INVESTIGATIONS ON POWER SYSTEM TRANSFER CAPABILITY IN ELECTRICITY MARKET

A Thesis submitted in fulfillment of the requirements for the award of the degree of

Doctor of Philosophy

Submitted by

Divya Gupta

(Reg. No. 950904021)

Under the Supervision of

Dr. Sanjay K. Jain

Electrical & Instrumentation Engineering Department

Thapar Institute of Engineering & Technology

PATIALA-147004

November 2022

Certificate

I hereby certify that the work which is being presented in the Thesis entitled, ***"INVESTIGATIONS ON POWER SYSTEM TRANSFER CAPABILITY IN ELECTRICITY MARKET"*** in fulfillment of the requirement for the award of the Degree of ***Doctor of Philosophy*** submitted in the ***Electrical & Instrumentation Engineering Department*** of the **Thapar Institute of Engineering and Technology** is an authentic record of my work carried out under the supervision of **Dr. Sanjay K. Jain** and refer other researcher's work, which is duly listed in the reference section.

The matter presented in this Thesis has not been submitted for the award of any other degree of this or any other University.

Divya Gupta
Reg. No. 950904021

This is to certify that the above statement made by the candidate is correct to the best of my knowledge.

Dr. Sanjay K. Jain
Professor

Date: 03 Nov 2022

Abstract

The structure of the power system is undergoing the transition from a vertically integrated arrangement to the deregulated one to adapt to competitive market practices for the benefit of all the participants. However, the want of market participants for profit maximization is a security risk and threat to the reliable operation of the system. Accordingly, it becomes essential for the system operator to enumerate the Available Transfer Capability (ATC) of the network and earmark the same to the market applicants in a well-organized way.

The optimal allocation of the Flexible Alternating Current Transmission Systems (FACTS) can be worked out to improve the power flow and minimize the losses. Among various FACTS devices, the series compensator namely Thyristor Controlled Series Capacitor (TCSC) can be utilized to compensate for line reactance and thus improve the ATC. In the present work, the allocation of TCSC has been accomplished by the Sensitivity and Power loss-based Congestion Reduction (SPCR) method. The SPCR method presents the technique of finding the optimal location of TCSC by computing the sensitivity of lines while utilizing the DC Power Flow Sensitivity Index and Reactive Power Loss Sensitivity Index after considering N-1 contingency. The reactive and real power losses along with real power flow are compared on the sensitive lines. With the placement of TCSC, the loadability of lines increases which ensures the relief of congestion on sensitive lines. The real power flows are analyzed by comparing the SPCR method with Power System Analysis Toolbox (PSAT). The efficacy of the proposed method is authenticated on 6-bus and 30-bus test systems.

The Metaheuristic Evolutionary Particle Swarm Optimization (MEEPSO) is proposed to enhance the ATC considering line flow limits termed as Static ATC (SATC). MEEPSO resulted in a higher rate of convergence and helped in optimizing the value of SATC. The acceleration parameter is selected at 2. The minimum and maximum inertia weights are fixed at 1 and 1.2 respectively. The maximum compensation is limited to 50% of line reactance. The base case values of SATC are calculated using the Newton–Raphson load flow and the AC Power Transfer Distribution Factor (ACPTDF) are used under different transactions. The SATC value is then optimized using the MEEPSO method and compared with conventional techniques like the DC Power Transfer Distribution Factor (DCPTDF) technique. MEEPSO resulted in a higher rate of convergence and helped in

optimizing the value of SATC by improving it through 25.85% and 9.34% as compared to DCPTDF and ACPTDF respectively for 6-bus system. These values were nearly 33% and 34% for 30-bus system. The performance of the developed algorithm in obtaining SATC values is compared with PWS. The results with PWS have been taken using Single Linear (SL) step solution technique. The system is divided into areas. The optimum cost of an individual case is calculated to visualize the influence of the modification in transactions amongst areas. The outcomes of the transactions are compared based on the above factors to obtain the economic operation.

The ATC determined under dynamic stability limits is known as Dynamic ATC (DATC). The DATC has been calculated using the novice Single Machine Infinite Bus Eigen Area-based Modal Bifurcation (SEAMB) method and is executed using PWS by dividing the system into areas. The critical sensitivity is ascertained using eigen values. The three-phase faults are applied at the designated buses for 0.1s. The respective line is tripped at 0.15s and the simulation is performed for 5s. The DATC calculation is accomplished till the accurate Hopf Bifurcation (HB) point of eigen value is reached. A comparison between ATC values observed by taking static load and dynamic load is presented. The effectiveness and accuracy of the proposed method are verified on WSCC 9 bus as well as the New England 39 bus system.

Keywords: Available Transfer Capability, Static ATC, TCSC allocation, Eigen values, Dynamic ATC

Acknowledgements

This study was an elaborate mission and it would have been unachievable without the help and gratitude of many people. I honestly feel short of words to acknowledge all those who helped me directly and indirectly during this mission.

The author expresses her deep sense of gratitude to **Dr. Sanjay K. Jain**, Professor, Electrical and Instrumentation Engineering Department, Thapar Institute of Engineering and Technology, Patiala. for his kind support, skillful guidance, and proficient evaluation, persistent encouragement, and conscientious supervision throughout this academic endeavour. His vibrant persona, hard-working nature, and methodical directions were a constant source of encouragement for me. Due to his extremely valuable guidance, expertise, inquisitive attitude, and tireless efforts throughout the tenure of the work, I found my vision even more broadened. I earnestly thank him from the core of my heart for being a consistent source of inspiration right from the beginning to the end.

I am also thankful to **Dr. Mandeep Singh**, Professor, **Dr. Sunil Kumar Singla**, Associate Professor, Electrical and Instrumentation Engineering Department and **Dr. Kulbir Singh**, Professor, Electronics and Communication Engineering Department, for being the members of the Doctoral Committee and spending their valuable time in reviewing and critically examining the work during regular progress monitoring meetings.

The author feels highly honoured and gratefully acknowledges the continuous encouragement from the present Chairman of the Doctoral Committee **Dr. R. S. Kaler**, Senior Professor and Head, Electrical and Instrumentation Engineering Department for the much-needed support throughout the work. My heartfelt gratitude to **Dr. Rafat Siddique**, Senior Professor and Dean, Research and Sponsored Projects, and Honourable Director **Dr. Prakash Gopalan** for the encouragement, support, and providing the necessary facilities to carry out and complete this work on a steady course.

The author is highly thankful to **Dr. Gursewak Singh Brar,** Professor, and Head, Department of Electrical Engineering, Baba Banda Singh Bahadur Engineering College, Fatehgarh Sahib for his help and support to provide her adequate time for the success of the work. The author would like to express her sincere thanks for the extreme help and support of her colleagues and friends particularly **Dr. Navdeep Kaur** and **Ms. Akanksha Sharma**, who with their valuable support, and suggestions have contributed directly or indirectly in a significant way towards the completion of this work.

The author also expresses her sense of sacrosanctity for her beloved parents and mentors **Late Er. Sushil Kumar** and **Smt. Anita Gupta** and brother **Er. Prasun Gupta**. The author appreciates the care and support of her life partner, **Er. Ashish Kumar**, who sacrificed many opportunities and firmly stood by her all the time. He took the author's family responsibility many times and compromised his comforts. A sense of apology is owed to the author's lovely daughter, **Manyata**, and son **Ruhaan Kumar**, who lost many precious moments of mother's care and love. They have been the victim of the author's frustrations which are deeply regretted. This thesis is dedicated to the author's lovely kids.

Above all, the author is highly grateful to the Almighty for blessing her with spiritual support and providing strength at every stage of the work.

Divya Gupta

Table of Contents

List of Figures

List of Tables

List of Abbreviations

AC	Alternating Current
ACO	Ant Colony Optimization
ACPTDF	AC Power Transfer Distribution Factors
AHP	Analytical Hierarchy Process
AI	Artificial Intelligence
AIS	Artificial Immune System
ANN	Artificial Neural Network
ANOVA	Analysis of Variance
ATC	Available Transfer Capability
AWNN	Adaptive Wavelet Neural Network
BPA	Back Propagation Algorithm
BSO	Bacterial Swarm Optimization
CBM	Capacity Benefit Margin
CCT	Critical Clearing Time
CEED	Combined Economic Emission Dispatch
CPF	Continuation Power Flow
CPU	Central Processing Unit
CSO	Cat Swarm Optimization
DATC	Dynamic Available Transfer Capability
DC	Direct Current
DCO	Dynamic Constrained Optimization
DCPTDF	DC Power Transfer Distribution Factors
DE	Differential Evolution
DFS	Depth First Search
DL	Dynamic Load
EA	Evolutionary Algorithm
EMS	Energy Management System
EP	Evolutionary Programming
ETC	Existing Transmission Commitments
FACTS	Flexible AC Transmission Systems
FERC	Federal Energy Regulatory Commission
GA	Genetic Algorithm

GENROU	Round Rotor Generator
GODF	Generator Outage Distribution Factor
GOS	Glover, Overbye & Sarma
HB	Hopf Bifurcation
HBA	Human-Based Algorithm
HE	Holomorphic Embedding
HMPSO	Hybrid Technique of Mutation Particle Swarm Optimization
IGA	Immune Genetic Algorithm
IPPs	Independent Power Producers
ISO	Independent System Operator
LAM	Linear Approximation Methods
LBAC	Load Bus's Available Capacity
LMP	Locational Marginal Pricing
MATLAB	Matrix Laboratory
MEA	Mind Evolution Algorithm
MEEPSO	Metaheuristic Evolutionary Particle Swarm Optimization
MVA	Mega Volt Ampere
MW	Mega Watt
NA	Neural Algorithm
NATC	Non-recallable ATC
NERC	North American Electric Reliability Council
NP	Non-deterministic Polynomial
NRLF	Newton Raphson Load Flow method
NSHCSA	Non-dominated Sorting Hybrid Cuckoo Search Algorithm
OASIS	Open Access Same Time Information System
OLS	Ordinary Least Square
OPF	Optimal Power Flow
OTDF	Outage Transfer Distribution Factor
PA	Probabilistic Algorithms
PBM	Physics-Based Mechanism
PEBS	Potential Energy Boundary Surface
PI	Proportional Integral
PSAT	Power System Analysis Toolbox
PSO	Particle Swarm Optimization
PTC	Power Transfer Capability

PTDF	Power Transfer Distribution Factor
PU	Per Unit
PV	Photo-Voltaic
PWS	Power World Simulator
RATC	Recallable ATC
RBF	Radial Basis Function
RBFNN	Radial Basis Function Neural Network
RGA	Real Genetic Algorithm
RPF	Repeated Power Flow
RTS	Reliability Test System
SA	Stochastic Algorithm
SATC	Static Available Transfer Capability
SCOPF	Security Constrained Optimal Power Flow
SEAMB	SMIB Eigen Area-based Modal Bifurcation
SGA	Standard Genetic Algorithm
SIA	Swarm – Intelligence Algorithm
SMIB	Single Machine Infinite Bus
SNB	Saddle Node Bifurcation
SPCR	Sensitivity and Power loss-based Congestion Reduction
SSSC	Static Synchronous Series Compensator
STATCOM	Static Synchronous Compensator
SVC	Static Var Compensator
SVM	Support Vector Machine
TCPAR	Thyristor-Controlled Phase Angle Regulators
TCPS	Thyristor Controlled Phase Shifter
TCR	Thyristor Controlled Reactor
TCSC	Thyristor Controlled Series Capacitor
TRM	Transmission Reliability Margin
TS	Tabu Search
TSCOPF	Transfer-based Security Constrained OPF
TTC	Total Transfer Capability
UPFC	Unified Power Flow Controller
VAR	Volt-Ampere Reactive
VDFs	Voltage Distribution Factors
VIU	Vertically Integrated Utility

List of Symbols

T_m	Mechanical torque in p.u.
T_e	Electromagnetic torque in p.u.
ω_r	Angular velocity of the rotor, electrical rad/s
δ	Rotor angle in p.u.
t	Time, s
D	Damping coefficient in p.u.
H	Inertia constant in s
R_a	Armature resistance in p.u.
X_l	Leakage reactance in p.u.
X_d	d-axis synchronous reactance in p.u.
$X_d{}'$	d-axis transient reactance in p.u.
$X_d{}''$	d-axis sub-transient reactance in p.u.
X_q	q-axis synchronous reactance in p.u.
$X_q{}'$	q-axis transient reactance in p.u.
$X_q{}''$	q-axis sub-transient reactance in p.u.
$T_{d0}{}'$	d-axis open circuit transient time constant in s
$T_{d0}{}''$	d-axis open circuit sub-transient time constant in s
$T_{q0}{}'$	q-axis open circuit transient time constant in s
$T_{q0}{}''$	q-axis open circuit sub-transient time constant in s
s_{10}	Saturation behavior parameter
s_{12}	Saturation behavior parameter
T_R	Voltage sensor time constant in s
K_A	Voltage regulator gain in s
T_A	Voltage regulator time constant in s
V_{RMAX}	Power source upper limit in s
V_{RMIN}	Power source lower limit in s
K_E	Exciter equivalent gain in p.u.
T_E	Exciter equivalent time constant in p.u.
K_F	Feedback loop equivalent gain in p.u.
T_F	Feedback loop equivalent time constant in s
E_1	Field voltage value in p.u.

$S_E E_1$	Saturation factor in p.u.
E_2	Field voltage value in p.u.
$S_E E_2$	Saturation factor in p.u.
θ	Phase shift angle in p.u.
φ_d	d-axis flux linkage in p.u.
$\varphi_d{}'$	d-axis transient flux linkage in p.u.
$\varphi_d{}''$	d-axis sub transient flux linkage in p.u.
φ_q	q-axis flux linkage in p.u.
$\varphi_q{}'$	q-axis transient flux linkage in p.u.
$\varphi_q{}''$	q-axis sub transient flux linkage in p.u.
i_d	d-axis stator current in p.u.
i_q	q-axis stator current in p.u.
u_d	d-axis stator voltage in p.u.
u_q	q-axis stator current in p.u.

Chapter 1 Introduction

Across the world, the power utilities are undergoing a major transformation from monopolistic to deregulated one. The power utilities were characterized by vertically integrated arrangement, as shown in Figure 1.1, in a monopolistic structure. In this model, generation, transmission, and distribution activities are within the direct control of a central agency or a single utility. Its transformation towards a more competitive deregulated system is directed to improving efficiency, quality, and reliability of production along with a reduction in prices. The transmission system is becoming more impartial to each participant in the power industry. The representative structure of deregulated power system is shown in Figure 1.2. Contrary to the vertically integrated utility structure, alternative paths seem to exist where the money flows in a deregulated arrangement.

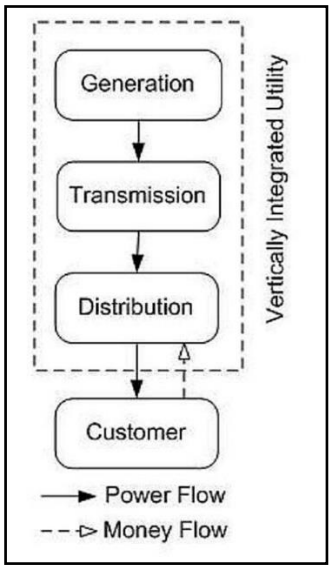

Figure 1.1 Block Diagram of Vertically Integrated Utility

Due to deregulation, the grid integration has reallocated itself from regional self-sufficiency to optimal application of resources amongst significant topographical areas. Hence, it is imperative on the part of the system operator to measure the ATC of the network and allocate the same to the market participants in a resourceful manner.

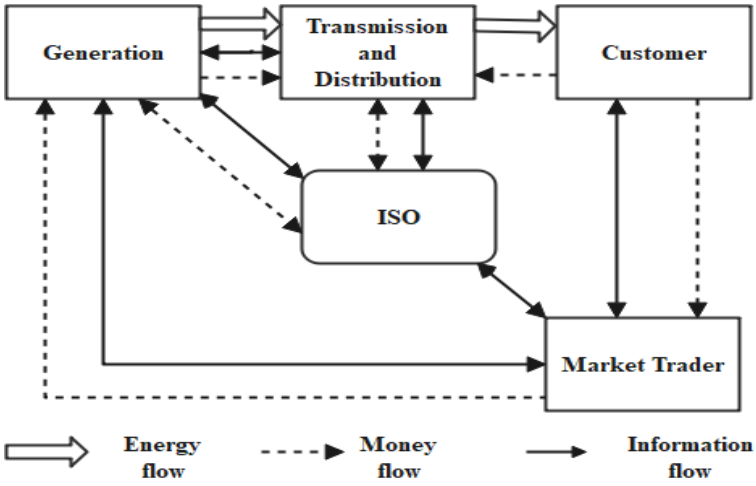

Figure 1.2 Flow chart showing deregulated power system [1]

For computing [2] and display of the ATC [3], an open access [4] system is needed where market participants are connected through public communications and the internet. The power sector in India has been the joint responsibility of the state and central governments. It was governed by the Indian Electricity Act, 1910, the Electricity (supply) Act, 1948 and the Electricity Regulatory Commissions Act, 1998. The enactment of the Electricity Act 2003 has given way to the deregulated structure and formulation of Independent Power Producers (IPPs) and Independent Regulatory Commissions.

Every buyer desire to purchase power from an inexpensive generator regardless of the topographical location. If all such transactions are permitted, the transmission corridors withdrawing the power of economical generators would get burdened or resulted in congestion. The congestion is the situation when the system operator discovers that every transaction cannot be permitted owing to overload on the transmission network. Congestion management is very important in the deregulated structure, which is a process to arrange the transactions on priority and make a committed schedule that would not burden the network.

The system operator supervises the circumstances such as forced outage and manages the congestion through real-time congestion management. This effectually implies that generations are dispatched in such a way so that the line power flow limits are not violated. Congestion has been handled through market-based, technical and non-market-based methods [5]. Among technical methods, the FACTS devices [6] were used to decrease the flows in heavily loaded lines and improve the loadability of lines and for ATC enhancement [7]. These devices improve the system performance by controlling

steady-state power flow without generation re-scheduling or any topological alterations [8]. FACTS devices such as TCSC can aid in reducing congestion [9]. The allocation of FACTS devices such as TCSC is very important and it has been investigated through approaches like sensitivity analysis [10] or using Power System Analysis Toolbox (PSAT) [11, 12].

The conventional methods used for calculating ATC include Newton Raphson (NR) technique, Linear Approximation Methods (LAM) [13] utilizing Power Transfer Distribution Factor (PTDF) [14] and SCOPF methods etc. The PWS was also used for analyzing ATC and related factors [15]. Various Artificial Intelligence (AI) techniques [16] have been used for the computation of transfer capability and the allocation of FACTS devices. Among these, the population-based heuristic searches and optimization methods [17, 18] are extremely competent in dealing with vastly constrained, multimodal, distinct and multi-objective systems.

The power system is always subjected to various types of disturbances arising due to changes in operating conditions. Under such dynamic conditions, the ATC must be calculated while considering the complete system and is referred to as DATC [19]. It is the value of maximum ATC while keeping the feasibility and stability of the transient response. The constraints such as saddle-node and Hopf bifurcation limits shall be accounted for in computing DATC through methods such as SCOPF or Dynamic Constrained Optimization (DCO) [20].

Hence, there is a need for the System Operator to manage the transmission network while ensuring its open access [21]. Since it is shared by all the market entities, they should be apprised of the transfer capability available for further commercial transactions. All the additional power transfer contracts must be within the bounds of the ATC and within the system limits. The introduction of deregulation in the electricity sector has brought forward many new entities, and the scope of the existing system has been redefined.

1.1 AVAILABLE TRANSFER CAPABILITY

ATC may be stated mathematically as the difference between the sum of Total Transfer Capability (TTC) and the sum of Transmission Reliability Margin (TRM) and Existing Transmission Commitments (ETC) including Capacity Benefit Margin (CBM) [13, 22].

$$ATC = TTC - (TRM + ETC + CBM) \quad (1.1)$$

Figure 1.3 depicts the ATC and related terms, which are forming the basis to schedule transmission services in the open power market. These are briefed here under as:

The TTC [23] is defined as the maximum transferable power from one control area to the others without violating thermal limits and voltage limits, no voltage collapse, or any transient instability. The ambiguities connected to these parameters trigger key problems while calculating the ATC values. TRM and CBM are used for modelling ambiguities in ATC calculation. TRM gives the value of ambiguity in the transmitting system and presents its effect on the determination of ATC, while CBM is responsible for uncertainty in the generation [24]. The ETC is the sum of the current commitment to transmission between those regions.

The conservative ATC estimate may result in inefficient use of the transmission network. Accordingly, it must be rapidly and accurately calculated. The ATC value will direct the business behaviour of the participants in electricity markets with open access transmission and then develop the transmission capacity to be used proficiently. The assets must be pooled intensively for the tractability, steadfastness, and frugality of the interconnected power networks. More than one line can be encumbered in the transmission network during open access and, hence, causes congestion. The management of congestion can be effectively achieved by convalescing the ATC of the network.

Re-callability refers to the service provider's right to disrupt a complete or fragment of a transmission facility because of some reason arising may be due to economic, which adheres to FERC policy. Non-recallable ATC (NATC) may be stated as TTC, excluding TRM and non-recallable reserved transmission service. Recallable ATC (RATC) is expressed as TTC, excluding TRM, recallable transmission service, and non-recallable transmission service (including CBM).

Power transactions between a specific seller and a buyer can be committed only when the ATC is available for that interface to ensure system security. It is the accountability of the System Operator (SO) to regulate, apprise and display the existing value of ATC because private participants are concerned only with the marketable facets. Governing principles for the determination of ATC are given as under:

1. The results of the ATC calculation must be commercially viable and the ATC calculated should indicate reasonable and dependable transfer capabilities available to the power market.

2. ATC calculations must identify its dependency on points of injection, directions of transfers and the points of power extraction across the interconnected transmission network.

3. Its evaluation must follow the regulatory guidelines in the country.

4. The determination of ATC must accommodate tolerable uncertainties and offer flexibility to certify the secure operation of the interconnected network.

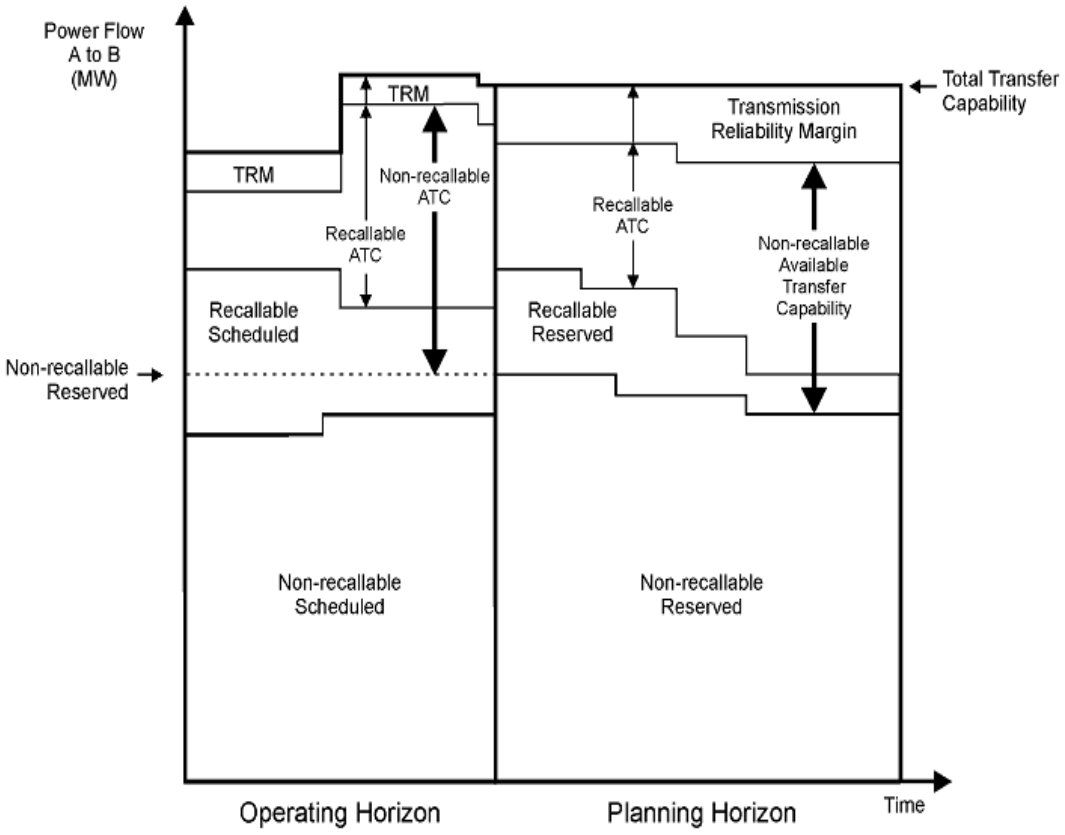

Figure 1.3 Various terms for scheduling the transmission service

The elementary purpose behind the analysis of ATC [1] is to communicate to the market entities regarding the limitations of the system, in advance, in terms of the supplementary amount of power that can be transported from one area to another. The limits pondered for the evaluation of ATC are categorized as flow limits, voltage limits and stability limits. Most electric devices fail to operate properly at under-voltage while voltages stress the insulation and may be destructive. When the generation and loadings in

a power system are gradually increased such that power balance is maintained, a limit is reached at which the load flow fails to converge. This is known as the steady-state stability limit of the transmission system.

With the consideration of constraints, ATC can be classified as Static Available Transfer Capability (SATC) and Dynamic Available Transfer Capability (DATC) [25]. The line flow limits considered for the evaluation of SATC may be defined as the maximum real power transfer capability of a line determined from considerations of its thermal and stability limit. ATC calculation is non-trivial [26] when static security constraints are included. The SATC can be evaluated by the Continuation Power Flow (CPF) method, Optimal Power Flow (OPF) method and methods based on sensitivity factors.

The ATC determination [27] can be formulated as an optimization problem that finds out the maximum value of the transaction between a given interface while satisfying the network power balance (equality constraints) and security constraints such as line flow, voltage limits and voltage instability conditions. The various methods for calculating ATC are broadly classified as Deterministic and Probabilistic. Artificial Intelligence techniques are exceptional in dealing with complex nonlinear problems.

Rapid calculation of the ATC can be accomplished through the linear approximation method. There are some advantages of static methods including simplicity, transparency, flexibility, and rapidity. Whereas optimism, inaccuracy, and not considering all constraints are the disadvantages and defects of these techniques. Dynamic stability is the capacity to maintain constant operation in the presence of small and large disturbances [25]. Transient stability constrained by maximum permissible transfer refers to the dynamic method [28]. This method consists of screening several contingencies. The maximum power transfer through the network is restricted by stability issues.

It is essential to ensure the system settles down to a new stable condition after a given disturbance, for the appropriate system operation [29]. Zhang *et al.* [20] suggested a technique for the evaluation of the dynamic ATC with the constraint of transient rotor angle stability. A bifurcation-based approach can be used for the dynamic ATC determination along with saddle-node and Hopf bifurcation limit. At zero eigenvalue, the SNB limit is reached and the response becomes monotonic. The HB limit generates oscillatory instabilities. A stable equilibrium point becomes unstable when the loading parameter variation forces a pair of complex eigen values to cross the imaginary axis in the complex plane. HB limit further leads to dynamic voltage instability.

1.2 CONGESTION MANAGEMENT

A substantial reason for transmission congestion [30] is the absence of power transmission line capacity for transactions. Thus, the dearth of attention will result in massive blackouts, and hence will destroy the electrical equipment of the system and will lead to differences in the price in several parts of the network [31]. Each transaction wishes the highest revenue from the system. Therefore, the possibility of congestion is higher in the deregulation scenario. For this reason, congestion management (CM) has been an important part of the analysis on enabling competition amongst utilities. For solving this, researchers all over the world have presented several techniques to prevent or diminish congestion restoring quicker power transfer to purchasers.

The general classification of congestion management methods can be done as technical and non-technical methods [32]. The non–technical methods include market-based and non-market-based methods. The technical methods shall include the outage of congested lines, controlling transformer tap settings and allocation of FACTS devices. Another classification is based on application. The applications are directed towards the generator side, transmission side and load side. Among various methods, optimal allocation of FACTS devices is an effective alternative. The FACTS devices can help in managing congestion, improving loadability, enhancing ATC, reducing transmission losses, fulfilling contractual obligations and improving stability [33]. However, the efficacy depends upon the locations where these devices are installed [34].

1.3 POWER WORLD SIMULATOR FRAMEWORK

The Power World Simulator (PWS) is a product of Power World Corporation, which was incorporated in 1996 and was developed by Professor Overbye [35] at Urbana–Champaign. Its graphical user interface (GUI) menu-driven interface is of great help to the user. It is easier to understand power system actions. The menu helped the users to have a certain number of case information displayed simultaneously in the interface. The power system simulation is manageable and highly communicative in the simulator. Different solutions like contingency analysis, fault analysis, optimal power flow, available transfer capability tools, etc. can be found. The main advantage of finding optimal power flow using this software is that it removes transmission line overload.

The static models provided in the framework can be augmented with generator cost information, reactive capability curve, power world simulator case options, interface definitions, injection group definitions and contingency definitions. ATC can be determined while using PWS for a normal mode operation for different bus systems in the case of normal and line outage contingency mode operation, with the thermal limit as a constraint and reactive power as constant. ATC may be determined for the bilateral and multilateral transactions in the simulator [36].

The solution technique used in the simulator for determining ATC among areas is the Single Linear (SL) Step technique. Sureban *et al.* present the step-by-step procedure to evaluate the ATC of the interconnected transmission network using PWS. Kumar *et al.* justified the accuracy of the calculation method by comparing the obtained results with standard Newton Raphson load flow and PWS results. The ATC values obtained from MATLAB are compared with that of PWS. Quick results and comparisons are obtained with detailed analysis using the simulator. It can be easily utilized for observing both Static and Dynamic ATC [37-39].

1.4 META HEURISTIC TECHNIQUES

Engineering design problems have long been solved with conventional methods. Despite yielding promising results in many cases, these methods find limited scope in more complex design problems. The number of decision variables may be large in case of real design problems and their effect can be complicated on the objective function. These complex problems are difficult to handle and efficient optimization methods are needed.

Meta-heuristic evolutionary algorithms, inspired by natural processes, have shown favourable performance for real-world optimization problems. Meta-heuristic techniques have improved abilities to avoid local optima compared with the conventional optimization methods. This is because of the stochastic nature of meta-heuristics which enables them to prevent inertia in local solutions and search the whole search space comprehensively. Search space of real problems is generally undetermined and is very complex with a vast count of local optima. Thus, meta-heuristics offer a good option for the optimization of these tough real problems.

A metaheuristic technique is a higher-level procedure created to find, generate, or select a heuristic which provides a good solution for an optimization problem, in case of incomplete, imperfect information and a limited computation capacity [40]. These

techniques are different from exact methods. They are not subject to combinatorial explosion. The computing time essential to find the optimal solution to Non-deterministic Polynomial (NP) hard problems intensifies as an exponential function of the size of the problem.

1.5 STATE OF THE ART

Power transactions between a source bus and a sinking bus can be committed only when sufficient power transfer capability is available. The ISO must estimate the required ATC between interfaces and update the same on OASIS at regular time intervals. Therefore, the methods required for the computation of ATC must be fast and accurate. A framework for determining the ATC of the interconnected transmission networks for a commercially viable wholesale market has been established by the NERC [41, 42] and FERC [2, 43] as per its report.

FERC in 1996 opened the transmission network and resultantly large power transactions have increased between utilities since then [44]. In future, these are expected to increase too in order to provide a reliable and economical power supply. These may involve two or more control areas in large networks. A system operator is required to ensure the transfer of power between two buses reliably to maintain system security. The useful information regarding the total power transfer feasible between two nodes without affecting the system reliability can be provided by ATC and TTC. The FERC mandates the ATC information to be made available on a real-time basis openly. TTC is the indicator of the power which can be transferred between two buses in the system in a consistent way in every time frame. ATC is the maximum transfer value between the source and the sink (control areas) available without infringement of operating properties (thermal overload and voltage limits) of the power system.

Environmental aspects and a search for optimal utilization of transmission capacities are inspiring many planners to work on ATC enhancement in place of building new transmission lines [45-49]. Hence, the use of FACTS devices appears to be a favourable strategy for reducing transmission congestion and for improving the ATC of the line [8, 50]. There are sensitivity-based methodologies for optimizing the location of FACTS controllers and improvement of ATC [51-53]. Singh *et al.* [9] presented a simple and efficient model for optimizing the location of FACTS devices for congestion management by controlling the device parameters.

Power transactions between a specific seller bus/area and a buyer bus/area [54] can be committed depending on the value of ATC. There are various deterministic mathematical techniques for ATC calculations such as CPF [3, 55], RPF [56], Optimum Power Flow (OPF) [57], DC load flow-based method [58, 59], and PTDF methods [60-64] and Heuristic-based methods [65-83]. Sensitivity-based power flow methods, based on PTDFs, have been proposed by many researchers for fast computation of ATC [61, 84, 85]. Christie *et al.* [86] have reported a DC load flow-based method for fast ATC calculation using DCPTDF. Ilic et al [59] discussed some theoretical aspects of ATC and its evaluation under open access environment. A method based on repeated AC power flow to determine risk assessment of ATC with margins has been proposed by Yan *et al.* [87].

Various optimization techniques such as sequential programming [88], evolutionary algorithms [89] and particle swarm optimization [90] have been used to find the ATC in different areas. Hiskens *et al.* [91], Tuglie *et al.* [92] and Gnanadass *et al.* [93] proposed an iterative approach for computing the dynamic ATC. Researchers have applied bifurcation analysis to studies of voltage stability [94-96]. HB is related to dynamic voltage instability while SNB is associated with the static voltage stability limit. Kumar *et al.* [64] had made the first attempt to address the bifurcation approach for the determination of DATC in the deregulated electricity market and the impact of SVC had also been presented. In addition to consideration of the static limits, the bifurcation analysis application would be an outstanding scheme in the calculation of DATC.

1.6 RESEARCH OBJECTIVES

In a deregulated scenario, the ATC is evaluated by ISO to control the power transactions and for congestion management. From the review, the following paucities concerning the optimal allocation of TCSC and enhancement and comparison of ATC procedure have been recognized from erstwhile work, and the scope has been identified as –

- Very few researchers have cited the hybrid methodology of using sensitivity indices along with reducing the reactive power losses accompanied by congestion management which includes real power reduction [9, 97-99].
- There is an absence of a comparison of intelligent techniques with the conventional methods and power world simulator results. Additionally, there is very least literature available on the use of PWS [46-49, 72, 79, 80, 82, 89, 100-108].

- Literature is scarce regarding the calculation of DATC with PWS. Area-based systems are very less explored. The hybrid analysis of SMIB, eigen values and Hopf. bifurcation limits combined with contingency analysis have not yet been reported in the literature [20, 24, 96, 109-115].

The research work entitled "INVESTIGATIONS ON POWER SYSTEM TRANSFER CAPABILITY IN ELECTRICITY MARKET" has been carried out with the following objectives:

- To develop the methodology for optimal placement of FACTS devices to enhance Available Transfer Capability.
- To develop the algorithm to determine Static ATC.
- To develop the algorithm to determine Dynamic ATC

1.7 THESIS ORGANIZATION

The thesis comprises six chapters and summarizes the specific contributions directed to achieving the objectives and presents the results obtained during this research. A brief description of these chapters is summarized as follows:

The *Chapter-1* presents an introduction to the basic terms related to investigations on power system transfer capability in the electricity market. The Available Transfer Capability (ATC) along with its principle of determination, limits and methods of calculating Static ATC and Dynamic ATC are mentioned. It introduces Congestion Management, Power World Simulator framework and meta-heuristic techniques, which are useful in calculating ATC. The state of the art in the field is also addressed. This chapter also outlines the identified research objectives and organization of the thesis.

The *Chapter-2* provides a brief description of various studies regarding ATC. The literature review is classified into categories namely usage of FACTS devices, review of different aspects of Static ATC and review of various aspects of Dynamic ATC. The later part of this chapter describes the author's contributions to the identified research areas.

The *Chapter-3* deals with the analysis of the optimal allocation of Thyristor Controlled Series Compensator (TCSC). The characteristic and mathematical model of

TCSC is summarized. It introduces the novice SPCR algorithm that has been developed to decide the allocation utilizing the DC power flow sensitivity index and Reactive power loss sensitivity index. The allocation is investigated for the different bus systems and the results are compared with PSAT.

Chapter-4 presents the calculation of static ATC using MEEPSO. It introduces the market operation, and the process of computing SATC using PWS and ACPTDF. The presented MEEPSO is a metaheuristic algorithm that utilizes ACPTDF to compute ATC following TCSC placement. The performance has been tested on different systems and the results are compared with PWS.

The *Chapter-5* presents the performance of ATC under the dynamic scenario. The dynamic model of the power system components namely the generator, load and exciter is presented. It also summarizes the eigen value analysis and different bifurcation methods. The technique is proposed to calculate DATC utilizing eigen values in conjunction with inequality constraints and SMIB eigen analysis. The DATC values are presented for different test systems when subjected to various faults and contingencies.

The *Chapter-6* presents the summary of the main conclusions of the studies offered in previous chapters. It also enlists the direction for further research.

Chapter 2 Literature Review

The power demand has increased substantially and growing with the rising dependency on electricity, however, power origination and transmission capacities have not been enhanced in that proportion. Consequently, a very small margin is left for the commercial activity. This margin is measured in terms of Available Transfer Capability (ATC), which indicates the ability of the power system to enhance the power transfer for efficient commercial transactions between two control areas (zones or points). A substantial enhancement in power transfer consists of unbiased open access to transmission networks. To surmount these problems, the scope for existing power transfer for the transmission network can be enhanced.

Investigators worldwide had addressed this issue of ATC enhancement by employing FACTS devices. The placement of such devices can be an encouraging strategy to drop congestion of the transmission lines and escalate ATC. Consequently, there is an interest in learning the stimulus of these devices on ATC plus optimally locating them to augment the transfer capabilities [116]. The ATC can be classified as Static ATC (SATC) and Dynamic ATC (DATC), which are calculated by considering static and dynamic limits respectively.

A reliable and cost-effective evaluation of SATC is crucial for the smooth functioning of the power system. The factors such as thermal limits, optimization parameters and motivation for the increase in ATC deeply influence the research in this area. The conventional techniques to calculate ATC are heavily dependent on mathematical equations. Such formulations shall not be suited for in present age power system because ATC will be a function of variable and interdependent parameters. Consequently, ATC calculations may need to be periodically updated and thus require the use of intelligent techniques in online conditions. In addition to numerous studies through probabilistic and deterministic methods, many metaheuristic techniques have been reported in optimizing the value of SATC.

The benefits of static methods include simplicity, transparency, flexibility, and rapidity. Inaccuracy, and not considering all constraints are the drawbacks and defects of these methods. Several methods for DATC evaluation are those based on SMIB and bifurcation theory. To enlist the contributions of various researchers, a brief literature review is carried out on the usage of FACTS devices, SATC and DATC computations.

2.1 USAGE OF FACTS DEVICES

It may not be always viable to transmit all the contracted power transactions in the deregulated electricity market due to congestion of the transmission corridors. The current power system restructuring needs an opening of unused transmission system potentials due to environmental and cost-related issues which are major barriers to the expansion of the power transmission network. FACTS devices play an important role in improving the performance of a power system by improving the voltage profile and removing the congestion in the transmission lines, but these devices are very costly and hence need to be placed optimally in the power system [117]. The thyristor-controlled series compensator (TCSC), a FACTS device, can be employed to reduce the flows in heavily loaded lines, resulting in a low system loss and improved stability of the network.

The TCSC offers series compensation and comprises a series capacitor bank shunted by Thyristor Controlled Reactor (TCR). With the thyristor's control, TCR can change its reactance smoothly and quickly. TCSC's static model is used as a series reactance with the control parameter [101]. Thakre *et al.* [118] suggested a criterion for determining the change in the reactance of TCSC for achieving the chosen transfer capability. The changes in the line flow and selection of a line for the installation of TCSC are computed by the sensitivity analysis. Many researchers have presented methods for determining the optimal location and capacity of TCSC to enhance ATC along with the voltage profile. Network strengthening has been given by Huang *et al.* [119] to enhance the ATC of a unified power system with TCSC. Pankajam *et al.* [101] analyzed the viability and technical merits of boosting ATC while using TCSC. Karthiga et al.[120] analyzed the feasibility and technical benefits of furthering ATC by TCSC.

Albatsh *et al.* [121] conducted a review on the usage of the FACTS controllers to improve the ATC combined with the Power Transfer Capability (PTC) of power networks. Schnurr *et al.* [122] deliberated a sensitivity established method to enhance the place of the multi-functional FACTS devices and their ability in the ATC development. The performance of the FACTS devices was assessed within ATC besides PTC improvement regarding various control algorithms.

Kulkarni *et al.* [123] suggested methods for the determination of the size and optimal location of TCSC to improve the capability of power transfer of a transmission system using a variable model of TCSC reactance under static conditions. These methods utilized various sensitivity parameters to optimize the TCSC location on IEEE 6 bus system

using Power System Analysis Toolbox (PSAT), which is a MATLAB toolbox for electric power system analysis and simulation. Many other researchers have stated the use of PSAT [124]. Milano *et al.* [125, 126] described the PSAT as an open-source software package for the analysis and design of small to medium size electric power systems through static and dynamic models.

The insertion of FACTS devices in electrical systems is a promising strategy to enhance ATC. Rao *et al.* [127] investigated ATC enhancement using FACTS devices utilizing the VAR loss sensitivity index method and Real power loss index method. The performance of FACTS devices was compared based on the optimal location methods. ATC was improved by multi-type FACTS devices i.e., the combination of TCSC and TCPAR for the IEEE-9 bus system with PWS. Xiao *et al.* [128] evaluated the effect of various categories of FACTS devices on ATC improvement for the IEEE 118-bus system. Verma *et al.* [51] located TCSC suitably based on the real power flow performance index sensitivity. A sensitivity-based approach was developed for finding the suitable placement of these devices for the enhancement of transfer capability. The placement of TCSC was ascertained through critical sensitivity.

2.2 REVIEW ON STATIC ATC

A real deregulation scheme was obtained by successfully verifying the correct amount of ATC [129]. The evaluation of ATC in presence of static limits is known as SATC. The linear ATC method [61] utilized linear distribution factors and provided the approximate ATC value. Ejebe *et al.* [130] presented a detailed formulation and implementation of speedy ATC calculations. The formulations were based upon the incremental power flow which is linear to justify the line flow with effects of thermal loading. The linear ATC application was found suitable for enhancing speed in administering many contingencies to ascertain ATC for every specified transfer.

The ability to obtain sensitivities swiftly in connection with many parameters makes it feasible to credit for the impacts of many unclear parameters in significant power system modes. The sensitivity indices-based methods can rapidly calculate ATC. However, due to significant changes in the system, accuracy cannot be maintained [131]. The techniques that are based upon DC load flow [132] involve less computation complexity and are faster. The methods assume the network to be loss-free and can only model real power flow (in MW). Venkatesh *et al.* [63] assessed ATC using the sensitivity-based approach to derive

ACPTDF. The results of ATC were compared with those of the Newton Raphson Load Flow method (NRLF) for checking the accuracy and the results were encouraging. Ashwani *et al.* [62] proposed a set of ACPTDFs, VDFs and OTDF to ascertain SATC more precisely. The coefficient of the linear relationship between the amount of a transaction and the flow on a line has been termed PTDF [133].

Corniere et. al [134] presented a probabilistic method for assessing congestion cost plus the risk coupled with ATC. The aim was to give accurate and realistic information on the capability of connected networks which reliably boost power transfer sandwiched between geographical zones and commercial entities. The existing methods established online capability for a set of conditions as well as applicable safety margins.

Weber *et al.* [135] described methods employing a single linear step, iterated linear step, and full AC formulation for calculating ATC in the Power World Simulator. Nagalakshmi *et al.* [136] estimated ATC for base case normal operating state, probable cases linking single line outage, generator outage through bilateral transactions using PTDF, Outage Transfer Distribution Factor (OTDF), Generator Outage Distribution Factor (GODF) approaches respectively. The simulation study was completed on IEEE 6 bus standard test system. The methods that are based on Optimal Power Flow (OPF) provide optimal settings of controllable variable quantity by optimizing the objective function conditional on equality along with inequality constraints. The methods based on distribution factors [137] can accommodate the scenario that is nearby the base. The ATC was calculated with very little computation time utilizing the distribution factor method, which shall be beneficial for the decontrolled electricity market applicants.

The accurate and fast estimation of SATC, including margins of transmission, remains the key factor in congestion management [138]. Various Artificial Intelligence (AI) techniques, which are emulating one or the other life characteristic, have evolved. Among these, the techniques based on Artificial Neural networks (ANN), Fuzzy Logic, and Evolutionary search algorithms have been used extensively in the power system. Because of the toughness, speed, and capacity to handle imperfect or noisy data, the ANNs have been used to estimate transfer capability [139-141]. For the complicated nonlinear and non-differentiable objective functions, the population-based heuristic or metaheuristic searches, and optimization methods have been used to obtain an optimal solution. Most common are the variants of Genetic Algorithm (GA), Evolutionary Programming (EP) and Particle Swarm Optimization (PSO). These methods are inspired by the various phenomenon that is happening in nature and science. A sample illustration is presented in

Figure 2.1 (a) [142], which suggests that insect behaviour has been predominantly captured in developing metaheuristics and has a share of about 23% of the total metaheuristics. The various disciplines of metaheuristics are presented in Figure 2.1 (b) [143], which suggests that bio-inspired metaheuristics are dominant with about 55% share [144].

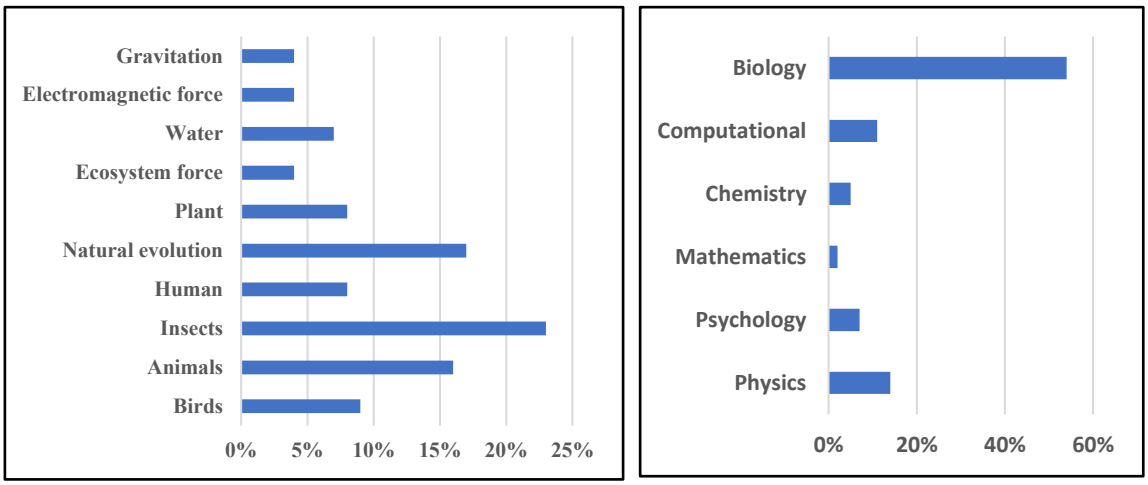

(a) (b)

Figure 2.1 Metaheuristic technique: (a) The topmost prominent areas, (b) The leading metaheuristic disciplines [142]

For deterministic calculations, RPF and CPF methods involve full AC load flow and integrate constant voltage reduction, reactive power flow, traditional thermal loading effects and voltage breakdown [145]. OPF methods adopt new optimization techniques easily but the problem of complexity and convergence arises [146]. Accurate results are guaranteed through stability constrained methods but they are highly complex [147]. ATC can be estimated based on probabilistic methods [65] that are suited for offline planning analysis. This classification includes numerical, analytical, approximate and AI methods. The numerical methods easily handle many uncertainties but are unable to deal with the relativity amongst system components [148]. Analytical methods are computationally efficient but accuracy degrades due to assumptions and linearization [149]. Approximate probabilistic methods are seldom used for real-time applications [61] and AI methods guarantee the accuracy of results [150]. The summary of these methods along with relative advantages and disadvantages are presented in Table 2.1.

Table 2.1 Comparison of deterministic and probabilistic methods for calculating ATC

Methods	Advantages	Disadvantages
Deterministic		
RPF and CPF [145]	• Divergence avoided around voltage limit point • Integrates constant voltage reduction, reactive power flow, traditional thermal loading effects and voltage breakdown • Full AC load flow is considered • Accurate results	• More computational time • Conservative results
OPF-conventional [146]	• Incorporates various complex constraints • Adopts new techniques of optimization effortlessly. • Feasibility of maximum power transfer • Simple and fast	• Optimal solution not guaranteed • Problem of complexity and convergence
Stability-constrained [147]	• Accurate ATC results are guaranteed.	• Highly complex • Rarely used for online applications
Probabilistic		
Numerical method [148]	• Includes uncertainties of the system • Easily handles many uncertainties • Accurate ATC results obtained	• Unable to deal with the relativity amongst system components • Accuracy degrades with the decrease in system size • More computation time required
Analytical method [149]	• Considers several system uncertainties • Computationally efficient	• Assumptions deteriorate the accuracy and linearization of the involved formulations
Approximate method [61]	• Accurate ATC results • Faster computational time	• Seldom used for real-time application
Artificial intelligent method [150]	• Outstanding in handling complex nonlinear problems • Accuracy of results guaranteed	• Considerable ATC data input is required • Larger computational resources required

The PSO [73], because of its inherent ability to maintain elitism, better exploration and exploitation capability, has been used for various power systems optimization purposes such as economic dispatch [151-153], reactive power control [145], optimal power flow [146], unit commitment [154] and ATC [155]. Test results indicated that optimal placing of FACTS controllers by PSO can improve the power transfer capability compared with

those from EP. It was reported that PSO gives a higher benefit to cost ratio, faster convergence, and less Central Processing Unit (CPU) time than EP for all transfer areas. The comparison of ATC enhancement methods along with the technologies used is described in Table 2.2 and Table 2.3 for IEEE 6 bus and 30 bus systems respectively.

Table 2.2 Comparison of ATC enhancement methods and technologies used for the IEEE-6 bus system

References	Methods	Technology
Yousefi et al. [114]	Losses estimation	Dynamic transmission line ratings
Prajapati et al. [156]	Optimal location of TCSC	DCPTDF ACPTDF
Gaur et al. [157]	Optimal placement of FACTS devices	Optimization Techniques
Ankaliki et al. [158]	Using TCR	PTDF Repeated Power Flow (RPF) PWS
Thakre et al. [159]	TCSC	Sensitivity Analysis
Jayalakshmi et al. [160]	Optimal setting of TCSC	A Static Optimization Approach

Table 2.3 Comparison of methods for ATC enhancement and technologies used for IEEE-30 bus system

References	Methods	Technology
Gharaveisi *et al.* [97]	Optimal location and capacity of TCSC	Real genetic algorithm (RGA) associated with analytical hierarchy process (AHP) and fuzzy sets
Shukla *et al.* [161]	Estimation of Available Transfer Capability	PS-NR (pattern search and Newton Raphson) based technique
Shayesteh *et al.* [162]	Incorporation of FACTS devices and Demand Response programs	Direct load control program and economic feasibility study
Poluru *et al.* [163]	Optimization of TCSC configuration	Adaptive Moth Flame Optimization Algorithm
Kesherwani *et al.* [164]	Intact system conditions and N-1 contingency situations	Holomorphic embedding (HE)
Rao *et al.* [165]	Using TCSC and TCPAR	Voltage stability
Karan *et al.* [166]	Using FACTS devices	Modified DE based
Idris *et al.* [167]	Optimal allocation of FACTS devices	Bees Algorithm

2.3 REVIEW ON DYNAMIC ATC

ATC determined with a dynamic stability range is said to be the dynamic ATC. Hiskens *et al.* [168] used an iterative approach to calculate dynamic ATC. Trajectory sensitivities along with some differential algebraic-discrete expressions for a given model of power systems. Enrico *et al.* [169] developed a nonlinear program to evaluate ATC and capability for the treatment of static and dynamic security constraints in the software. The algorithm was applied and tested in real-time on the actual power system.

Idhaya *et al.* [25] determined the possibility of bilateral contracts and estimated DATC on open access same-time information system on an hourly/daily basis. A rapid and effective online technique for dynamic ATC was estimated. The method was applied to New England 10 machine 39-bus dynamic system for estimating DATC values for different cases. By applying contingency screening analysis, the most sensitive lines were identified. Jain *et al.* [109] optimized dynamic ATC considering Hopf bifurcation limit, in bilateral as well as multilateral transactions. The effectiveness of the method was presented on the 39-bus New England system and the 246-bus Indian system for AC hybrid of static and dynamic load models. An oscillatory stability-based contingency index for screening was used to determine the ATC considering critical contingencies.

Kumar *et al.* [112] calculated dynamic ATC using intelligent techniques. Serious faults were designated for the determination of dynamic ATC to decrease the calculation time. The critical contingencies were used to calculate the dynamic ATC between a pair of sources and a sink bus. The results were compared with other techniques. Manikandan [36] carried out area-wise transactions to evaluate multi-area ATC with ACPTDF. IEEE 30 bus and 118 bus systems were used for the determination of multi-area ATC for normal as well as line outage contingency. The multi-area ATC values so obtained were compared with Power World Simulator (PWS) for validation.

Kumar *et al.* [64] described a submission of bifurcation criteria which is planned for dynamic available transfer capability fortitude in a cutthroat power market having bilateral along with multilateral transactions. The Hopf bifurcation limit had been quantified for a finding of the dynamic ATC. The saddle-node bifurcation coupled with bus voltage limits had been utilized for static ATC determination. ATC values decreased in all the cases due to Dynamic Load (DL) in the system. HB occurred before SNB for all the considered transactions. Thus, the dynamic ATC was observed to be less than that corresponding to the static ATC considering SNB.

2.4 RESEARCH CONTRIBUTIONS

As per the identified research objectives, the following contributions are made during the work:

Development of methodology for placing FACTS device to enhance the ATC

- In this study, the sensitivity factor-based method is proposed to optimally allocate TCSC, which is termed the Sensitivity and Power loss-based Congestion Reduction (SPCR) method.
- For the proposed technique, the two sensitive indices viz., DC power flow sensitivity index and Reactive power loss sensitivity index are calculated while considering N-1 contingency.
- This method finds the optimal location of TCSC by first calculating the sensitivity of all the lines and then analyzing the effect of TCSC placement in a few most sensitive lines.
- The line where TCSC placement leads to the most reduction in real and reactive power loss along with real power flow is considered optimal. This ensures the increase of ATC in these lines and, a decrease in congestion in the system.

Development of a heuristic algorithm for determining static ATC

- In this study, the power market operations are observed for single and multi-area systems.
- The available transfer capability considering static limits is analyzed using the proposed Metaheuristic Evolutionary Particle Swarm Optimization (MEEPSO) technique and PWS.
- The SATC is optimized using the MEEPSO technique for a single area system. The reduction in the total system cost along with congestion on heavily loaded lines is observed for the different levels of transactions between the neighbouring areas using PWS.
- The values of SATC obtained by the MEEPSO technique are compared with that of ACPTDF, DCPTDF, and PWS.

- The efficacy of the developed method has been proved by making various transactions between different buses and is validated by presenting results for SATC, with and without FACTS device employing the 6 bus and 30 bus system.

Development of an algorithm for determining DATC

- This study comprises the computation of DATC using the proposed Single Machine Infinite Bus Eigen Area-based Modal Bifurcation (SEAMB) method.
- The calculation using the SEAMB method includes firstly the division of the system into areas and then running of SMIB eigen analysis for finding eigen values. The critical eigen values are obtained based on SNB and HB limits. The DATC is considered for transactions between the two areas for the 9-bus system and three areas for the 39-bus system.
- The proposed SEAMB method finds the DATC at which the eigen value reaches the accurate HB point, after increasing transferred power until the saddle-node limit is reached.
- The DATC values are computed and compared for static load and dynamic load for various contingencies.
- The effectiveness and accuracy of the proposed approach have been ascertained through investigations of the WSCC-9 bus system and the New England 39-bus system.

Chapter 3 Optimal Allocation of FACTS Device

The power system is experiencing twin challenges due to continuously increasing demand and the commercial activities that are happening due to deregulation. Thereby, the system is experiencing congestion in some of the lines. Further, it is highly unrealistic to replace the existing system to evacuate a higher amount of power to facilitate both commercial activities and meet the power demand. Therefore, the inherent option is to use the existing transmission lines/system to the extent possible by increasing the line loadability close to the stability limits.

The Flexible AC Transmission System (FACTS) devices, can be used to cater above objective and to meet various other objectives. The FACTS devices are a family of power electronics-based static devices that are characterized by low maintenance cost and operational robustness. By controlling series reactance and shunt admittances, the equivalents of different FACTS devices can be formulated. However, the FACTS controllers are a costly proposition and judiciously require the optimal allocation. As the objective is to enhance the Available Transfer Capability (ATC), the performance of the system with the series FACTS device namely Thyristor Controlled Series Capacitor (TCSC) has been investigated. The equivalent of TCSC carrying a series capacitor, C, in parallel with a TCR is shown in Figure 3.1,

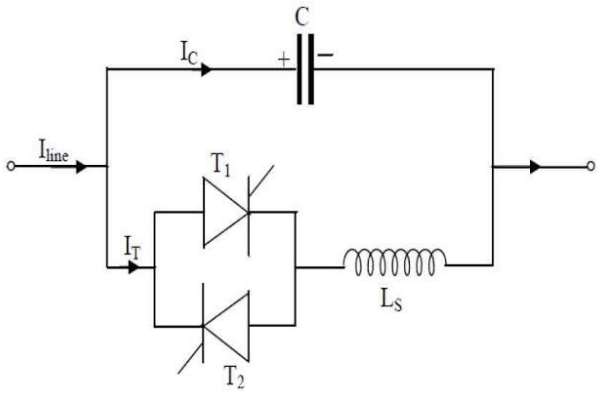

Figure 3.1 Basic module of Thyristor Controlled Series Compensator

where I_{line} is the line current, I_c is the capacitive current, I_T is the thyristor current, T_1 and T_2 are the thyristors 1 and 2 and L_s is the series inductance.

TCSC brings several benefits [170] for the user of the grid which includes upgrading in transmission capability of old and new transmission lines, growth in system stability, improvement in voltage regulation, reactive power balance, load sharing amongst parallel lines in addition to decrease in transmission losses.

Kimbark *et al.* [171, 172] investigated the enhancement in transient stability of power systems utilizing switched series capacitors. The elementary TCSC arrangement was suggested in 1986 as a technique for quick tuning of network impedance. It is described as a capacitive reactance compensator containing a series capacitor bank shunted by TCR to deliver smooth adjustable series capacitive reactance. For realistic TCSC applications, numerous such elementary compensators might be coupled in series to obtain the preferred voltage rating besides operating characteristics [173]. The degree of compensation can be varied rapidly by limiting the response speed of TCSC. This device founds applications in damping active power oscillations and post-contingency power flow control.

The placement of TCSC is being investigated for reducing congestion by decreasing losses and increasing the loadability of the lines. Faster computation can be achieved by using linear sensitivity factors. In this study, the sensitivity factor-based method is proposed to optimally allocate TCSC, which is termed the Sensitivity and Power loss-based Congestion Reduction (SPCR) method. This method finds the optimal location of TCSC by first calculating the sensitivity of all the lines and then analyzing the effect of TCSC placement in a few most sensitive lines. The line where TCSC placement leads to the most reduction in real and reactive power loss along with real power flow is considered optimal. This ensures the increase of ATC and a decrease in congestion in the system. For the proposed technique, the two sensitive indices viz., DC power flow sensitivity index and Reactive power loss sensitivity index are calculated while considering N-1 contingency. This study deals with the standard IEEE 6-bus and 30-bus systems.

3.1 CHARACTERISTICS AND STATIC MODELLING OF TCSC

3.1.1 CHARACTERISTICS OF TCSC

TCSC, a series compensator, enhances the capacity of the transmission line by decreasing the series impedances of lines and increasing the reliability of the network. The capacitor is included in series directly with the transmission line and the capacitor is mounted directly in parallel with the thyristor-controlled inductor. Consequently, no interfacing apparatus like a high voltage transformer is involved. The two-way thyristor valve is fired with an

angle α which ranges between 90° and 180° for the capacitor voltage. This makes TCSC more economical, simple, and easy to understand the operation than other competing FACTS technologies.

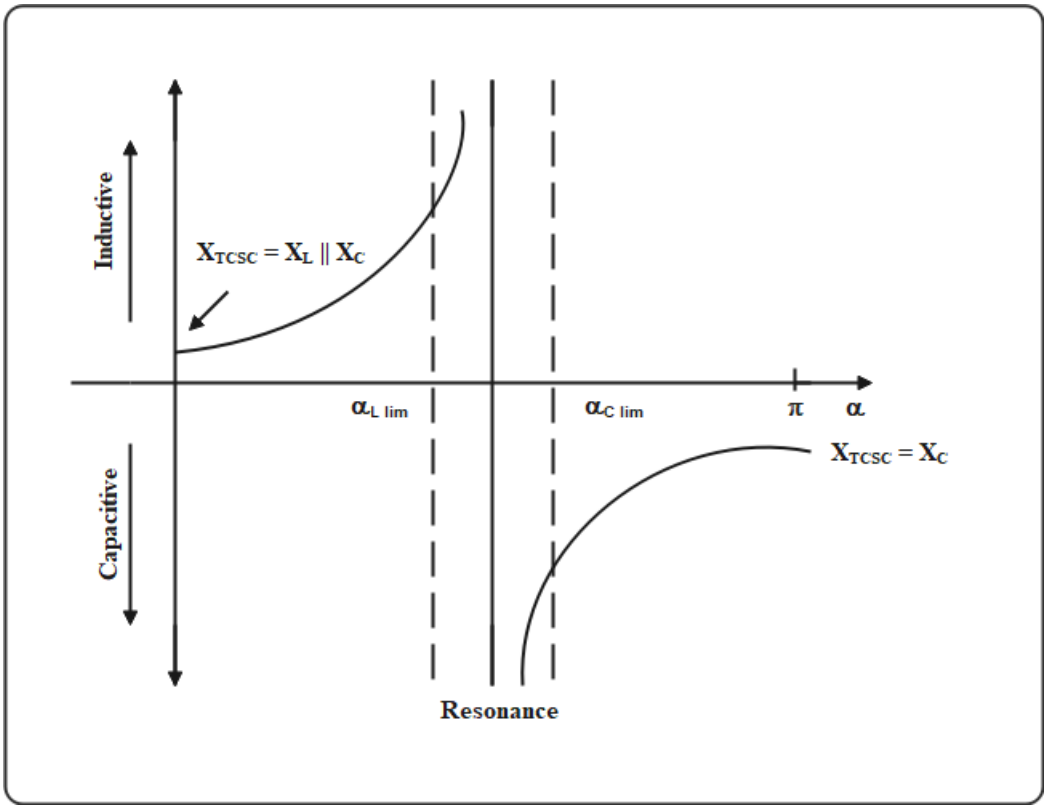

Figure 3.2 Variation of impedance in TCSC

Figure 3.2 portrays the trend curve of impedance for a TCSC device [174] between the effective firing angle α and the reactance of TCSC. This reactance starts increasing from the X_L value up till the existence of a parallel condition of resonance $X_L(\alpha) = X_C$. Since it is in the inductive region, an increase of $X_L(\alpha)$ provides a capacitive region. It decreases from the point at infinity to the least value of capacitive reactance X_C. Consequently, the impedance characteristics of TCSC exhibit that both capacitive and inductive regions are feasible by changing the angle of firing (α). Below are depicted the different regions based on firing angle:

- $90^o < \alpha < \alpha_{L\ lim}$ Inductive region
- $\alpha_{C\ lim} < \alpha < 180^o$ Capacitive region
- $\alpha_{L\ lim} < \alpha < \alpha_{C\ lim}$ Resonance region

During the selection of inductance, X_L should be infinitesimally small as compared to that of the capacitor X_c. Assuming X_c smaller than X_L , then the only capacitive area is viable in the impedance characteristics. The actual value of reactance in any shunt network follows the minor reactance present. Hence, only one capacitive reactance area will be visible. The value of X_L should not be equal to X_c value, else resonance develops those results in infinite impedance which is an unacceptable condition and may result in the opening of a transmission line. The impedance of the TCSC circuit for a parallel LC circuit is given by:

$$X_{TCSC}\,(\alpha) = \frac{X_c\, X_l(\alpha)}{X_l(\alpha) - X_c} \tag{3.1}$$

where

$$X_l(\alpha) = X_L \frac{\pi}{\pi - 2\alpha - sin\,\alpha} \tag{3.2}$$

α is the firing angle, X_L is the reactance of the inductor and $X_l(\alpha)$ is the effective reactance of the inductor at firing angle α and is limited as:

$$X_L \leq X_l(\alpha) \leq \infty \tag{3.3}$$

3.1.2 STATIC MODELLING OF TCSC

Let the complex voltages at bus-i and bus-j be denoted by $V_i \angle\delta_i \;\; and \; V_j \angle\delta_j$, respectively. The real power flow from buses i to j (P_{ij}) can be written as:

$$P_{ij} = V_i^2 G_{ij} - V_i V_j (G_{ij}\, cos\, \delta_{ij} + B_{ij}\, sin\, \delta_{ij}) \tag{3.4}$$

$$P_{ji} = V_j^2 G_{ij} - V_i V_j (G_{ij}\, cos\, \delta_{ij} - B_{ij}\, sin\, \delta_{ij}) \tag{3.5}$$

The model of a transmission line with a TCSC connected between bus i and bus j is shown in Figure 3.3. In this model, Z_{ij} and r_{ij} are the impedance and resistance respectively, X_{ij} is the reactance, X_c is the capacitive reactance of line ij, B_{i0} and B_{j0} are the initial shunt susceptance of buses i and j respectively. During the steady-state, the TCSC can be considered as a static reactance $-jX_c$. The real power flow from buses i to j (P_{ij}^c), and from buses j to i (P_{ji}^c) of a line having series impedance,

$$Z_{ij} = r_{ij} + jX_{ij} \tag{3.6}$$

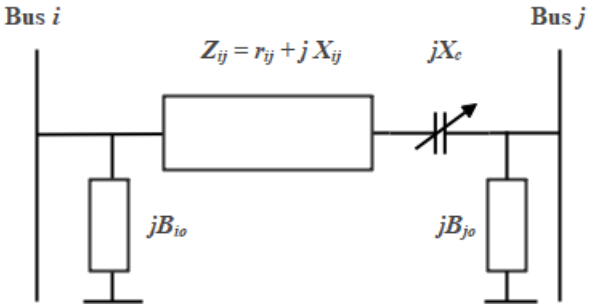

Figure 3.3 Model of a transmission line with TCSC

and a series reactance $-jX_c$ are

$$P_{ij}^c = V_i^2 G_{ij}^{'} - V_i V_j (G_{ij}^{'} \cos\delta_{ij} + B_{ij}^{'} \sin\delta_{ij}) \quad (3.7)$$

$$P_{ji}^c = V_j^2 G_{ij}^{'} - V_i V_j (G_{ij}^{'} \cos\delta_{ij} - B_{ij}^{'} \sin\delta_{ij}) \quad (3.8)$$

where

$$G_{ij}' = \frac{r_{ij}}{r_{ij}^2 + (X_{ij} - X_c)^2} \quad (3.9)$$

$$B_{ij}' = \frac{-(X_{ij} - X_c)}{r_{ij}^2 + (X_{ij} - X_c)^2} \quad (3.10)$$

The change in the line flow due to series capacitance can be represented as a line without series capacitance with additional power (complex) injections at the receiving (S_{jc}) and sending (S_{ic}) ends as shown in Figure 3.4.

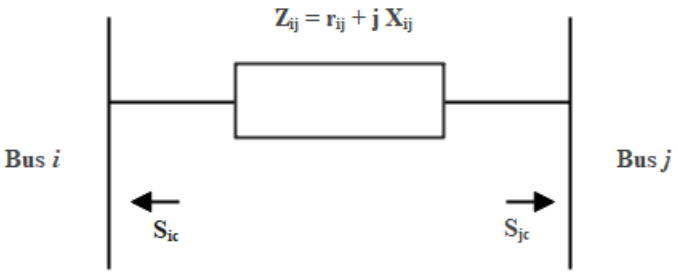

Figure 3.4 Injection Model of TCSC

The real power injections due to series capacitor at bus i (P_{ic}) and bus j (P_{jc}) using Equations (3.6 -(3.10) are:

$$P_{ic} = P_{ij} - P_{ij}^c = V_i^2 \Delta G_{ij} - V_i V_j (\Delta G_{ij} \cos\delta_{ij} + \Delta B_{ij} \sin\delta_{ij}) \quad (3.11)$$

$$P_{jc} = P_{ji} - P_{ji}^{c} = V_j^2 \Delta G_{ij} - V_i V_j (\Delta G_{ij} \cos \delta_{ij} - \Delta B_{ij} \sin \delta_{ij}) \quad (3.12)$$

where

$$\Delta G_{ij} = \frac{X_c r_{ij} (X_c - 2X_{ij})}{(r_{ij}^2 + {X_{ij}}^2)(r_{ij}^2 + (X_{ij} - X_c)^2)} \quad (3.13)$$

$$\Delta B_{ij} = \frac{-X_c (r_{ij}^2 - {X_{ij}}^2 + X_c X_{ij})}{(r_{ij}^2 + {X_{ij}}^2)(r_{ij}^2 + (X_{ij} - X_c)^2)} \quad (3.14)$$

The frequent active power oscillations are a limiting factor in the power transmission capacity and it can be dampened through periodic modulation of the line reactance. The fundamental notion after the TCSC structure is to make available an incessantly variable capacitor while using partly annulling the actual reimbursing capacitance by the TCR. The main controlling factor is transmission reactance, X_T. The range of X_T is taken from 0 to 0.5 X_T.

3.2 OPTIMAL ALLOCATION USING THE SPCR METHOD

The proposed SPCR method presents the technique of first calculating the sensitivity indices of all the lines by DC power flow sensitivity index and the Reactive power loss sensitivity index in the considered system [175] and then comparing the reduction of reactive [176] and real power losses along with real power flow ensuring the increase of ATC in the sensitive lines to reduce congestion in the system. These sensitivity indices are calculated after considering N-1 contingency. The TCSC shall be located among the most sensitive lines. With such consideration, the criteria used for the optimal placement are described as:

- Calculate the DC power flow sensitivity index d_{qr}.
- Calculate the Reactive power loss sensitivity index c_{ij}.
- Identify a few lines on which the sensitivity indices d_{qr} or c_{ij} has the largest value.
- Explore the placement of TCSC with consideration of real and reactive power loss and real power flow.
- Identify the best location (line) for TCSC placement.

3.2.1 DC POWER FLOW SENSITIVITY INDEX

For the calculation of the DC power flow sensitivity index, the sensitivity of real power flow is observed. The parameter d_{qr} represents this sensitivity factor, and is defined by the following equation:

$$d_{qr} = \frac{\Delta f_q}{f_r^0} \tag{3.15}$$

where q, r and d are the line outage sensitivity factors and f_r^o, Δf_q are the original power flow on line r before outage and change in real power flow on line q respectively. In this method, the sensitivity matrix $[x]$ is calculated while using the dc load flow equation as:

$$\theta = [x][P] \tag{3.16}$$

where $[\theta]$ is the bus angle vector and $[P]$ is the real power injection vector. The DC power flow sensitivity index is calculated with the help of the following equation:

$$d_{qr} = \frac{\frac{x_r}{x_q}[X_{os} - X_{ps} - X_{ot} + X_{pt}]}{x_r - [X_{oo} + X_{pp} - 2X_{op}]} \tag{3.17}$$

where r refers to the line that is at fault and it is linked amongst buses o and p, x_q is the reactance of the line on which TCSC is to be positioned amongst buses s and t. Greater sensitivity factors point toward greater reliance.

3.2.2 REACTIVE POWER LOSS SENSITIVITY INDEX

For the calculation of the Reactive power loss sensitivity index, the methodology adopted is grounded on finding the sensitivity of total reactive power loss. It gives the loss sensitivity, which depends upon the control parameter X_{ij}. The following equation provides the parameter c_{ij} representing the given index:

$$c_{ij} = \frac{\partial Q_L}{\partial X_{ij}} = \left(V_i^2 + V_j^2 - 2V_iV_jcos\delta_{ij}\right)\frac{r_{ij}^2 - X_{ij}^2}{\left(r_{ij}^2 + X_{ij}^2\right)^2} \tag{3.18}$$

where X_{ij} is the series reactance of the line with TCSC located amidst i and j buses, V_i and V_j are the voltages at line i and j respectively, Q_L is the reactive power of the line and δ_{ij}

is the angle between buses i and j. Here, the reactance of the TCSC and the resistance of the line are assumed to be negligible.

3.2.3 ALGORITHM AND FLOW CHART

The flowchart of the recommended SPCR method is shown in Figure 3.5. The placement of the TCSC is accomplished through the following steps:

1. Read the bus data and line data of the system.
2. Set line number as i = 1, 2, …., N.
3. Consider N-1 contingency and calculate the sensitivity of all lines by applying the DC power flow sensitivity index, d_{qr} from equation (3.17) and Reactive power loss sensitivity index, c_{ij} from equation (3.18).
4. Identify a few most sensitive lines having the largest values of d_{qr} and c_{ij} indices respectively.
5. Evaluate the reactive power losses, real power losses and real power flow after placing TCSC on the most sensitive lines.
6. The placement giving reduced reactive and real power losses along with decreased real power flow are best suited for optimally placing TCSC.

3.3 RESULTS AND DISCUSSION

The research study has been accomplished by optimizing the location of the FACTS device by the SPCR method. The TCSC is used as a FACTS device to control the reactance of the transmission line. The effectiveness of the proposed method is validated, utilizing the 6-bus as well as the 30-bus system. The program has been implemented on MATLAB version 2017 on the Intel Core i5 system. The factors considered for the optimization of location in this investigation included the DC power flow sensitivity index, reactive power loss sensitivity index, reactive power losses, real power losses, and real power flows.

3.3.1 6 BUS TEST SYSTEM RESULTS

When considering the 6-bus system having three generators and eleven lines, the sensitivity indices are calculated and the sensitive lines are identified. The analysis of TCSC placement is carried out with the consideration of reactive power loss, real power loss and the line flows. Table 3.1 summarizes the calculated values of the DC power flow sensitivity index. where the lines with the largest values of d_{qr} are 10 and 11.

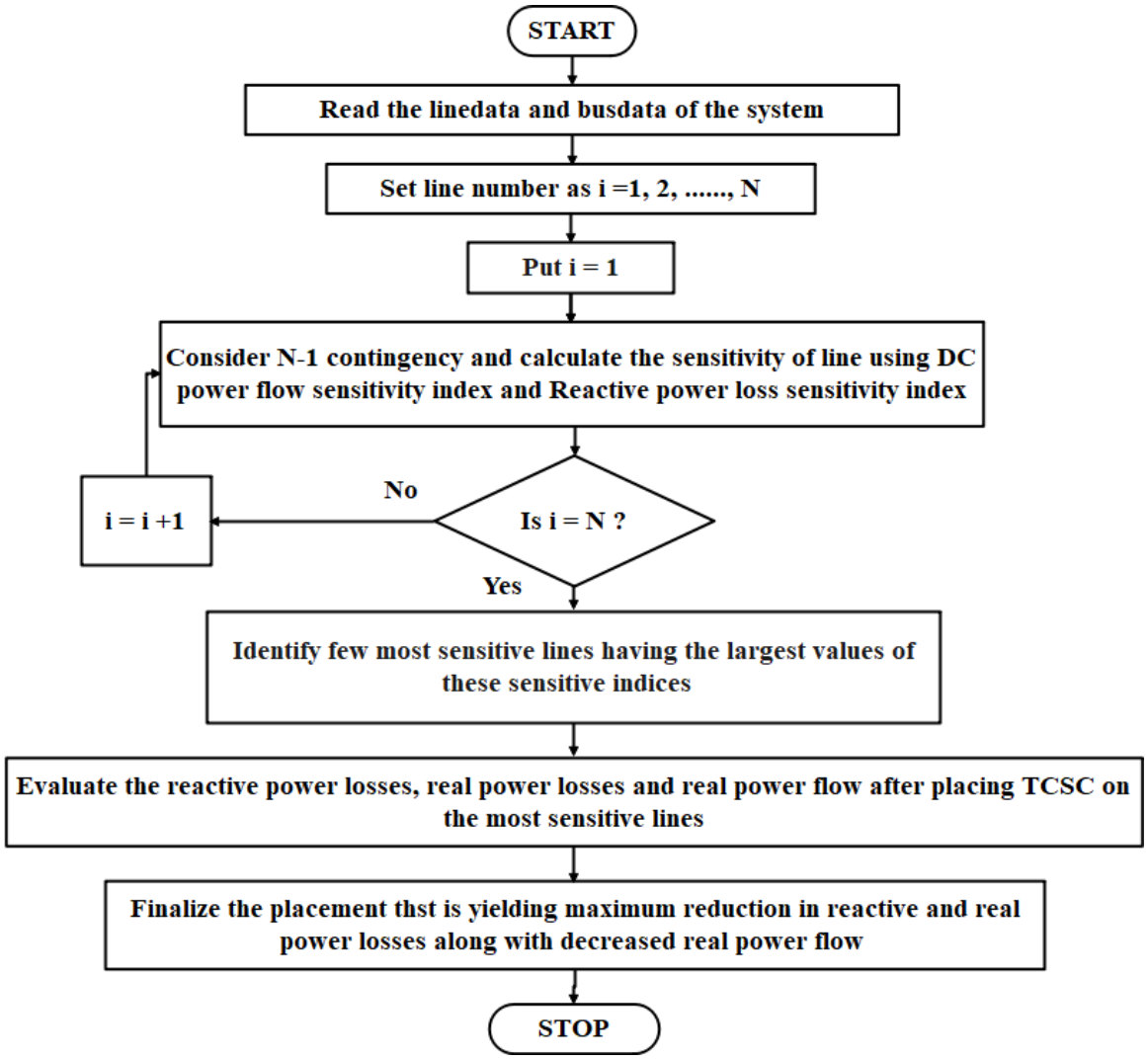

Figure 3.5 Flow chart of the proposed SPCR method

Table 3.1 Calculated values of DC power flow sensitivity index, d_{qr}

Line No.	d_{qr}
1	−0.0006
2	−0.1533
3	−0.0901
4	−0.0007
5	−0.2363
6	−0.0457
7	−0.0762
8	−0.0821
9	−0.4504
10	−0.0005
11	0.0007

Table 3.2 Reactive power loss sensitivity index, c_{ij} for contingency at each line

l/k	k=1	2	3	4	5	6	7	8	9	10	11
l=1	0	0.635	0.543	-0.11	-0.5	-0.21	-0.12	-0.14	0.013	0.01	0.132
2	0.59	0	0.457	-0.03	0.61	-0.062	-0.04	-0.04	0.004	-0.33	0.039
3	0.41	0.365	0	0.146	-0.11	0.2721	0.158	0.177	-0.02	0.317	-0.17
4	-0.1	-0.03	0.178	0	0.12	0.2262	0.466	-0.4	-0.53	0.171	0.132
5	-0.59	0.765	-0.17	0.159	0	0.2969	0.172	0.193	-0.02	-0.67	-0.19
6	-0.19	-0.06	0.325	0.221	0.23	0	0.239	0.268	-0.03	0.311	-0.26
7	-0.12	-0.04	0.21	0.507	0.15	0.2667	0	-0.2	0.584	0.201	0.443
8	-0.12	-0.04	0.204	-0.38	0.14	0.2583	-0.17	0	0.475	0.195	-0.42
9	0.01	0.005	-0.03	-0.62	-0.02	-0.032	0.638	0.6	0	-0.02	0.557
10	0.01	-0.24	0.286	0.126	-0.39	0.235	0.136	0.153	-0.02	0	-0.15
11	0.11	0.034	-0.18	0.117	-0.13	-0.235	0.362	-0.4	0.416	-0.18	0

Table 3.3 Calculated values of reactive power loss sensitivity index, c_{ij}

Line No.	$\boldsymbol{c_{ij}}$
1	0.013
2	0.004
3	−0.020
4	−0.530
5	−0.020
6	−0.030
7	0.584
8	0.475
9	0.000
10	−0.020
11	0.416

Table 3.2 summarizes the reactive power loss sensitivity index, for contingency at each line. Table 3.3 shows the sample illustration of calculated values of the reactive power loss sensitivity index for contingency at line 9. It is observed that the largest values of c_{ij} of 0.584 and 0.475 pertains to lines 7 and 8 respectively. Hence, the identified sensitive lines are 7 and 8. It is not a surprise that different lines have been identified as sensitive from d_{qr} and c_{ij}. As it is known that TCSC placement is a costly proposition, the best location needs to be identified by analyzing its placement effect in each of the sensitive lines in a one-by-one manner. The maximum compensation is 50%. The optimal value of the control parameter of TCSC, X_{TCSC} at sensitive lines 7, 8, 10 and 11 are presented in Table 3.4.

Table 3.5 shows the reactive power losses after placing TCSC in the sensitive lines. When it is placed on line 7 and line 8, the reactive power losses are reduced in lines 5 and

9. As indicated by d_{qr}, the lines for placement of TCSC are 10 and 11. After placing TCSC in line 11, the reactive power losses are reduced in line 5. Table 3.6 summarizes the comparison of total reactive power losses when TCSC is placed on sensitive lines. It is not possible to deduce a definite conclusion from this comparison. Table 3.7 shows the real power losses that are calculated after placing TCSC on sensitive lines 7, 8, 10, and 11 in a one-by-one manner.

Table 3.4 Control Parameter, X_{TCSC}

Line	Compensation	TCSC (p.u.)
7	0.35	-0.060
8	0.45	-0.104
10	0.35	-0.140
11	0.45	-0.135

Table 3.5 Comparison of Reactive power losses after placement of TCSC on sensitive lines

	Reactive power losses				
Lines	**Without TCSC (MVAR)**	**With TCSC at Line 7 (MVAR)**	**With TCSC at Line 8 (MVAR)**	**With TCSC at Line 10 (MVAR)**	**With TCSC at Line 11 (MVAR)**
1	−4.058	−4.050	−4.052	−4.058	−4.051
2	−1.167	−1.164	−1.169	−1.162	−1.176
3	−3.680	−3.707	−3.717	−3.686	−3.755
4	−6.587	−6.585	−6.588	−6.587	−6.588
5	1.3650	1.3550	1.350	1.3650	1.3370
6	−2.530	−2.553	−2.567	−2.531	−2.603
7	−3.833	−3.924	−3.827	−3.836	−3.760
8	−2.586	−2.582	−2.651	−2.584	−2.690
9	3.225	3.0960	3.183	3.2270	3.3980
10	−7.752	−7.756	−7.760	−7.753	−7.768
11	−5.820	−5.819	−5.830	−5.818	−5.851

Table 3.6 Comparison of Total reactive power losses after placement of TCSC on sensitive lines

TCSC place (Lines)	Total reactive power losses without TCSC (MVAR)	Total reactive power losses with TCSC (MVAR)
7	−33.425	−33.6900
8	−33.425	−33.6270
10	−33.425	−33.4266
11	−33.425	−33.5090

The losses have reduced at lines 3, 5–7, 9, and 10 after placing TCSC at line 7. After placing it on lines 8 and 10, the real power losses have reduced at lines 2–6, 8–11, and lines 1, 3 6, 7, 10, respectively. Similarly, real losses are found to be reducing on lines 2, 3, 5, 6, 8, 10, and 11, after placing TCSC in line 11.

Table 3.7 Calculation of Real power losses after placement of TCSC at sensitive lines

	Real power losses				
Lines	**Without TCSC (MVAR)**	**With TCSC at Line 7 (MVAR)**	**With TCSC at Line 8 (MVAR)**	**With TCSC at Line 10 (MVAR)**	**With TCSC at Line 11 (MVAR)**
1	0.176	0.180	0.179	0.17590	0.179
2	0.747	0.748	0.747	0.74873	0.745
3	0.677	0.670	0.668	0.67483	0.659
4	0.031	0.031	0.031	0.03101	0.031
5	1.722	1.717	1.714	1.72204	1.708
6	0.538	0.531	0.527	0.53768	0.516
7	0.506	0.476	0.509	0.50541	0.530
8	1.247	1.249	1.218	1.24738	1.202
9	1.076	1.050	1.068	1.07633	1.110
10	0.016	0.015	0.015	0.01508	0.015
11	0.039	0.042	0.037	0.03982	0.030

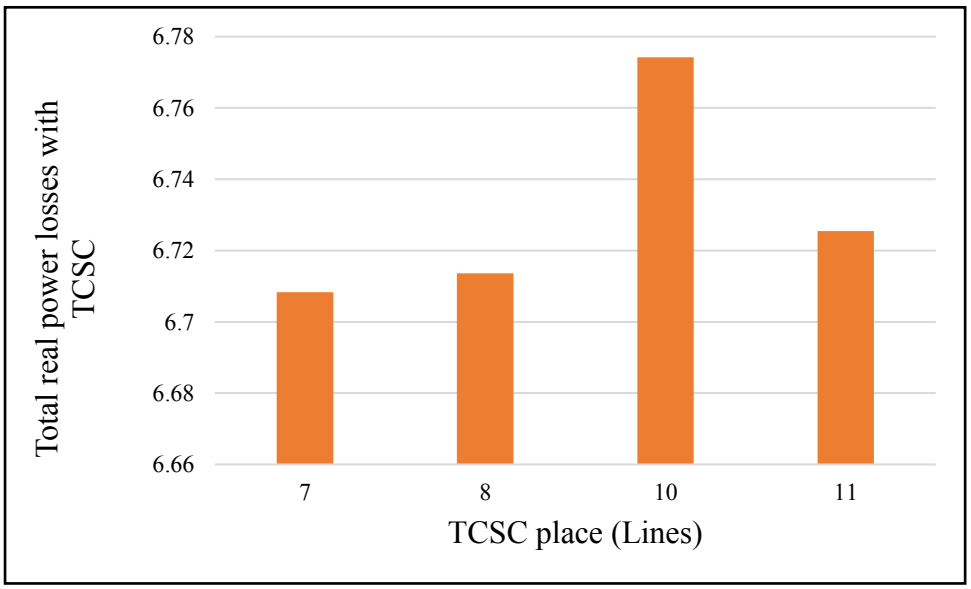

Figure 3.6 Comparison of total real power losses with TCSC at sensitive lines (6 bus system)

The total real power losses get reduced when TCSC is placed at lines 7, 8, 10, and 11 in the six-bus system, as shown in Table 3.8. The variation of real power losses for the six-bus system has been represented in the bar graph, shown in Figure 3.6. It is evident from

the graph that the total real power losses are reduced after placing TCSC. Among all the considered lines, the seventh line has witnessed the minimum total real power loss, which is about 6.70 MW.

Table 3.8 Comparison of Total real power losses after placing TCSC on sensitive lines

TCSC place (Lines)	Total real power losses without TCSC (MW)	Total real power losses with TCSC (MW)
7	6.77575	6.70832
8	6.77575	6.71365
10	6.77575	6.77421
11	6.77575	6.72544

Table 3.9 shows the values of real power flows, after placing TCSC at sensitive lines. The flows are considerably reduced when it is placed on lines 7, 8, and 11. At line 7, the real power flows have decreased in lines 7, 9 and 11. When TCSC is placed at line 8, power flow on lines 3, 5, 6, 8, 9, and 10 has reduced and, when placed at line 11, it has reduced in lines 6, 8, and 10.

Table 3.9 Comparison of Real Power Flows at different locations of TCSC

	Real power flows				
Lines	Without TCSC (MVAR)	With TCSC at Line 7 (MVAR)	With TCSC at Line 8 (MVAR)	With TCSC at Line 10 (MVAR)	With TCSC at Line 11 (MVAR)
1	12.548	12.619	13.882	12.5424	12.641
2	31.762	31.787	32.262	31.8514	31.785
3	25.635	25.543	24.258	25.5546	25.505
4	−2.293	−2.601	1.5803	−2.3334	−2.193
5	43.440	43.345	41.543	43.5864	43.262
6	17.222	17.082	14.769	17.1521	16.996
7	23.363	22.820	25.135	23.3214	23.758
8	25.068	25.154	19.097	25.0268	24.691
9	50.077	49.684	44.755	50.0788	50.555
10	2.7340	2.6650	1.4160	2.65960	2.5900
11	−1.819	−2.026	1.6710	−1.7787	−1.343

The decrease in real power flows suggests that the available transfer capability has increased in these lines. A noticeable reduction in real power flows is noticed when TCSC is placed at lines 7, 8, and 11. This results in relieving congestion of these lines and, hence, allow them to be able to transfer power more than already committed usage and prevents

overloading in the future. Therefore, the efficacy of the proposed SPCR technique in optimally locating TCSC to relieve congestion is established.

The comparison of real power flows calculated after placing the TCSC device at optimal locations on lines 7 and 11 are shown in Table 3.10. The values found using the proposed SPCR method are compared with that calculated with PSAT [117]. The results are almost comparable and prove the validity of the proposed method.

Table 3.10 Comparison of real power flows after placing TCSC at optimal lines 7 and 11 by using PSAT and SPCR method for 6 bus system

			FACTS at Line 7		**FACTS at Line 11**	
Line	**From**	**To**	**PSAT (p.u.)**	**SPCR (p.u.)**	**PSAT (p.u.)**	**SPCR (p.u.)**
2	1	4	0.2527	0.3178	0.4287	0.3178
6	2	5	0.0271	0.1708	0.0264	0.1699
7	2	6	0.1951	0.2282	0.1665	0.2375

3.3.1 30 BUS TEST SYSTEM RESULTS

A standard IEEE 30-bus system is taken into consideration which consists of six generators and forty-one lines. The analysis of TCSC placement is carried out with the consideration of reactive power loss, real power loss and the line flows. The Reactive power loss sensitivity index, c_{ij} for contingency at lines, 1 to 12 are shown in Table 3.11 and lines 13 to 24 are represented in Table 3.12.

The sample illustration of data by considering the outage of line 14 is shown in Table 3.13. It summarizes the calculated values of the DC power flow sensitivity index and Reactive power loss sensitivity index. The lines with the largest values of d_{qr} are 11 and 31. It is observed that largest values of c_{ij} of 0.6298 and 0.7747 pertains to line 12 and 15 respectively. Hence, the identified sensitive lines are 12 and 15. It is not a surprise that different lines have been identified as sensitive from d_{qr} and c_{ij}. As it is known that TCSC placement is a costly proposition, best location needs to be identified by analyzing its placement effect in each of the sensitive lines in a one-by-one manner.

The value of the control parameter of TCSC, X_{TCSC} for computing power flow is taken as per Table 3.14. The maximum compensation is 50%. The value of the control parameter is calculated at sensitive lines 11, 12, 15 and 31.

Table 3.11 Reactive power loss sensitivity index, c_{ij} for contingency at lines 1-12

l/k	k = 1	2	3	4	5	6	7	8	9	10	11	12
l = 1	0	2.2574	-0.1417	5.4610	0.0365	0.0243	0.6376	0.0042	0.0127	0.0617	0.5903	0.3780
2	-6.6593	0	0.5839	-2.6658	0.3815	0.5336	-0.2513	0.4499	-0.4852	0.0343	0.3609	0.2331
3	0.7233	1.0106	0	2.4448	0.5047	0.7154	-0.5660	0.6090	-0.6628	0.0247	0.2814	0.1828
4	-6.7705	-1.1204	0.5936	0	0.3878	0.5425	-0.2555	0.4575	-0.4933	0.0348	0.3670	0.2370
5	-0.1078	0.3823	0.2923	0.9249	0	0.3986	0.3676	-1.3336	1.4676	0.0114	0.0948	0.0599
6	-0.1139	0.8480	0.6569	2.0513	0.6321	0	0.8223	0.7613	-0.8279	0.0252	0.2100	0.1327
7	-3.5868	-0.4793	-0.6237	-1.1594	0.6994	0.9868	0	0.8373	-0.9084	0.0085	-0.2507	-0.1798
8	-0.0105	0.3857	0.3016	0.9330	-1.1405	0.4106	0.3763	0	1.5119	0.0115	0.0955	0.0603
9	-0.0289	-0.3736	-0.2949	-0.9038	1.1275	-0.4011	-0.3668	1.3582	0	-0.0111	-0.0925	-0.0584
10	-0.2337	0.0440	0.0183	0.1064	0.0145	0.0204	0.0057	0.0172	-0.0185	0	0.0669	0.0446
11	-1.3838	0.2868	0.1292	0.6938	0.0751	0.1050	-0.1044	0.0885	-0.0954	0.0415	0	0.7579
12	-0.7538	0.1575	0.0714	0.3811	0.0404	0.0564	-0.0637	0.0476	-0.0513	0.0235	0.6448	0
13	-0.0020	0.0003	0.0001	0.0008	0.0001	0.0002	0.0002	0.0002	-0.0002	0.0000	0.0005	0.0002
14	-1.1959	0.2545	0.1169	0.6158	0.0622	0.0869	-0.1251	0.0732	-0.0788	0.0405	-1.0101	0.7521
15	-2.2671	0.3532	0.1202	0.8544	0.1713	0.2403	0.4375	0.2030	-0.2194	0.0457	0.8037	0.5360
16	-0.0021	0.0004	0.0002	0.0010	0.0001	0.0002	0.0001	0.0002	-0.0002	0.0000	0.0003	0.0002
17	-0.2445	0.0365	0.0117	0.0882	0.0191	0.0269	0.0557	0.0227	-0.0246	0.0074	0.0886	0.0591
18	-0.3280	0.0238	-0.0040	0.0577	0.0360	0.0507	0.2055	0.0429	-0.0465	0.0235	0.2646	0.1770
19	0.0461	-0.0480	-0.0344	-0.1161	0.0134	0.0190	0.2040	0.0162	-0.0176	0.0035	0.3062	0.2055
20	0.1047	-0.0319	-0.0178	-0.0772	-0.0015	-0.0020	0.0611	-0.0016	0.0017	0.0057	0.0568	0.0382
21	0.0524	-0.0486	-0.0345	-0.1175	0.0127	0.0181	0.2007	0.0154	-0.0168	0.0034	0.3006	0.2017
22	0.0986	-0.0399	-0.0245	-0.0965	0.0027	0.0039	0.1090	0.0034	-0.0037	-0.0022	0.1731	0.1163
23	0.1030	-0.0408	-0.0248	-0.0986	0.0024	0.0035	0.1090	0.0031	-0.0034	-0.0023	0.1727	0.1160
24	0.1072	-0.0415	-0.0251	-0.1003	0.0021	0.0031	0.1085	0.0027	-0.0030	-0.0023	0.1715	0.1152
25	-0.1138	0.0423	0.0253	0.1024	-0.0016	-0.0023	-0.1064	-0.0020	0.0023	0.0024	-0.1673	-0.1124
26	-0.0584	0.0493	0.0346	0.1192	-0.0122	-0.0173	-0.1983	-0.0147	0.0161	-0.0033	-0.2963	-0.1989
27	-0.0814	0.0199	0.0100	0.0482	0.0032	0.0044	-0.0220	0.0037	-0.0040	0.0336	-0.1863	-0.1252
28	-0.0421	0.0108	0.0055	0.0260	0.0014	0.0020	-0.0138	0.0017	-0.0018	0.0202	-0.1141	-0.0767
29	-0.0305	0.0110	0.0065	0.0265	-0.0003	-0.0004	-0.0265	-0.0004	0.0004	0.0342	-0.2037	-0.1368
30	0.1185	-0.0465	-0.0283	-0.1125	0.0026	0.0038	0.1233	0.0033	-0.0037	0.0250	0.0621	0.0418
31	-0.0189	0.0125	0.0085	0.0301	-0.0025	-0.0036	-0.0460	-0.0030	0.0033	0.0560	-0.3423	-0.2298
32	0.1225	-0.0471	-0.0285	-0.1139	0.0023	0.0034	0.1225	0.0030	-0.0033	0.0248	0.0612	0.0411
33	0.1453	-0.0433	-0.0239	-0.1047	-0.0025	-0.0033	0.0797	-0.0027	0.0029	0.0794	-0.2751	-0.1846
34	-0.0021	0.0004	0.0001	0.0009	0.0001	0.0002	0.0002	0.0002	-0.0002	0.0001	0.0003	0.0002
35	0.1706	-0.0474	-0.0254	-0.1147	-0.0043	-0.0059	0.0757	-0.0049	0.0052	0.0769	-0.2729	-0.1831
36	-0.7518	0.1470	0.0632	0.3555	0.0445	0.0622	-0.0105	0.0525	-0.0566	-0.0431	0.2963	0.1979
37	-0.0046	0.0008	0.0003	0.0020	0.0003	0.0004	0.0004	0.0004	-0.0004	0.0002	0.0005	0.0003
38	-0.0036	0.0006	0.0002	0.0015	0.0002	0.0003	0.0003	0.0003	-0.0003	0.0001	0.0004	0.0002
39	-0.0005	0.0001	0.0000	0.0002	0.0000	0.0000	0.0000	0.0000	-0.0000	0.0000	0.0000	0.0000
40	-0.1900	0.0365	0.0155	0.0883	0.0115	0.0161	0.0008	0.0136	-0.0147	-1.4828	0.0653	0.0436
41	-0.7893	0.1509	0.0638	0.3651	0.0481	0.0673	0.0063	0.0568	-0.0613	1.4312	0.2622	0.1749

Table 3.12 Reactive power loss sensitivity index, c_{ij} for contingency at lines 13 -24

l/k	k = 13	14	15	16	17	18	19	20	21	22	23	24
l = 1	-1.1686	0.5022	2.0267	-1.1240	0.1202	0.1132	-0.0283	-0.1031	-0.0318	-0.0811	-0.1625	0.2050
2	-0.6094	0.3153	0.9314	-0.6225	0.0529	0.0243	-0.0870	-0.0927	-0.0871	-0.0969	-0.1897	0.2340
3	-0.4145	0.2506	0.5485	-0.4480	0.0293	-0.0070	-0.1081	-0.0894	-0.1069	-0.1029	-0.2000	0.2451
4	-0.6196	0.3206	0.9469	-0.6329	0.0538	0.0247	-0.0885	-0.0943	-0.0885	-0.0985	-0.1929	0.2379
5	-0.2310	0.0772	0.4526	-0.2072	0.0278	0.0368	0.0243	-0.0043	0.0229	0.0065	0.0113	-0.0120
6	-0.5133	0.1710	1.0069	-0.4600	0.0619	0.0820	0.0547	-0.0092	0.0515	0.0151	0.0261	-0.0280
7	-0.5484	-0.2954	2.2002	-0.1659	0.1541	0.3991	0.7053	0.3388	0.6859	0.5051	0.9674	-1.1676
8	-0.2338	0.0777	0.4589	-0.2094	0.0282	0.0375	0.0251	-0.0040	0.0237	0.0070	0.0122	-0.0131
9	0.2267	-0.0752	-0.4455	0.2030	-0.0274	-0.0365	-0.0246	0.0038	-0.0232	-0.0070	-0.0122	0.0131
10	-0.0380	0.0644	0.1547	-0.0396	0.0138	0.0307	0.0082	0.0211	0.0078	-0.0069	-0.0135	0.0167
11	-0.7583	-0.9943	1.6842	-0.3622	0.1021	0.2141	0.4411	0.1312	0.4280	0.3341	0.6385	-0.7688
12	-0.2433	0.6298	0.9555	-0.2036	0.0579	0.1219	0.2518	0.0751	0.2443	0.1909	0.3649	-0.4394
13	0	-0.0001	0.0007	-0.0002	0.0000	0.0001	0.0001	0.0000	0.0001	0.0001	0.0001	-0.0002
14	0.2089	0	1.6491	-0.3452	0.1000	0.2116	0.4398	0.1320	0.4268	0.3341	0.6385	-0.7690
15	-0.4356	0.7747	0	-0.8189	-0.0633	-0.3404	-0.8054	-0.4667	-0.7871	0.6310	-1.2150	1.4744
16	-0.0003	0.0003	0.0014	0	-0.0000	-0.0001	-0.0002	-0.0001	-0.0002	-0.0002	-0.0004	0.0004
17	-0.0480	0.0854	-0.1150	0.0046	0	0.8066	0.1480	-3.7748	0.1441	-0.2513	-0.4831	0.5852
18	-0.1143	0.2574	-0.8817	0.1270	1.1487	0	0.6609	3.0287	0.6438	-0.9467	-1.8193	2.2031
19	-0.0973	0.3006	-1.1716	0.1975	0.1184	0.3712	0	0.3802	-1.4832	0.6257	1.2011	-1.4529
20	-0.0119	0.0563	-0.4235	0.0766	-1.8838	1.0613	0.2372	0	0.2312	-0.2886	-0.5545	0.6713
21	-0.0950	0.2951	-1.1584	0.1956	0.1166	0.3659	-1.5007	0.3749	0	0.6168	1.1841	-1.4323
22	-0.0490	0.1704	-0.6852	0.1197	-0.1501	-0.3970	0.4670	-0.3453	0.4551	0	-3.2154	3.8925
23	-0.0485	0.1700	-0.6885	0.1206	-0.1505	-0.3981	0.4678	-0.3462	0.4559	-1.6779	0	3.8952
24	-0.0478	0.1688	-0.6890	0.1209	-0.1504	-0.3976	0.4667	-0.3457	0.4548	-1.6752	-3.2125	0
25	0.0460	-0.1648	0.6824	-0.1202	0.1484	0.3922	-0.4594	0.3409	-0.4477	1.6515	3.1671	-3.8271
26	0.0931	-0.2909	0.0304	-0.1945	-0.1153	-0.3620	1.4862	-0.3711	1.4460	-0.6104	-1.1717	1.4173
27	0.0493	-0.1837	0.1871	-0.0359	0.0625	0.1681	-0.2631	0.1490	-0.2563	-0.3448	-0.6619	0.8007
28	0.0308	-0.1124	0.1102	-0.0208	0.0376	0.1013	-0.1596	0.0900	-0.1554	-0.2088	-0.4008	0.4848
29	0.0586	-0.2004	0.1719	-0.0304	0.0633	0.1714	-0.2757	0.1531	-0.2685	-0.3590	-0.6891	0.8335
30	-0.0158	0.0613	-0.7804	0.1367	-0.1492	-0.3909	0.3979	-0.3366	0.3878	0.5887	1.1307	-1.3684
31	0.1010	-0.3365	0.2709	-0.0461	0.1036	0.2813	-0.4568	0.2519	-0.4448	-0.5935	-1.1391	1.3778
32	-0.0152	0.0604	-0.7792	0.1368	-0.1487	-0.3898	0.3962	-0.3355	0.3862	0.5865	1.1265	-1.3633
33	0.0872	-0.2700	-0.5591	0.1016	-0.0546	-0.1330	-0.0341	-0.1043	-0.0328	0.0315	0.0612	-0.0749
34	-0.0002	0.0002	0.0007	-0.0002	0.0001	0.0001	0.0000	0.0001	0.0000	-0.0000	-0.0000	0.0001
35	0.0887	-0.2677	-0.5572	0.1027	-0.0543	-0.1317	-0.0338	-0.1029	-0.0325	0.0311	0.0605	-0.0741
36	-0.1444	0.2869	0.6581	-0.1541	0.0602	0.1382	0.0364	0.0994	0.0349	-0.0316	-0.0618	0.0761
37	-0.0005	0.0004	0.0014	-0.0005	0.0001	0.0002	0.0001	0.0001	0.0001	-0.0000	-0.0001	0.0001
38	-0.0004	0.0003	0.0011	-0.0004	0.0001	0.0001	0.0000	0.0001	0.0000	-0.0000	-0.0001	0.0001
39	-0.0001	0.0000	0.0001	-0.0001	0.0000	0.0000	0.0000	0.0000	0.0000	-0.0000	-0.0000	0.0000
40	-0.0339	0.0630	0.1472	-0.0358	0.0133	0.0302	0.0080	0.0214	0.0077	-0.0069	-0.0134	0.0166
41	-0.1383	0.2530	0.5939	-0.1457	0.0536	0.1212	0.0321	0.0853	0.0307	-0.0275	-0.0538	0.0663

Table 3.13 Calculated values of d_{qr} and c_{ij} for 30 bus

Line No.	d_{qr}	c_{ij}
1	−1.7892	0.5022
2	−0.4472	0.3153
3	−0.1018	0.2506
4	−0.3803	0.3206
5	−0.2001	0.0772
6	3.4922	0.1710
7	6.6495	−0.2954
8	0.2636	0.0777
9	2.1356	−0.0752
10	2.5852	0.0644
11	10.4489	−0.9943
12	0.5046	0.6298
13	0.0695	−0.0001
14	4.6528	0.0000
15	0.4842	0.7747
16	0.8399	0.0003
17	2.9897	0.0854
18	1.0709	0.2574
19	7.3753	0.3006
20	9.6101	0.0563
21	2.0937	0.2951
22	2.2205	0.1704
23	0.6347	0.1700
24	2.5254	0.1688
25	1.0705	−0.1648
26	1.2230	−0.2909
27	1.0185	−0.1837
28	1.2278	−0.1124
29	1.2848	−0.2004
30	3.1627	0.0613
31	11.1062	−0.3365
32	1.2400	0.0604
33	1.5269	−0.2700
34	0.7036	0.0002
35	0.4730	−0.2677
36	0.3341	0.2869
37	1.0920	0.0004
38	0.2544	0.0003
39	0.1222	0.0000
40	0.1393	0.6300
41	0.2663	0.2530

Table 3.14 Control Parameter, X_{TCSC} for 30 bus system

Line	Compensation	TCSC
11	0.40	-0.0315
12	0.35	-0.1960
15	0.11	-0.0332
31	0.21	-0.0377

Table 3.15 shows the reactive power losses after placing TCSC on the sensitive lines. When it is placed on line 11, the reactive power losses are reduced in lines 1, 2, 4, 11 and 12, whereas the losses are reduced in lines 1, 2 and 4, when TCSC is placed in line 31. As indicated by c_{ij}, the lines for placement of TCSC are 12 and 15. After placing TCSC in line 12, the reactive power losses are reduced on lines 2, 4, 11 and 12, whereas the losses are found to be reduced on lines 1, 2 and 4 when TCSC is placed in line 15.

Table 3.15 Calculation of Reactive power losses after placement of TCSC on sensitive lines

	Reactive power losses				
Lines	Without TCSC (MVAR)	With TCSC at Line 11 (MVAR)	With TCSC at Line 12 (MVAR)	With TCSC at Line 15 (MVAR)	With TCSC at Line 31 (MVAR)
1	11.13451	11.12571	11.13942	11.12366	11.12410
2	7.535790	7.523160	7.501260	7.526900	7.526380
4	1.507510	1.504240	1.499650	1.505060	1.504950
11	1.426920	1.354390	1.186280	1.455510	1.465570
12	1.104380	1.070690	0.870690	1.108780	1.117790
15	−0.09130	−0.12165	−0.12085	−0.12268	−0.12308
19	−0.20679	−0.20856	−0.20908	−0.20852	−0.20866
20	−0.18536	−0.19069	−0.19756	−0.18957	−0.18869
31	−0.19328	−0.19655	−0.19768	−0.19647	−0.19798

Table 3.16 Comparison of Total Reactive power losses after placement of TCSC

TCSC Place (Lines)	Total Reactive power losses without TCSC (MVAR)	Total Reactive power losses with TCSC (MVAR)
11	22.03238	21.86074
12	22.03238	21.47213
15	22.03238	22.00267
31	22.03238	22.02039

Table 3.16 summarizes the decrease in total reactive power losses when TCSC is placed on the sensitive lines. It is observed in lines 11 and 12, that the losses decreased considerably. Table 3.17 shows the real power losses that are calculated after placing TCSC on sensitive lines 11, 12, 15, and 31 in a one-by-one manner.

The losses have reduced at lines 1, 2, 4, 11, 12, 15, 19, 20 and 31 after placing TCSC at line 11. After placing it on lines 12 and 15, the real power losses have reduced at lines 2, 4, 11, 12, 15, 19, 20 and 31 and lines 1, 2, 4, 12, 15, 19, 20 and 31 respectively. Similarly, real losses are found to be reducing on lines 1, 2, 4, 11, 15, 19, 20 and 31 after placing TCSC in line 11.

Table 3.17 Calculation of Real power losses after placement of TCSC at sensitive lines

	Real power losses				
Lines	**Without TCSC (MVAR)**	**With TCSC at Line 11 (MVAR)**	**With TCSC at Line 12 (MVAR)**	**With TCSC at Line 15 (MVAR)**	**With TCSC at Line 31 (MVAR)**
1	5.41374	5.41092	5.41531	5.41027	5.41041
2	2.83736	2.83486	2.82975	2.83571	2.83559
4	0.77990	0.77914	0.77769	0.77938	0.77935
11	0.00781	0.00747	0.00667	0.00795	0.00800
12	0.00235	0.00230	0.00194	0.00236	0.00238
15	0.00094	0.00072	0.00073	0.00071	0.00071
19	0.00604	0.00521	0.00467	0.00528	0.00516
20	0.01188	0.01012	0.00723	0.01062	0.01100
31	0.00611	0.00523	0.00472	0.00528	0.00461

The total real power losses get reduced when TCSC is placed at lines 11, 12, 15, and 31 in the thirty-bus system, as shown in Table 3.18. Figure 3.7 represents the bar graph of the comparison of real power losses for the 30-bus system. It is evident from the graph that the total real power losses are reduced after placing TCSC. Among all the considered cases, the 12^{th} line has witnessed the minimum total real power loss, which is about 9.048 MW.

Table 3.18 Comparison of Total real power losses after placing TCSC on sensitive lines

TCSC Place (Lines)	**Total real power losses without TCSC (MW)**	**Total real power losses with TCSC (MW)**
11	9.06613	9.05597
12	9.06613	9.04871
15	9.06613	9.05756
31	9.06613	9.05721

Table 3.19 shows the values of real power flows, after placing TCSC at sensitive lines. The real power flows have reduced considerably when TCSC is placed at lines 11, 12, 15, and 31. When it is placed at line 11, power flow has decreased at all lines, except line 4, as is evident from Table 3.19. Similarly, when it is placed at line 12, the real power flows have decreased at all lines, except in line 1.

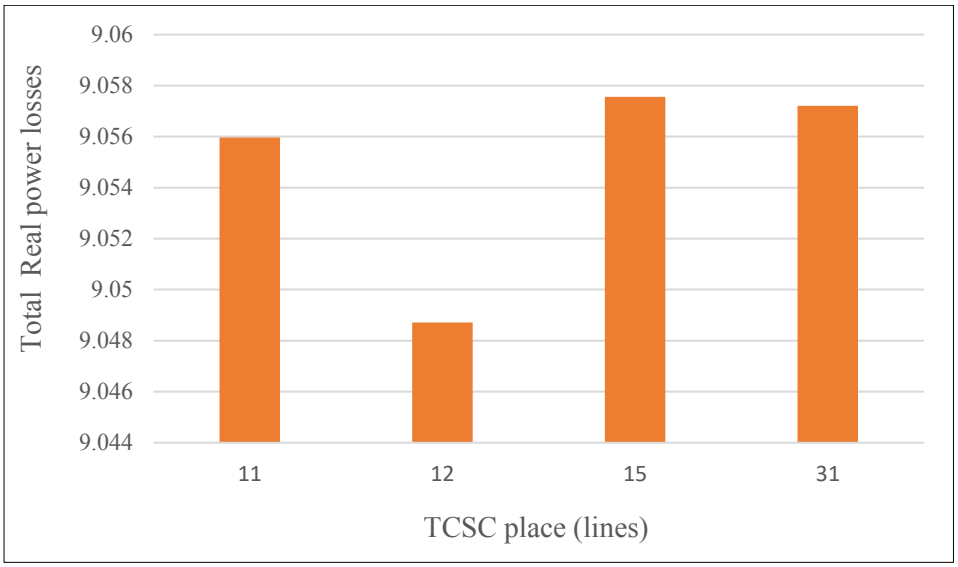

Figure 3.7 Assessment of total real power losses at sensitive lines by placing TCSC (30 bus system)

Table 3.19 Comparison of Real power flows at different locations of TCSC

	Real power flows				
Lines	**Without TCSC (MVAR)**	**With TCSC at Line 11 (MVAR)**	**With TCSC at Line 12 (MVAR)**	**With TCSC at Line 15 (MVAR)**	**With TCSC at Line 31 (MVAR)**
1	178.02707	177.98063	178.05303	177.9698	177.97217
2	83.702490	83.673090	83.598580	83.68524	83.683490
4	77.966460	77.969070	77.904550	77.97841	77.976950
11	28.672390	28.054870	26.514980	28.94278	29.029520
12	15.866640	15.680530	14.411640	15.91052	15.964390
15	10.241710	9.0201400	9.0546600	8.975770	8.9584600
19	1.6616300	1.5503000	1.4595300	1.562750	1.5426400
20	3.8824000	3.5959200	3.0220800	3.686900	3.7537700
31	2.1252100	1.9707200	1.8643200	1.982840	1.8434700

When TCSC is placed at lines 15 and 31, power flow on all lines has decreased, except lines 4, 11, and 12. The reduction of real power flows suggests that the available transfer capability has increased in the lines having lesser real power flows. This will result in

relieving the congestion of these lines. These results prove the efficacy of the proposed SPCR method in optimally locating the TCSC to relieve congestion.

3.4 CHAPTER SUMMARY

In this study, the SPCR method to optimally locate the TCSC has been devised. The optimization utilizes the DC power flow sensitivity index and reactive power loss sensitivity index. The IEEE 6-bus and 30-bus test systems are used for validating the results. The following conclusions are drawn from the study:

- The potential list of lines where TCSC can be placed is obtained by both sensitivity factors.
- The TCSC location is one among the sensitive lines, which is resulting in the most reduction in real and reactive power loss and decreased line flow.
- For 6 bus system, among all the cases, the line 7 has been found to be suited for TCSC location.
- For 30 bus system, among all the cases, the 15^{th} and 31^{st} line have been found to be suited for TCSC location.
- The allocation results in relieving congestion of these lines and, hence, allow them to be able to transfer power more than already committed usage and prevents overloading in the future.
- The results have been compared with published results based on PSAT and the performance is found comparable.

It is important to discuss the power market operation from the view point of single area system and multiarea system. Under such operation, the ATC calculation is although important but becomes complicated because the transaction shall be between the buses in single area system and among different areas in multi area system.

For the purpose, a heuristic algorithm MEEPSO (Metaheuristic Evolutionary Particle Swarm Optimization) has been developed to calculate Static ATC (SATC). The presented algorithm utilizes ACPTDF and can compute the SATC value under various bilateral transactions. For multiarea system, the SATC has been calculated using Power World Simulator (PWS). The efficacy of the presented algorithm is validated while comparing its performance with ACPTDF, DCPTDF and PWS. The comparison involves the performance with and without TCSC placement.

4.1 OPERATIONS IN THE POWER MARKET

While analyzing linear ATC, the calculation of transfer limitation [1] for every contingency of the transmission line is done and the limiters are listed. The list includes:

- name of the line exceeding the limit,
- limit of transfer (MW), and
- base case for limits

The number of determined transfer limiters is given as:

$$Transfer\ Limiters = X * (Y + n) \tag{4.1}$$

where X is the number of monitored transmission lines, Y is the number of contingencies and n is the number of the base case. The system operator balances buying and selling of energy to control generation and load and hence smaller transactions are performed in normal cases [177]. Taking a bilateral trading case of a 2-bus system shown in Figure 4.1 where 1, 2, and 3 are the generators, and I and II are the loads 1 and 2, respectively. Let there is a transaction between generator 1 and load 1, and between generator 2 and load 2, the allowable limit under contingency shall not exceed the total generation. If generator 1 gives generation to load 1 at x ₹/MWh price, generator 2 gives generation to load 2 at y ₹/MWh price, and generator 3 gives energy at z ₹/MWh, load 2 should not pay more than

$(z - y)$ ₹/MWh for rights of the transmission to avoid expensive pricing. Some prices are reserved for transmission. However, these are optional. Figure 4.2 explains the loop flow showing Kirchhoff's Voltage Law (KVL). The following formulae decide the power flows.

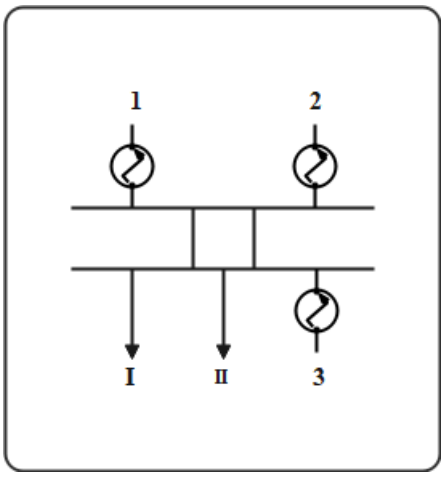

Figure 4.1 An illustration of bilateral trading in a 2-bus system

$$\overrightarrow{v_{ab}} = z_1\vec{\imath}_1 = z_2\vec{\imath}_2 \tag{4.2}$$

$$\vec{\imath} = \vec{\imath}_1 + \vec{\imath}_2 \tag{4.3}$$

$$\vec{\imath}_1 = \left[\frac{z_2}{(z_1 + z_2)}\right] * \vec{\imath} \tag{4.4}$$

$$\vec{\imath}_2 = \left[\frac{z_1}{(z_1 + z_2)}\right] * \vec{\imath} \tag{4.5}$$

$$Z \approx jX \tag{4.6}$$

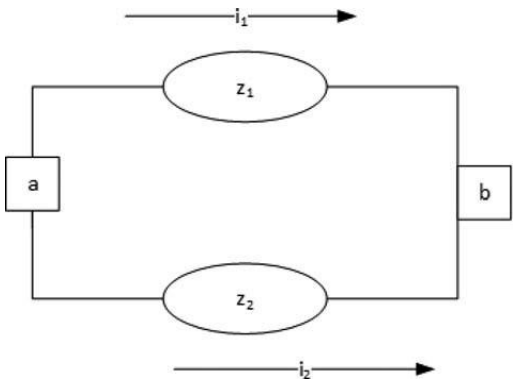

Figure 4.2 Loop showing Kirchhoff's Voltage Law (KVL)

where resistance is neglected in Equation (4.4) and Z is the impedance and X is the reactance of the line.

Also, reactive power and losses are neglected, where V_{ab} is the voltage between points a and b, z_1 and z_2 are the impedances at 1 and 2, i_1 and i_2 are the currents at points 1 and 2, and Z, X, and I are the total impedance, reactance, and current of the system. Figure 4.3 shows the power loop. The following equations show the power flow equations used for the 2-bus system.

$$P_a = P_b = P \tag{4.7}$$

$$f_1 = \left[\frac{X_1}{(X_1 + X_2)}\right] * P_1 = \left[\frac{X_1}{(X_1 + X_2)}\right] * P \tag{4.8}$$

$$f_2 = \left[\frac{X_1}{(X_1 + X_2)}\right] * P_2 = \left[\frac{X_1}{(X_1 + X_2)}\right] * P \tag{4.9}$$

where X_1 and X_2 is the reactance of branches 1 and 2, P_a and P_b are the values of power P at a and b, and f_1 and f_2 are the flow of power at branches 1 and 2.

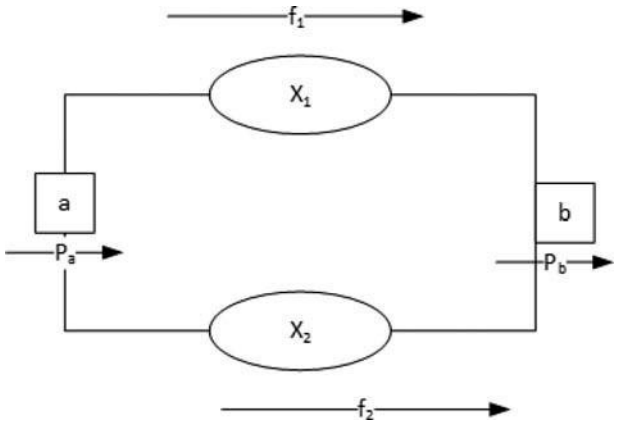

Figure 4.3 Power loop showing P_a and P_b

4.2 IMPORTANCE OF STATIC AVAILABLE TRANSFER CAPABILITY

The Static ATC (SATC) is defined as ATC under static limits namely thermal limit. The need for using SATC arises because of the need to reliably deliver the power and give the

flexibility to change the system as and when required so that the urge to enhance more installed generating capacity can be reduced.

The linear sensitivity elements have the potential for an instantaneous calculation of SATC. The use of these parameters provides an extraordinarily fast estimate for the determination of static ATC and offers a linear approximation of flow and, observes the variation in response to the transaction between the seller and buyer [138]. It is based on the Newton Raphson load flow approach. In the AC method, change occurs in line flow sensitivity factors. The calculation of line flows in the AC method is given as:

$$S_{ij} = V_i . I_{ij}^* = V_i \left[\frac{V_i - V_j}{r + jx} + j\, V_i B_{ij}\right]^* \tag{4.10}$$

$$S_{ij} = P_{ij} + jQ_{ij} \tag{4.11}$$

Using the equation for the N-R Jacobian method:

$$\Delta P_{ij} = \frac{\partial P_{ij}}{\partial \delta_i}\Delta\delta_i + \frac{\partial P_{ij}}{\partial \delta_j}\Delta\delta_j + \frac{\partial P_{ij}}{\partial V_i}\Delta V_i + \frac{\partial P_{ij}}{\partial V_j}\Delta V_j \tag{4.12}$$

where S_{ij} is complex power flowing between bus i and j, V_i is the voltage at the i^{th} bus, P_{ij} is $real(S_{ij})$ and Q_{ij} is $imag(S_{ij})$, ΔP_{ij} is change in real power, I_{ij} is current flowing between buses i and j and $\frac{\partial P_{ij}}{\partial \delta_i}$ is incremental change in real power for the change in angle.

4.3 CALCULATION OF SATC WITH PWS

The PWS uses Single Linear (SL) step technique to calculate SATC. The technique makes use of the mathematical data of the state derivatives of the present state. These derivatives are used while calculating PTDF. Considering the transmission line limit x, present loading y and PTDF $z\%$ without any line overloading, the maximum estimated transfer is given as:

$$Transfer\ limitation = \frac{Limit - Present\ loading}{PTDF} = (x - y)/z \tag{4.13}$$

The value of SATC is determined as the minimum amount of a transfer limitation value when considering the limitation of transfer on each line during every contingency. Each transfer may decrease the line flow till the flow limit is in the opposite direction. The

transfer of power among combinations of zones, participating groups, areas and super areas can give the value of SATC [99, 178]. The steady-state power system is included in the SATC environment and gives linear ATC values. For calculation of these values for the base case, the following equation is used,

$$T_m = \begin{cases} \dfrac{MW\ lim_m - flow_m}{PTDF_m}, & \forall\ PTDF_m > 0 \\ \infty, & \forall\ PTDF_m = 0 \\ \dfrac{-MW\ lim_m - flow_m}{PTDF_m}, & \forall\ PTDF_m < 0 \end{cases} \tag{4.14}$$

where T_m is the transfer limitation for monitored element m in the power system, $PTDF_m$ indicates the PTDF for the monitored element m, $MW\ limit_m$ is the power limit for monitored element m, $PTDF_m = 0$, implies that its value is negligible i.e., the transfer has a negligible effect on the limiting element.

In electricity markets involving the trading system in the decentralized and bilateral environment, the two main things which are involved in all transactions are a buyer and a seller. These two should agree on the points of quantity, price, and any other condition linked with trading. Then comes the role of the System Operator. It is not part of any transaction and does not fix the amount or prices of it but is concerned with the security and balancing of the system. It includes maintenance of security especially controlling the injection of power [20] which generators do at nodes of power systems.

The loss of branch or any of its insertion can be handled by linear analysis of ATC. The speed of the solution and simultaneously the need for the memory of the computer can be enhanced by decreasing the monitored elements of the power system and its contingencies for the analysis of ATC. For contingencies, the transfer limitation values for the monitored element [113, 179-181] are given as:

$$T_{m,c} = \begin{cases} \dfrac{MW\ lim_m - OMW_{m,c}}{OTDF_{m,c}}, & \forall\ OTDF_{m,c} > 0 \\ \infty, & \forall\ OTDF_{m,c} = 0 \\ \dfrac{MW\ lim_m - OMW_{m,c}}{OTDF_{m,c}}, & \forall\ OTDF_{m,c} < 0 \end{cases} \tag{4.15}$$

where OMW gives the limiting element's estimate before transferring of power and after the occurrence of a contingency and OTDF gives the sensitivity of the limiting element for the direction of transfer for the limiting contingency.

4.4 CALCULATION OF SATC USING ACPTDF

The ACPTDF for calculating SATC is used to determine different parameters for a variation in MW transaction at variable operating conditions e.g., a bilateral transaction between a seller and a buyer bus. The algorithm for the calculation of SATC using ACPTDF is presented below. The equations used in the process are described in the algorithm.

Step 1. Calculate the line flow sensitivity factors.

Step 2. Take bus number $1, \dots, g$ as PV buses and $g+1, \dots, .n$ as PQ buses for n number of total buses.

Step 3. Through sensitivity analysis, the power flow change on line $i-j$ is given as:

$$\Delta P_{ij} = \left[\frac{\partial P_{ij}}{\partial \delta_2}, \quad \dots, \quad \frac{\partial P_{ij}}{\partial \delta_n}, \frac{\partial P_{ij}}{\partial V_{g+1}} \quad \dots, \quad \frac{\partial P_{ij}}{\partial V_n}\right] \begin{bmatrix} \Delta\delta_2 \\ \vdots \\ \Delta\delta_n \\ \Delta|V_{g+1}| \\ \vdots \\ \Delta|V_n| \end{bmatrix} \tag{4.16}$$

Step 4. Transacted power is P_t between bus i to bus j:

$$\Delta P_m = +P_t \tag{4.17}$$

$$\Delta P_n = -P_t \tag{4.18}$$

Step 5. By the N-R Load Flow:

$$\begin{bmatrix} \Delta\delta_2 \\ \vdots \\ \Delta\delta_n \\ \Delta|V_{g+1}| \\ \vdots \\ \Delta|V_n| \end{bmatrix} = [J]^{-1} \begin{bmatrix} \Delta P_2 \\ \vdots \\ \Delta P_n \\ \Delta|Q_{g+1}| \\ \vdots \\ \Delta|Q_n| \end{bmatrix} \tag{4.19}$$

$$\Delta P_{ij} = \left[\frac{\partial P_{ij}}{\partial \delta_2}, \quad \dots, \quad \frac{\partial P_{ij}}{\partial \delta_n}, \ \frac{\partial P_{ij}}{\partial V_{g+1}} \quad \dots, \quad \frac{\partial P_{ij}}{\partial V_n}\right][J]^{-1}\begin{bmatrix} 0 \\ \vdots \\ +P_t \\ 0 \\ \vdots \\ -P_t \\ 0 \end{bmatrix} \tag{4.20}$$

$$= ACPTDF_t * P_t$$

$$ACPTDF_{ij,mn} = \left[\frac{\partial P_{ij}}{\partial \delta_2}, \quad \dots, \quad \frac{\partial P_{ij}}{\partial \delta_n}, \ \frac{\partial P_{ij}}{\partial V_{g+1}} \quad \dots, \quad \frac{\partial P_{ij}}{\partial V_n}\right][J]^{-1}\begin{bmatrix} 0 \\ \vdots \\ +1 \\ 0 \\ \vdots \\ -1 \\ 0 \end{bmatrix} \tag{4.21}$$

Step 6. ATC is calculated, as given below:

$$P_{ij,mn}^{max} = \begin{cases} \dfrac{Limit_{ij}^{max} - P_{ij}}{ACPTDF_{ij,mn}} & ; \quad ACPTDF_{ij,mn} > 0 \\ \infty\ (infinite) & ; \quad ACPTDF_{ij,mn} = 0 \\ \dfrac{-Limit_{ij}^{max} - P_{ij}}{ACPTDF_{ij,mn}} & ; \quad ACPTDF_{ij,mn} < 0 \end{cases} \tag{4.22}$$

$$ATC_{mn} = min\{P_{ij,mn}^{max} \quad ij\ \varepsilon\ N_1\} \tag{4.23}$$

4.5 MEEPSO TECHNIQUE

Particle Swarm Optimization is primarily credited to Kennedy, Eberhart, and Shi [78, 182]. It was initially prearranged for reenacting the community behavior of birds and fishes. The calculation after improvement was noticed to perform streamlining. Kennedy *et al.* [183] depicted many logical fragments of swarm optimization. A broader overview of its applications is presented by Poli [184, 185]. Recently, Bonyadi *et al.* [186] dispersed a far-reaching audit on the hypothesis and its test that takes a shot at PSO.

The presented MEEPSO is a metaheuristic technique inspired by PSO. It makes no suppositions and can look through the massive domain of the problem being rationalized. It is a technique that optimizes by iteratively attempting to improve an arrangement given a proportion of value. It considers a problem by having a population of applicants, known

as particles, and then moving these across the region of interest, as indicated by basic arithmetical formulae over the position of the particle and its speed. The development of each is impacted by its locality's most popular position, but, on the other hand, it is guided towards the most popular situations in the inquiry space, which are refreshed as better positions found by different particles. This is required to push the swarm toward the best arrangements. The choice of MEEPSO factors has a great influence on the performance of the optimization.

4.5.1 PARAMETER CHOICE

Choosing parameters that give sensible results has been the topic of abundant analysis. The gradual updating of every particle separately in the explored space is managed through its present position and velocity that can be observed while using the probable resolution in the problem space, whereby the existing velocity is governed with

- the previous velocity;
- the distance from the position where the particle attained its greatest fitness (personal best, $pbest$); and,
- the distance from the particle that accomplished the best fitness among all the particles (global best, $gbest$).

The position of an individual particle is a probable solution, besides the respective particle remembers the best position that it attains throughout the whole optimization process ($pbest$). The swarm together learns the best position that is attained with every particle ($gbest$). The position coupled with the velocity association after the i^{th} iteration amongst any two entities is attained through the subsequent updating expression:

$$v(i) = w * v(i) + c1 * r1 * \big(pbest(i) - pos(i)\big) + c2 * r2 * (gbest - pos(i)) \tag{4.24}$$

where,

- $c1$ and $c2$ are the acceleration factors and constants. They are not negative constants and regulate the comparative effect of the peculiar (local) and collective (global) information on the effort of every particle
- $v(i)$ is the velocity of i^{th} particle. This parameter is checked for minimum and maximum limits violations
- w is the inertia weight or function

- $r1, r2$ are the autonomous consistently dispersed random variables around the span of $(0,1)$
- $pbest(i)$ is the greatest preceding position of $pos(i)$
- $pos(i)$ is the position of the i^{th} particle
- $gbest$ is the finest global position that is attained through a particle surrounded by the complete population.

The inertia function, w, stabilizes the local and global explorations throughout the evolution procedure. At large, a huge inertia weight levied by the side of the primary search stages lets the search space be exhaustively discovered. By steadily reducing the inertia weight, further upgraded results are attained in the ultimate search stage. The main aim of this adjustment is to circumvent early convergence in the primary explored phases besides refining convergence to the global best solution throughout the concluding examined phases. The perception of linearly declining inertia weight that is related to MEEPSO is provided by:

$$w = \frac{w_{max} - (w_{max} - w_{min}) * ite}{maxiter} \tag{4.25}$$

where,

- w_{max} and w_{min} are the highest and the lowest values of the inertia weight,
- ite is the recent iterations, and
- $maxiter$ refers to the highest number of iterations.

The SATC is optimized and calculated with the help of the MEEPSO technique, which comprises first defining input parameters in the MEEPSO and initialization of velocity. Then, set the maximum limit of TCSC compensation and velocity. After that SATC is calculated. Finally, fitness function, objective function, particle best position and global best position are computed.

4.5.2 ALGORITHM FOR CALCULATION OF SATC WITH MEEPSO

A fundamental version of the MEEPSO algorithm works while utilizing a swarm of particles and these are progressed in the seek-space under some elementary formulae. The progress is guided via a function inside the seek-area in addition to the whole swarm's

known position. Once the upgraded positions are being located, they come to guide the moves of the swarm.

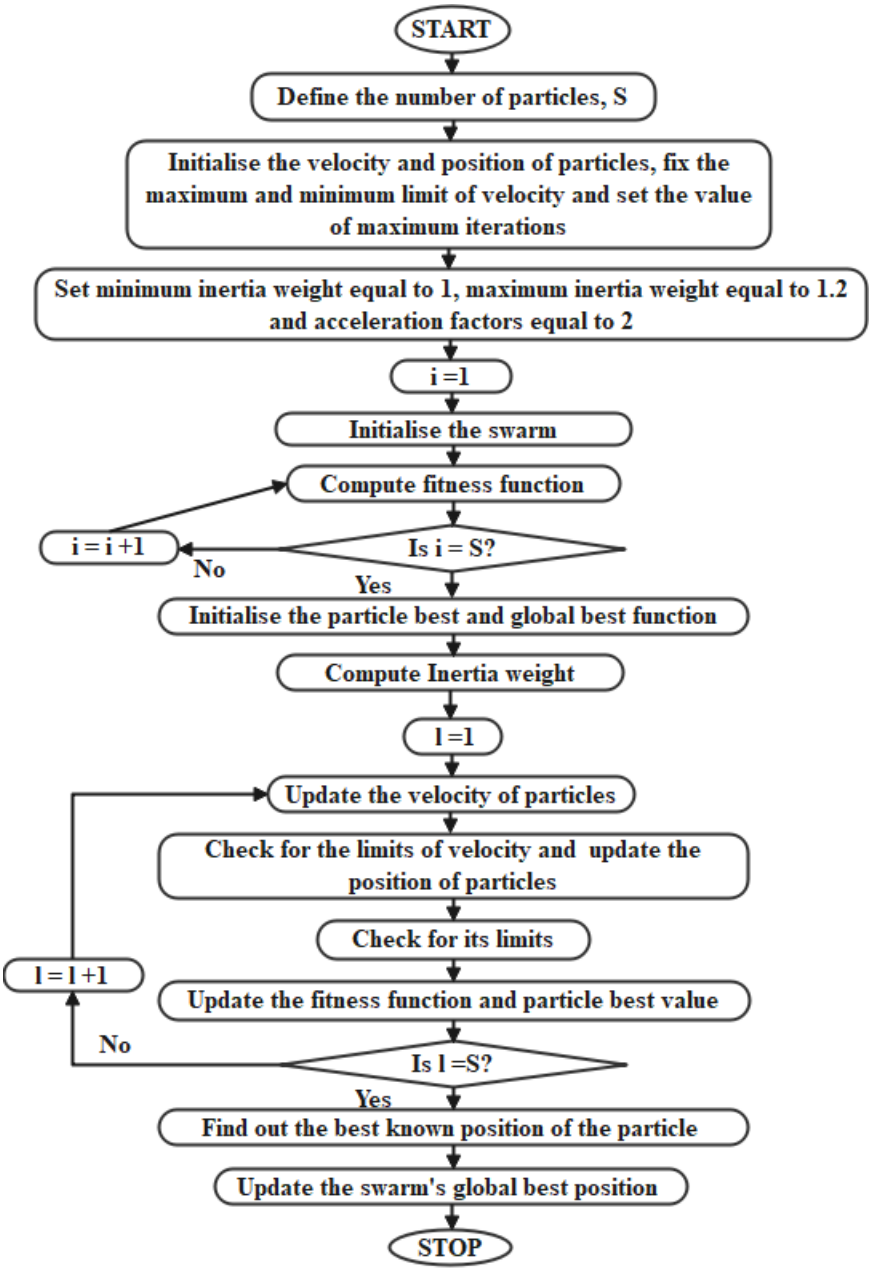

Figure 4.4 Flowchart depicting the MEEPSO algorithm

Consider $f(R_n)$ be the function of R, which is the prime characteristic that is required to be minimized. The aim is to find an answer 'a', for which

$$f(a) \leq f(b) \tag{4.26}$$

for all b in the search space, which gives a as the global minimum.

Let S be the number of particles within the swarm, each having a position $x_i \, \varepsilon \, R_n$ inside the seek-area and a pace $v_i \, \varepsilon \, R_n$. Let p_i be the best-acknowledged position of particle

i and allow g to be the absolute known position of the complete swarm. Figure 4.4 describes a simple flow chart. The steps of the algorithm are described below:

- **Step 1:** For every particle $i = 1 \dots \dots . S$, initialize the position of a particle.

$$x_i = U(b_{lo}, b_{up}) \tag{4.27}$$

- **Step 2:** Initialize the best-acknowledged position of the particle to its initial position, p_i.
- **Step 3:** If $f(p_i) < f(g)$ then update the swarm's best-known position, g.
- **Step 4:** Initialize the velocity of the particle,

$$v_i = U(-|b_{up} - b_{lo}|, |b_{up} - b_{lo}|) \tag{4.28}$$

  while a termination criterion is not met.

- **Step 5:** For every particle, $i = 1, \dots, \dots, S$ and for every dimension $d = 1, \dots, \dots, n$ pick random numbers r_p, r_g.
- **Step 6:** Update the velocity of the particle

$$v_{id} = w.v_{id} + \varphi_p.r_p.(p_{id} - x_{id}) + \varphi_g.r_g.(g_d - x_{id}) \tag{4.29}$$

- **Step 7:** Update the position of the particle

$$x_i = x_i + v_i \tag{4.30}$$

- **Step 8:** If $f(x_i) < f(p_i)$, then update the best-known position of the particle

$$p_i = x_i \tag{4.31}$$

- **Step 9:** If $f(p_i) < f(g)$, then update the swarm's best-acknowledged position.

$$g = p_i \tag{4.32}$$

The lower and upper limits of the search space are the values b_{lo} and b_{up}. The termination principle is the number of reiterations completed or where a satisfactory objective function value is reached [185-187]. The variables w, φ_p, and $\varphi_g$control the behavior and efficacy of the MEEPSO method.

4.6 RESULTS AND DISCUSSION

The SATC has been calculated using PWS and presented the MEEPSO technique for 6 bus and 30 bus test systems. The PWS has been used to analyze the results for a multiarea system while MEEPSO is used to analyze the result for a single-area system. The MEEPSO is used to analyze the performance with and without TCSC placement.

4.6.1 SATC WITH PWS

The PWS is utilized to calculate the static available transfer capability, system cost, and overloading of lines on 6-bus and 30-bus test systems. The values are computed for different transactions between areas and then to find out the combination. The analyzed cases are:

1. Isolated Areas (No Transaction)
2. Transaction from Area B to A of 5 MW
3. Transaction from Area B to A of 10 MW
4. Transaction from Area B to A of 15 MW

4.6.1.1 6 Bus System

The system is divided into two areas A and B. Different cases are considered for the same. Area A consists of bus numbers 1, 2 and 4 and Area B comprises buses 3, 5 and 6. The line data mentioning resistance R, reactance X, susceptance B and line limit is given in Table 4.1.

i. Case No. 1 (Isolated Areas (No Transaction)):

In this case, areas A and B do not carry any transaction between them. Power flow is from area B to area A. Table 4.2 shows the calculated static available transfer capability value for this case. These values are calculated in a power world simulator environment. Line 2–3 is loaded up to 65% and line number 3–6 is loaded up to 75%. The total cost spent is the sum of the hourly cost of areas A and B respectively.

$$\begin{aligned} Total\ Cost &= Hourly\ Cost\ of\ Area\ A + Hourly\ Cost\ of\ Area\ B \\ &= 925 + 1696 = 2621\ (₹/hr) \end{aligned} \tag{4.33}$$

Table 4.1 Branch data of 6-bus system

S. No.	From	To	R	X	B	Limit (MVA)
1	1	2	0.1	0.2	0.02	40
2	1	4	0.05	0.2	0.02	80
3	1	5	0.08	0.3	0.03	60
4	2	3	0.05	0.25	0.03	40
5	2	4	0.05	0.1	0.01	60
6	2	5	0.1	0.3	0.02	30
7	2	6	0.07	0.2	0.025	90
8	3	5	0.12	0.26	0.025	70
9	3	6	0.02	0.1	0.01	100
10	4	5	0.2	0.4	0.04	20
5	5	6	0.1	0.3	0.03	40

ii. Case No. 2 (Transaction from Area B to A of 5 MW):

When a power of 5 MW is transferred from area B to A, the value of the static available transfer capability decreases as shown in Table 4.2. The total cost spent hourly for transacting 5 MW from Area B to Area A is calculated as below:

$$\begin{aligned} Total\ Cost &= Hourly\ Cost\ of\ Area\ A \\ &\quad + Hourly\ Cost\ of\ Area\ B \\ &= 871 + 1760 = 2631\ (₹/hr) \end{aligned} \tag{4.34}$$

Line 2–3 is now 70% loaded and line 3–6 loading has increased to 76% after this transaction. In this case, the SATC value has decreased but the cost has increased. Further loading of lines 2–3 has increased from 65% to 70% and of lines, 3–6 has increased from 75% to 76% but they are within limits.

iii. Case No. 3 (Transaction from Area B to A of 10 MW):

When a transaction of 10 MW is done from Area B to Area A, the static available transfer capability value further reduces. The total cost hence obtained is evaluated below:

$$\begin{aligned} Total\ Cost &= Hourly\ cost\ of\ Area\ A \\ &\quad + Hourly\ cost\ of\ Area\ B \\ &= 818 + 1825 = 2643\ (₹/h) \end{aligned} \tag{4.35}$$

The loading on line 2–3 is further increased to 75% and on line 3–6, it has increased to 78% after this transaction. The value of SATC decreased further and the cost increases. The loading on lines 2–3 and 3-6 has increased.

Table 4.2 Calculated SATC values with PWS depicting the cost of each transaction and loading on specified lines for 6 bus system

	SATC (MW)	Costs (₹/hr)	Loading of line 2–3 (%)	Loading of line 3-6 (%-)
Case 1	37.64	2,621	65	75
Case 2	32.64	2,631	70	76
Case 3	27.64	2,643	75	78
Case 4	22.64	2,655	79	80

iv. Case No. 4 (Transaction from Area B to A of 15 MW):

A transfer of 15 MW is done from Area B to Area A. While performing so, the static available transfer capability values are indicated in Table 4.2 and the total cost for Case 4 is thus calculated as below:

$$\begin{aligned} Total\ Cost\ &= Hourly\ Cost\ of\ Area\ A \\ &\quad + Hourly\ Cost\ of\ Area\ B \\ &= 765 + 1890 = 2655\ (₹/hr) \end{aligned} \tag{4.36}$$

Due to these transactions, line 2–3 is loaded up to 79% but line 3–6 is loaded up to 80%, and the transaction amount is 15 MW. The SATC value is the least in this case and the cost is the highest. The loading on lines 2–3 and 3–6 is highest in this case.

The comparison between all the cases regarding SATC values, costs, and variation in loading of lines is summarized in Table 4.2. After scrutinizing all the cases, the best possible arrangement is that in case 1 because of the value of cost, SATC and loading on both lines are optimum. In the first case, the cost is minimum, SATC is maximum and none of the lines is overloaded; hence case 1 gives the best solution.

4.6.1.2 30 bus system

The system is divided into two areas A and B. Area B consists of bus numbers 1, 2, 3, 4, 5 and 7 and Area A comprises of all other remaining buses. The resistance R, reactance X, susceptance B and line limit are given in Table 4.3.

i. Case No. 1 (Isolated Areas (No Transaction)):

In this case, areas A and B do not carry any transaction between them. Power flow is from area A to area B. Table 4.4 shows the calculated static available transfer capability value

for this case. The total cost spent in this case is the sum of the hourly cost of area A and B respectively.

$$Total\ Cost = Hourly\ Cost\ of\ Area\ A + Hourly\ Cost\ of\ Area\ B = 300 + 3742 = 4042\ (₹/hr) \quad (4.37)$$

Line 1–2 is overloaded up to the maximum limit (127%) and line no. 6–8 is loaded up to 93%.

ii. Case No. 2 (Transaction from Area A to B of 5 MW):

When a power of 5 MW is transferred from area A to B, the value of the static available transfer capability decreases as shown in Table 4.4. The total cost spent hourly for transacting 5 MW from Area A to Area B is calculated as below:

$$Total\ Cost = Hourly\ Cost\ of\ Area\ A + Hourly\ Cost\ of\ Area\ B = 300 + 1943 = 2243\ (₹/hr) \quad (4.38)$$

Line 1–2 is now 83% loaded and line 6–8 loading has decreased to 37% after this transaction. In this case, the SATC value has decreased and the cost is also decreased. Further loading of lines 1–2 has decreased from 127% to 83% and of line, 6-8 has decreased from 93% to 37% but they are within limits.

iii. Case No. 3 (Transaction from Area A to B of 10 MW):

When a transaction of 10 MW is done from area A to area B, the static available transfer capability value further reduces. The total cost hence obtained is evaluated below:

$$Total\ Cost = Hourly\ cost\ of\ Area\ A + Hourly\ cost\ of\ Area\ B = 300 + 1879 = 2179\ (₹/h) \quad (4.39)$$

The loading on line 1–2 is further decreased to 80% and on line 6–8, it has increased to 41% after this transaction. The value of SATC decreased further and the cost also decreases. The loading on lines 1–2 has decreased and that on 6-8 increased.

Table 4.3 Line Data of 30 bus system

From	To	R	X	B	Limit (MVA)
1	2	0.0192	0.06	0.0528	130
1	3	0.0452	0.19	0.0408	130
2	4	0.057	0.17	0.0368	65
2	5	0.0472	0.2	0.0418	130
2	6	0.0581	0.18	0.0374	65
3	4	0.0132	0.04	0.0084	130
4	6	0.0119	0.04	0.009	90
4	12	0	0.26	0	65
5	7	0.046	0.12	0.0204	70
6	7	0.0267	0.08	0.017	130
6	8	0.012	0.04	0.009	32
6	9	0	0.21	0	65
6	10	0	0.56	0	32
6	28	0.0169	0.06	0.013	32
8	28	0.0636	0.2	0.0428	32
9	10	0	0.11	0	65
9	11	0	0.21	0	65
10	17	0.0324	0.08	0	32
10	20	0.0936	0.21	0	32
10	21	0.0348	0.07	0	32
10	22	0.0727	0.15	0	32
12	13	0	0.14	0	65
12	14	0.1231	0.26	0	32
12	15	0.0662	0.13	0	32
12	16	0.0945	0.2	0	32
14	15	0.221	0.2	0	16
15	18	0.1073	0.22	0	16
15	23	0.1	0.2	0	16
16	17	0.0524	0.19	0	16
18	19	0.0639	0.13	0	16
19	20	0.034	0.07	0	16
21	22	0.0116	0.02	0	32
22	24	0.115	0.18	0	16
23	24	0.132	0.27	0	16
24	25	0.1885	0.33	0	16
25	26	0.2544	0.38	0	16
25	27	0.1093	0.21	0	16
28	27	0	0.4	0	65
27	29	0.2198	0.42	0	16
27	30	0.3202	0.6	0	16
29	30	0.2399	0.45	0	16

iv. Case No. 4 (Transaction from Area A to B of 15 MW):

A transfer of 15 MW is done from area A to area B. While performing so, the static available transfer capability values are summarized in Table 4.4 and the total cost for Case 4 is thus calculated as below

$$\begin{aligned} Total\ Cost\ &= Hourly\ Cost\ of\ Area\ A \\ &\quad + Hourly\ Cost\ of\ Area\ B \\ &= 300 + 1816 = 2116\ (₹/hr) \end{aligned} \tag{4.40}$$

Due to these transactions, line 1–2 is loaded up to 78% but line 6–8 is loaded up to 46%, and the transaction amount is 15 MW. The SATC value and cost of the transaction are the least in this case. The loading on line 1–2 is least in this case but that on line 6–8 is 46%.

Table 4.4 Calculated SATC values with PWS depicting the cost of each transaction and loading on specified lines for 30 bus system

	SATC (MW)	**Costs (₹/hr)**	**Loading of line 1–2 (%)**	**Loading of line 6-8 (%)**
Case 1	189.52	4,042	127	93
Case 2	55.3	2,243	83	37
Case 3	50.3	2,179	80	41
Case 4	45.3	2,116	78	46

The comparison between all the cases regarding SATC values, costs, and variation in loading of lines is shown in Table 4.4. After scrutinizing all the cases, the best possible arrangement is that in case 3 because of the value of cost, ATC and loading on both lines are optimum. However, in the fourth case though the cost is minimum, the SATC value is least; hence case 3 is the best solution. Thus, area A should transfer 15 MW to area A for the best power system results.

4.6.2 SATC WITH MEEPSO

The procedure implemented for the intensification of SATC using the MEEPSO technique in this illustrated work is also analyzed on IEEE 6 bus and 30 bus systems. The MEEPSO algorithm is applied for augmenting and optimizing SATC after placing TCSC at an optimal location. The represented algorithm has been carried out by taking, into account,

the count of particles as 50 for maximum iterations of 200, w_{min} is 1 and w_{max} is 1.2, $c1$ and $c2$ are both 2.

The maximum amount of TCSC compensation is 50% and the minimum is 0. The base MVA taken is 100 MVA. All the parameters are taken per unit. The values are computed by exercising the ACPTDF procedure. A comparison involving with and without TCSC, exercising the MEEPSO technique is monitored and examined with the DCPTDF technique and the values of SATC are calculated with the help of the Power World Simulator software.

4.6.2.1 6 bus system

The 6-bus system consists of three generators and eleven lines. Figure 4.5 shows the calculated values of SATC. The values are calculated first for the base case at lines 2–3, 2–5, and 2–6. Transaction T1 means that the transaction is done between buses 2 and 3, transaction T2 means the transaction is done amongst buses 2 and 5, and transaction T3 implies that the transaction is performed for buses 2 and 6.

The base case values are calculated using the Newton–Raphson method (for calculating load flow) and the ACPTDF method for finding SATC at all transactions. The SATC is also calculated using the DCPTDF technique. Both methods are evaluated and compared with the calculated values of SATC using PWS.

To demonstrate the efficacy of the proposed method, the TCSC is placed at lines 7, 8, and 11 (optimal location found using the SPCR method), and SATC is then calculated using the MEEPSO technique at transactions T1, T2 and T3. Table 4.5 shows the comparison of SATC that is calculated by means of the MEEPSO technique by the evaluated results of ACPTDF, DCPTDF, and PWS software.

Here, MEEPSO 7, MEEPSO 8 and MEEPSO 11 represent that SATC is calculated using the MEEPSO technique while placing TCSC at line 7, line 8 and line 11 respectively in one-by-one manner. Figure 4.5 shows the enhanced values of SATC by using the proposed technique.

Table 4.5 Comparison of SATC values by several methods

Transactions	ACPTDF	PWS	DCPTDF	MEEPSO 7	MEEPSO 8	MEEPSO 11
T1	98.8	90.02	93.48	121.53	98.78	99.27
T2	42.18	41.15	42.73	51.12	56.86	46.98
T3	104.14	95.44	99.12	128.83	126.82	104.20

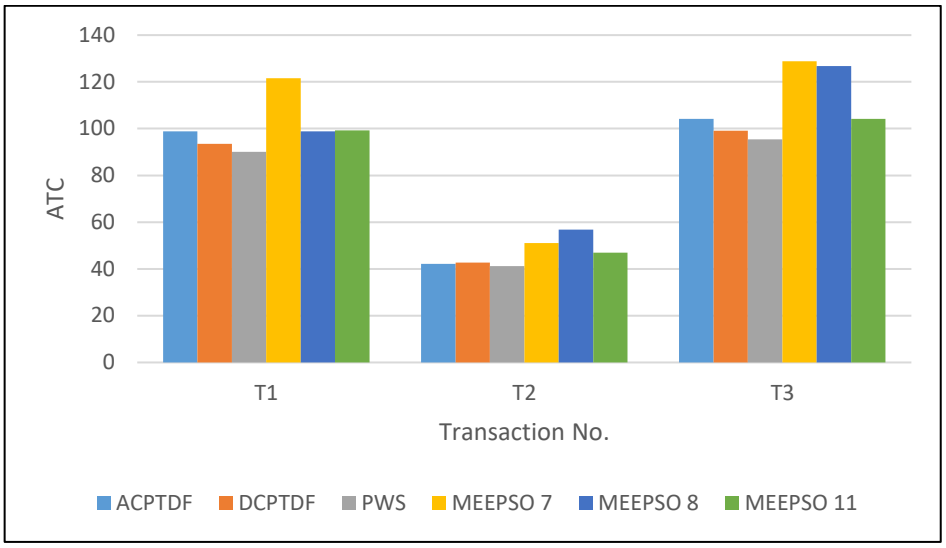

Figure 4.5 Evaluation of SATC values at various transactions by several methods (6 bus system)

Table 4.6 Comparison between SATC values calculated with and without TCSC at optimally located lines for various transactions for 6 bus system.

Transaction	Location of TCSC Line No.	SATC without TCSC (MW)	SATC with TCSC and MEEPSO (MW)
2-3	7	98.8	121.53
	8		98.78
	11		99.27
2-5	7	42.18	51.12
	8		56.86
	11		46.98
2-6	7	104.14	128.83
	8		126.82
	11		104.20

The comparison reveals the improvement in values of SATC (in MW) by 25.85% by using the currently developed MEEPSO method compared with that of DCPTDF in 6 bus system, whereas it showed an improvement of 9.34% as compared to ACPTDF. The efficacy of the developed method has been proved by taking various transactions between different buses. In six bus systems, SATC has improved considerably with the currently developed MEEPSO technique when TCSC was placed at line 7 during transaction T1.

In Table 4.6, the comparison between SATC values calculated with and without TCSC devices at optimally located lines for various transactions for 6 bus system is presented. Each transaction is analyzed after allocating TCSC at line 7, line 8 and line 11 separately. After placing TCSC at the 7th line, the SATC is 23% more than that without TCSC for

transaction T1. For transaction T2, after placing the TCSC device at the 8th line, SATC improves by 34%. It has increased by 24% when the TCSC device is located at the 7th line for transaction T3.

4.6.2.2 30 Bus System

The IEEE 30 bus system comprises six generators and 41 transmission lines [186]. Table 4.7 shows the calculated values of Static Available Transfer Capability. The values are calculated first for the base case in lines 11–25 and 9–11. Transaction T1 means that the transaction is done between buses 11 and 25 and transaction T2 means that the transaction is done between buses 9 and 11. The base case values are calculated using the Newton Raphson method (for calculating load flow) and the ACPTDF method for finding SATC at all transactions. The SATC is also calculated while using the DCPTDF technique. These values are further compared with the calculated values of SATC using PWS.

Table 4.7 Comparison of SATC values computed by different methods for 30 bus system

Transaction	ACPTDF	PWS	DCPTDF	MEEPSO 11	MEEPSO 12	MEEPSO 15	MEEPSO 31
T1	27.54	22.65	23.37	30.11	29.87	30.67	27.65
T2	64.99	65.89	65	65.14	65.05	65.00	65.00

The TCSC is placed at lines 11, 12, 15, and 31 (optimal location found using the SPCR method) and then SATC is calculated using the MEEPSO technique at transactions T1, T2 and T3 to prove the efficacy of the proposed method. Figure 4.6 displays the analysis of SATC calculated by MEEPSO, ACPTDF, DCPTDF, and PWS software. Here, MEEPSO 11, MEEPSO 12, MEEPSO 15 and MEEPSO 31 represent that SATC is calculated using the MEEPSO technique while placing TCSC at line 11, line 12, line 15, and line 31 respectively in a one-by-one manner. Figure 4.6 depicts the enhanced values of SATC by using the proposed technique. The validation and efficacy of the proposed methods are proved by comparing the results with the conventional methods of the ACPTDF and DCPTDF techniques. Additionally, the results are further verified by using the values that were observed through PWS software.

In Table 4.8, the comparison between SATC values calculated with and without TCSC devices at optimally located lines for various transactions for 30 bus system is listed. Each transaction is analyzed after allocating TCSC at line 11, line 12, line 15 and line 31 separately. For transaction T1, when it is placed at the 15th line, SATC is 9% more than

that without TCSC. For transaction T2, after placing the TCSC device at the 11th line, the SATC increases.

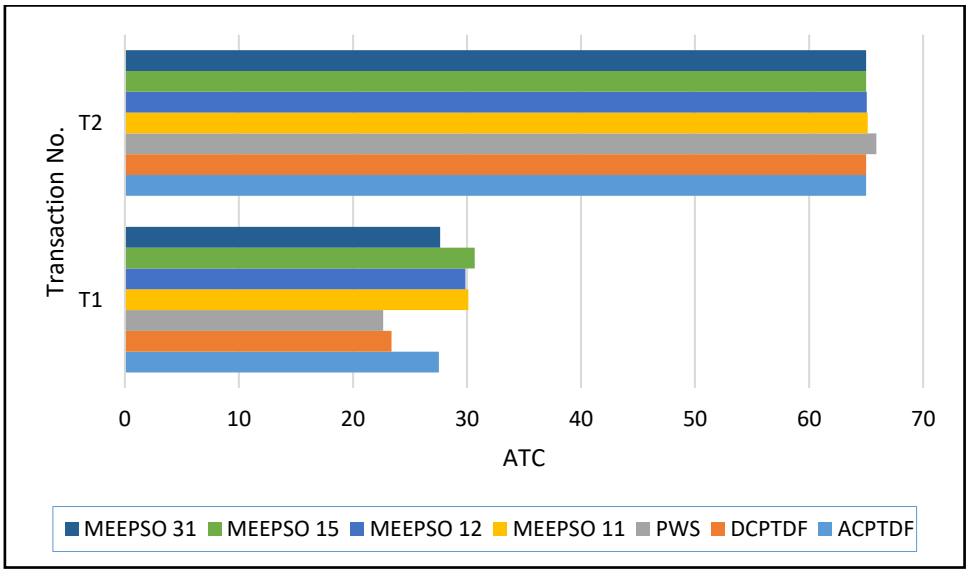

Figure 4.6 Analyzation of SATC at various transactions by several methods (30 bus system)

Table 4.8 Comparison between SATC values calculated with and without TCSC at optimally located lines of various transactions for 30 bus system

Transaction	Location of TCSC (Line No.)	SATC without TCSC (MW)	SATC with TCSC and MEEPSO (MW)
11-25	11	27.54	30.1143
	12		29.8702
	15		30.6754
	31		27.6526
9-11	11	64.99	65.1395
	12		65.0499
	15		65.0036
	31		65.0037

4.7 CHAPTER SUMMARY

The power market operations have been analyzed based on single area and muti area arrangements. A heuristic algorithm MEEPSO has been proposed to calculate SATC for a single area arrangement. The multi-area system has been analyzed for different transactions using PWS. The performance is validated through the analysis of 6-bus and 30-bus test systems. The following conclusions are drawn:

- The improved values of SATC are not resulted in all cases after placing TCSC at sensitive lines. However, the improvement in SATC has resulted in most of the lines.
- The values of SATC obtained by the presented MEEPSO algorithm are compared with that of ACPTDF, DCPTDF, and PWS. The higher SATC value has resulted from the presented MEEPSO method.
- The comparison reveals the improvement in values of SATC by 25.85% to that of DCPTDF and 9.34% to that of ACPTDF in the 6-bus system by using the MEEPSO method.
- In the 30-bus system, the comparison reveals the improvement in values of SATC by 33.06% to that of DCPTDF and 34.8% to that of ACPTDF by using the MEEPSO method.
- Among different transactions, the best arrangement is decided by the consideration of optimum cost, SATC and line loading.

Chapter 5 Dynamic ATC Calculation

The Dynamic ATC (DATC) refers to the calculation of ATC under dynamic stability conditions, which are arising due to changes in load, fault and even the outage of the line. The DATC calculation requires a dynamic model and representation of power system components. To facilitate this, the generator is represented by the *d-q* axis sub transient model. The excitation system is also represented by a dynamic model. The SEAMB method is presented for calculating the DATC. Firstly, the power system network is classified into areas and then the SEAMB eigen value analysis is done to find DATC for the transaction between areas. The critical limits are obtained by Hopf Bifurcation (HB) limit. The result has been analyzed using Power World Simulator for the transient conditions of three-phase fault at buses and line outage contingency.

5.1 MODELING OF POWER SYSTEM COMPONENTS

- **Generator Model:**

The round rotor generator (GENROU) model estimates the behaviour of a synchronous generator during a transient stability study. A solid rotor machine with three damper windings is represented by this model. Figure 5.1 shows the machine model GENROU represented by equal mutual inductance rotor modelling. It signifies a solid rotor generator on the d-axis consisting of a field and one iron circuit while on the q-axis it has two iron circuits and includes the saturation effect. One state variable needs to be incorporated into each rotor circuit. This kind of generator is a 6^{th} order round rotor generator.

In the individual synchronous machines [188], factors are transferred to the rotor reference frame. Whereas the quantities of the network are stated in the synchronous reference frame. Figure 5.2 shows the correlation between two coordinates, where a voltage source E behind a dynamic impedance X_s represents the generator. The rotor angle signifies the angular spatial positions of the shaft of rotor. The synchronously rotating reference axes leading the $d-q$ axes by angle

$$\theta = \frac{\pi}{2} - \delta \tag{5.1}$$

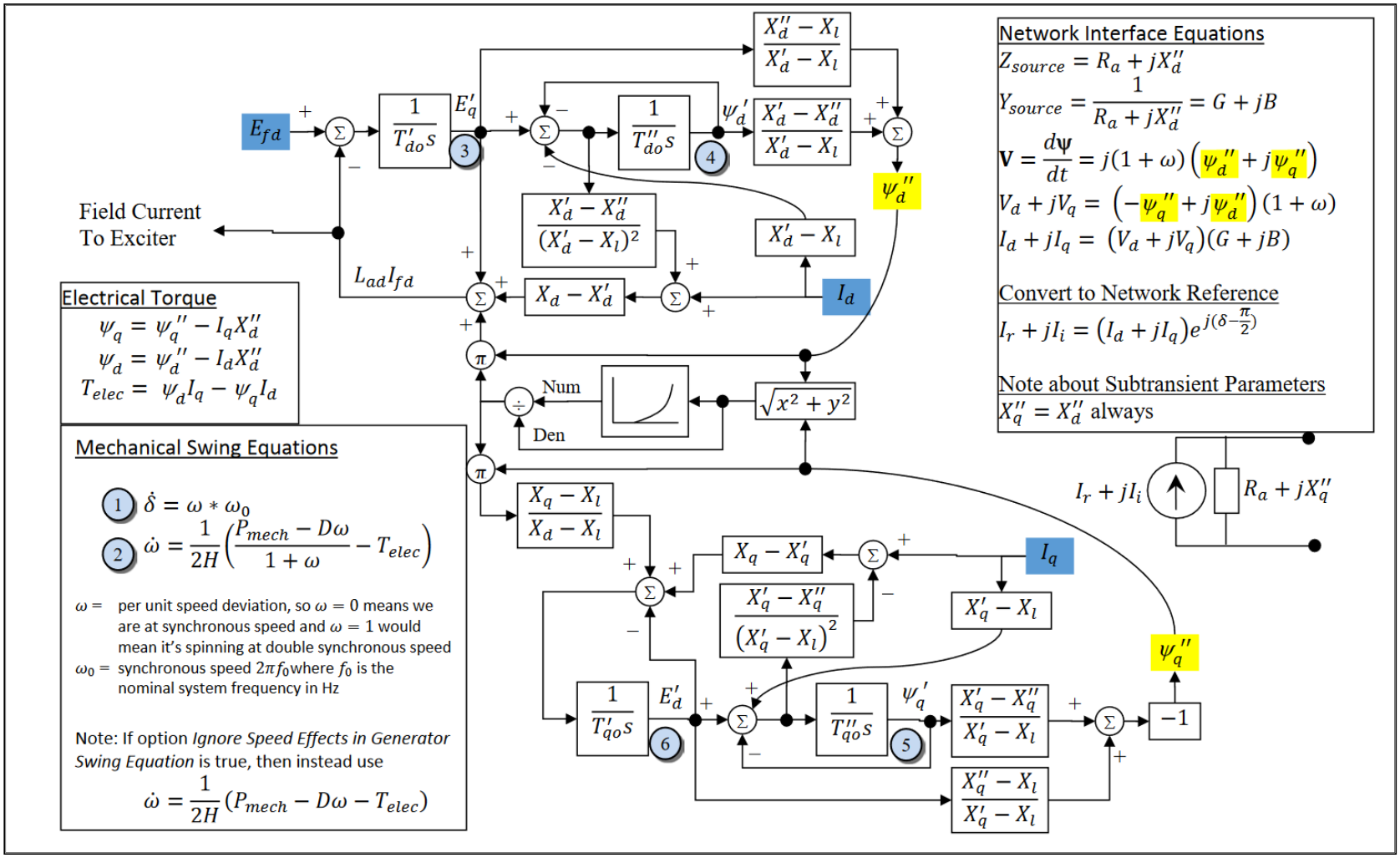

Figure 5.1 Block Diagram of Machine model GENROU

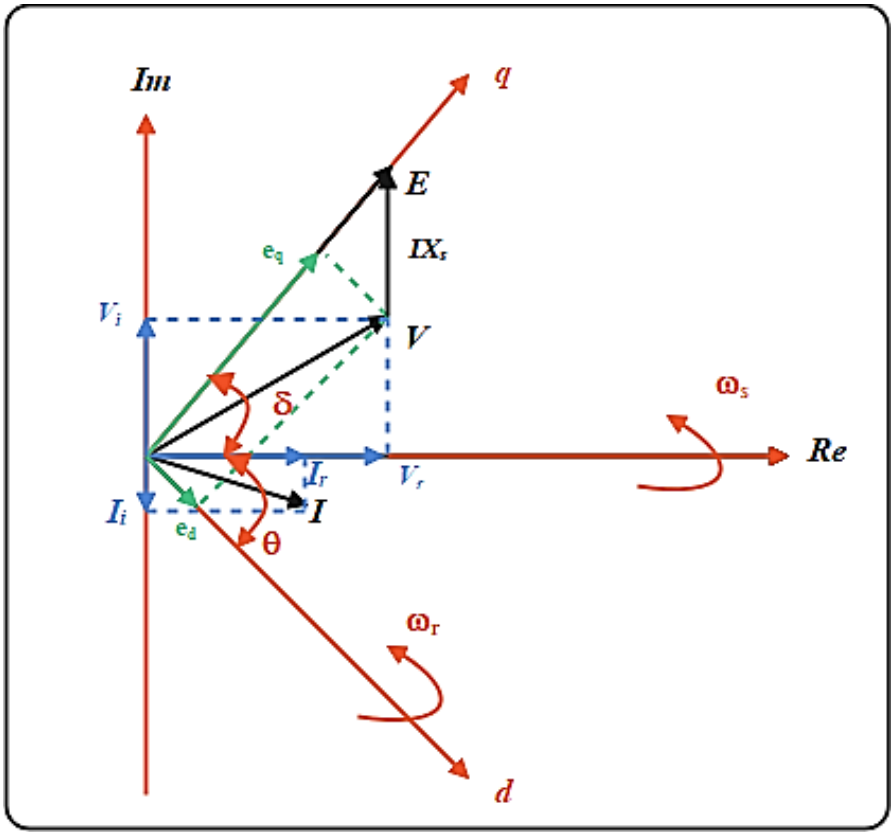

Figure 5.2 Synchronous and Rotor coordinates

The following equation gives the relation between the quantities expressed in $R-I$ axes and $d-q$ axes:

$$\begin{bmatrix} V_r \\ V_i \end{bmatrix} = \begin{bmatrix} sin(\delta) & cos(\delta) \\ -cos(\delta) & sin(\delta) \end{bmatrix} \times \begin{bmatrix} e_d \\ e_q \end{bmatrix} \tag{5.2}$$

The electromagnetic torque T_e induced by the three-phase currents in the stator are given by the current and flux linkages in the dq axis:

$$T_e = \varphi_d i_q - \varphi_q i_d \tag{5.3}$$

Mechanical torque T_m provided by the turbine governor takes the initial value. Since T_e revolves around the rotor, an unbalance between T_e and T_m leads to increased (or decreased) rotating energy and hence results in the speed variation of the generator. A term proportional to speed deviation is added to include the effect of damping torque. Therefore, the equation of motion is:

$$2H\frac{d\Delta\omega_r}{dt} = T_m - T_e - D_e\frac{d\Delta\omega_r}{\omega_r} \tag{5.4}$$

$$\frac{d\delta}{dt} = \omega_0\Delta\omega_r \tag{5.5}$$

The electro-magnetic relation between the terminal voltage of the generator, current and flux linkage is derived by equations of stator voltage. When the changes in flux are ignored in the model, the stator voltage is given as follows:

$$u_d = -\varphi_q\omega_r - R_a i_d \tag{5.6}$$

$$u_q = +\varphi_d\omega_r - R_a i_q \tag{5.7}$$

It is assumed that

$$\mathrm{X_d''} = \mathrm{X_q''} \tag{5.8}$$

In the newly developed models, these parameters are adjusted by considering the default value of R_a as zero. The algebraic equations mentioned above are the same for both the generators: salient and solid pole. But the electromagnetic performance of these is required to be modelled separately. In the case of salient pole generator modelling, saturation is normally supposed to take place only in the direct axis. The saturation can be significant in the case of solid iron rotor turbine generators for both the axes: direct and quadrature. The equations given below correspond to a solid rotor generator. The saturation curve for the open-circuit generator determines the saturation factor *S*. The equations stated with standard synchronous machine parameters are given below:

$$\dot{E}_q' = \frac{1}{T_{d0}'}(E_{fd} - X_{ad}I_{fd}) \tag{5.9}$$

$$\dot{E}_d' = \frac{1}{T_{q0}'}(-1)(X_{aq}I_{1q}) \tag{5.10}$$

$$\dot{\varphi}_{kd} = \frac{1}{T_{d0}''}(E_q' - \varphi_{kd} - (X_d' - X_l)i_d) \tag{5.11}$$

$$\dot{\varphi}_{kq} = \frac{1}{T_{q0}''}(E_d' - \varphi_{kq} + (X_q' - X_l)i_q) \tag{5.12}$$

$$X_{ad}I_{fd} = \frac{(X_d' - X_d'')(X_d - X_d')}{(X_d' - X_l)^2}\left[E_q' - \varphi_{kd} - (X_d' - X_l)i_d\right] + i_d(X_d - X_d') + E_q' + S_e(|\varphi''|\varphi_d'') \tag{5.13}$$

$$X_{aq}I_{lq} = \frac{(X'_q - X''_q)(X_q - X'_q)}{(X'_q - X_l)^2}\left[E'_d - \varphi_{kq} - (X'_d - X_l)i_q\right] \\ -i_q(X_q - X'_q) + E'_d - S_e(|\varphi''|\frac{X_q - X_l}{X_d - X_l}\varphi''_q) \tag{5.14}$$

$$\varphi''_d = \frac{E'_q(X''_d - X_l) + \varphi_{kd}(X'_d - X''_d)}{X'_d - X_l} \tag{5.15}$$

$$\varphi''_q = \frac{-E'_d(X''_q - X_l) + \varphi_{kq}(X'_q - X''_q)}{X'_q - X_l} \tag{5.16}$$

$$|\varphi''| = \sqrt{(\varphi''_d)^2 + (\varphi''_d)^2} \tag{5.17}$$

$$\varphi_d = \varphi''_d - X''_d i_d \tag{5.18}$$

$$\varphi_q = \varphi''_q - X''_q i_q \tag{5.19}$$

The initialization of the generator model GENROU is elaborated in the below equations. All the derivatives of state variables at a steady-state are equated to zero and additionally, all the generators stay synchronous i.e.,

$$\omega_r = \omega_{ref} = 1 \tag{5.20}$$

The speed derivate is zero, i.e.,

$$\Delta\omega_r = 0 \tag{5.21}$$

The following set of equations is obtained for the GENROU model, from Equation (5.9) to (5.19):

$$0 = \frac{P_m - D\Delta\omega_r}{\omega_r} \quad - T_e \tag{5.22}$$

$$0 = \omega_0\Delta\omega_r \tag{5.23}$$

$$0 = \frac{1}{T'_{d0}}(E_{fd} - X_{ad}I_{fd}) \tag{5.24}$$

$$0 = \frac{1}{T'_{q0}}(-1)(X_{aq}I_{1q}) \tag{5.25}$$

$$0 = \frac{1}{T''_{d0}}(E'_q - \varphi_{kd} - (X'_d - X_l)i_d) \tag{5.26}$$

$$0 = \frac{1}{T''_{q0}}(E'_d - \varphi_{kq} + (X'_q - X_l)i_q) \tag{5.27}$$

which implies that

$$0 = P_{m0} - T_{e0} \tag{5.28}$$

$$0 = E_{fd0} - X_{ad0}I_{fd0} \tag{5.29}$$

$$0 = X_{aq0}I_{1q0} \tag{5.30}$$

$$0 = E'_{q0} - \varphi_{kd0} - (X'_d - X_l)i_{d0} \tag{5.31}$$

$$0 = E'_{d0} - \varphi_{kq0} + (X'_q - X_l)i_{q0} \tag{5.32}$$

Also,

$$X_{ad0}I_{fd0} = i_{d0}(X_d - X'_d) + E'_{q0} + S_e(|\varphi''_0|\varphi''_{d0}) \tag{5.33}$$

$$0 = -i_{q0}(X_q - X'_q) + E'_{d0} + S_e|\varphi''_0|\frac{X_q - X_l}{X_d - X_l}\varphi''_{q0} \tag{5.34}$$

By doing proper transformation, the equation above can be reduced to:

$$(X_q{}' - X''_q)i_{q0} + \varphi''_{q0}K = 0 \tag{5.35}$$

$$K = \left(1 + S_e|\varphi''_0|\frac{X_q - X_l}{X_d - X_l}\right) \tag{5.36}$$

With the stator voltage equation, all the variables with initial value are determined provided that the amount of the flux linkage and current are mentioned. But the voltage and current phasor $V_t\angle\theta_v$, $I_{t0}\angle\theta_{i0}$ represented by the power flow solution are stated in the synchronous reference frame. However, the initial position of the rotor is also unknown. Proper transformation is required to be made to solve these equalities. By transferring the quantities from *d-q* axes to network coordinate, the Equations (5.35) and (5.36) can be transformed to be stated with δ_0, and on synchronous reference frame $I_{t0}\angle\theta_{i0}$, and $\varphi''_0\angle\theta_{p0}$:

$$(X_q{}' - X''_q)(i_{r0}\,cos(\delta_0) + i_{i0}\,sin(\delta_0)) + K(\varphi_{r0}cos(\delta_0) + \varphi_{i0}sin(\delta_0)) = 0 \tag{5.37}$$

$$|I_{t0}|(X_q{}' - X''_q)cos(\theta_{i0} - \delta_0) + K|\varphi''_0|\,cos(\theta_{p0} - \delta_0) = 0 \tag{5.38}$$

- **Exciter model:**

The model IEEET1 shown in Figure 5.3 represents dc exciters or alternator exciters. When representing dc exciter systems, the constants K_e, V_{max}, V_{min}, are entered as zero to adjust the values automatically. While indicating alternator rectifier systems, the constant K_e is set to unity, and V_{max}, V_{min} are set to zero so that their values are assigned by the routines inside the model. Each block is initialized by assigning an initial value to its state. To initialize the states, the inverse Laplace transform is applied to the given block diagram. For the sake of analysis, the input and output of each block are identified by a letter. After transformation, the following relationship is obtained:

$$a = b + T_R\dot{b} \tag{5.39}$$

$$K_{AC} = d + T_R\dot{d} \tag{5.40}$$

$$e = T_E\dot{f} \tag{5.41}$$

$$K_{Fg} = h + T_F\dot{h} \tag{5.42}$$

The time derivative of all states at steady state is zero and the output of the exciter is kept the same as the field voltage at steady state. Without compensating circuit, the input of the exciter is taken as the preliminary value of measured generator bus voltage.

$$a_0 = V_{t0} \tag{5.43}$$

$$a_0 = b_0 \tag{5.44}$$

$$K_{AC_0} = d_0 \tag{5.45}$$

$$e_0 = 0 \tag{5.46}$$

$$h_0 = 0 \tag{5.47}$$

$$f_0 = E_{fd0} \tag{5.48}$$

where d_0, the initial regulator output V_{R0} can be calculated as follows:

$$V_{R0} = (S_e(E_{fd0}) + 1 + K_E)E_{fd0} \tag{5.49}$$

and the reference voltage is set as:

$$V_{ref} = \frac{V_{R0}}{K_A} - V_{S0} + V_{t0} \tag{5.50}$$

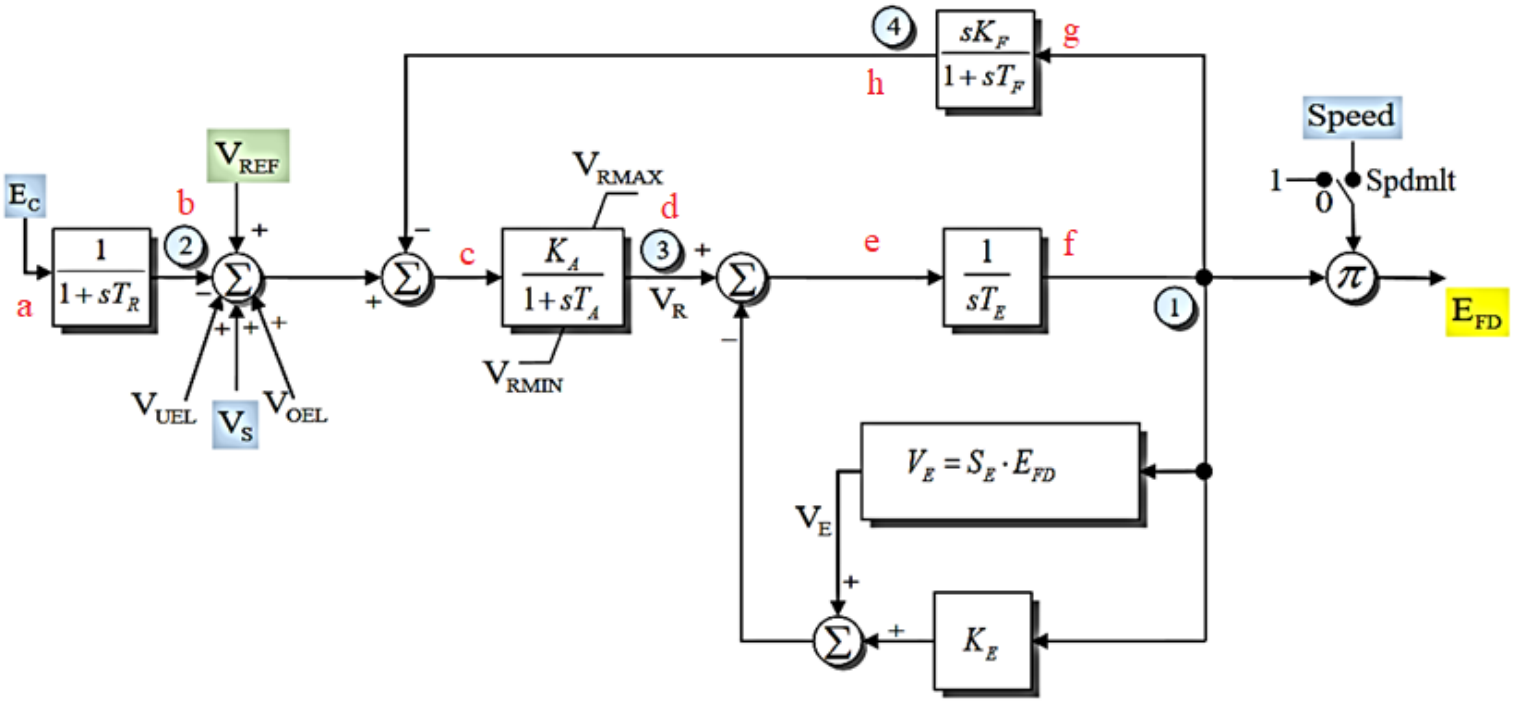

Figure 5.3 Block Diagram of Exciter Model IEEET1

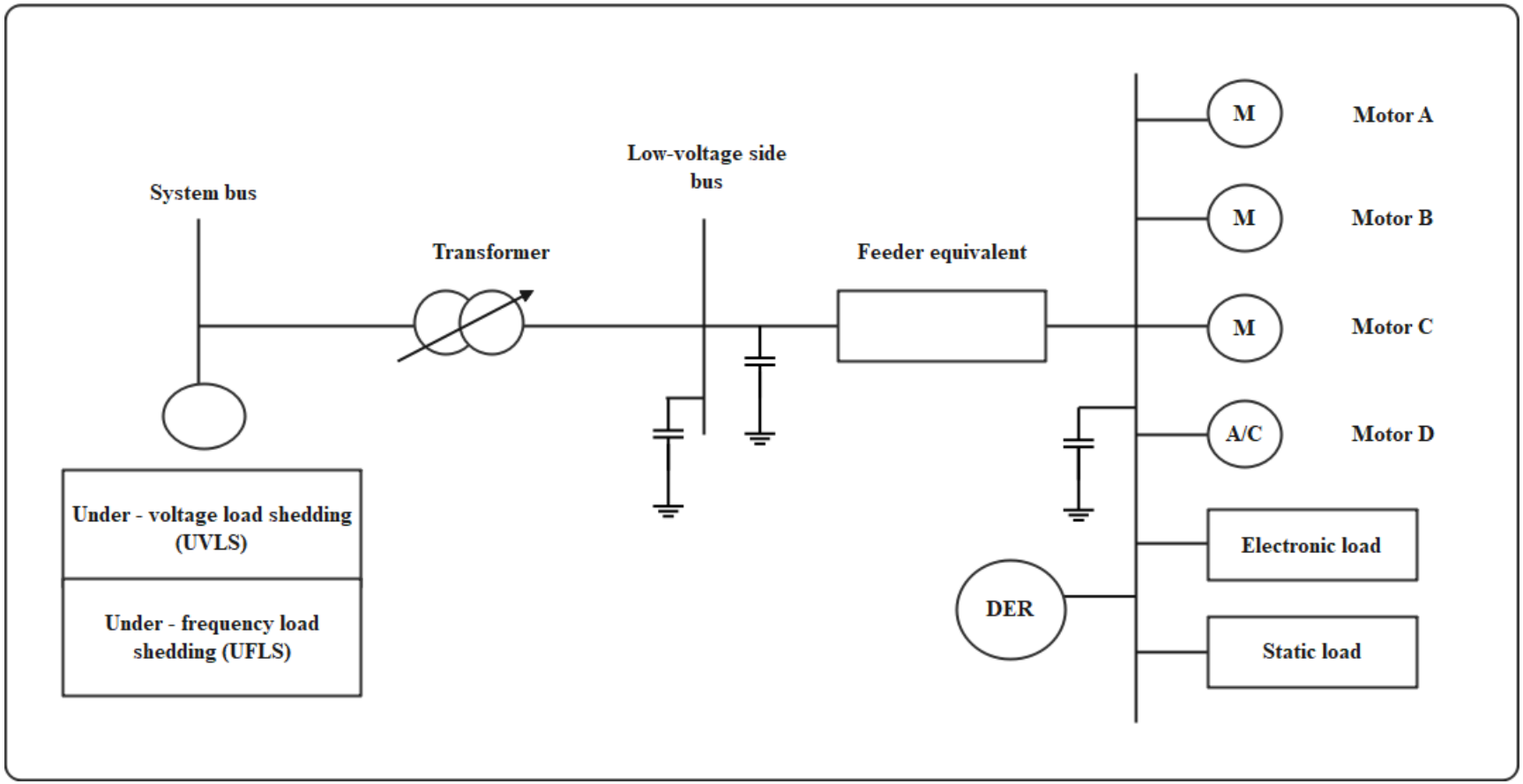

Figure 5.4 Schematic diagram of CMPLDW

- **Composite load model:**

The dynamic composite load model used here is CMPLDW as shown in Figure 5.4 [189]. The internal model produces two buses i.e. low side bus and load bus and is used in the numerical simulation for transient stability. The model works as below:

- Produces a transformer between the transmission bus and the low side bus.
- It develops a capacitor in the bus on the lower side.
- It develops a branch between the load bus and the low side bus.
- The load is moved from the transmission bus to the load bus in this system.

The model involves an electrical representation of a distribution system with a transformer, a feeder equivalent and a shunt reactance. On the distribution system side, it comprises one model with static load, one power electronic model, three three-phase motor models, one A.C. single-phase motor and one Distributed Energy Resource (DER).

5.2 EIGEN VALUE ANALYSIS

The system behaviour depends upon the point of operation. The same system may be stable for a given set of operating points while being unstable at others. The local stability of such systems can be estimated by analyzing eigen values of the system around the operating point. The dynamic and algebraic system equations are linearized around the operating point to calculate these values. Eigen values are calculated using dynamic models of the generator. A linear matrix is constructed from the dynamic states at the equilibrium solution and an analysis of the eigen value and eigen vector is carried out of this matrix. If A is an n-by-n matrix, the n numbers λ that satisfy:

$$\boldsymbol{A}x = \lambda x \tag{5.51}$$

are the eigen values of A. They are found using $eig(A)$, which returns the eigen values in a column vector. Eigen values and eigen vectors can be obtained with a double assignment statement:

$$[X, D] = eig(\boldsymbol{A}) \tag{5.52}$$

The diagonal elements of D are the eigen values and the columns of X are the corresponding eigen vectors such that:

$$\boldsymbol{AX} = \boldsymbol{XD} \tag{5.53}$$

The eigen values of A are the roots of the characteristic equation:

$$det[\boldsymbol{A} - \lambda \boldsymbol{I}] = |\boldsymbol{A} - \lambda \boldsymbol{I}| = 0 \tag{5.54}$$

Assume $\lambda_1, \lambda_2, \ldots\ldots, \lambda_n$ as distinct eigen values. For each eigenvalue λ_i, there exists an eigen vector such that:

$$\boldsymbol{A}\boldsymbol{v}_i = \lambda_i \boldsymbol{v}_i \tag{5.55}$$

where $\boldsymbol{v}_i$ is the right eigen vector. If λ_i is complex, then $\boldsymbol{v}_i$ has complex entries. For each eigen value λ_i, there exists a left eigen vector w_i such that:

$$\boldsymbol{w}_i^t \boldsymbol{A} = \boldsymbol{w}_i^t \lambda_i \tag{5.56}$$

Equivalently, the left eigenvector is the right eigen vector of A^T; that is,

$$\boldsymbol{A}^t \boldsymbol{w}_i = \lambda_i \boldsymbol{w}_i \tag{5.57}$$

The right and left eigen vectors are orthogonal i.e.

$$\mathbf{w}_\mathbf{i}^\mathbf{t}\, \mathbf{v}_\mathbf{i} \neq 0, \mathbf{w}_\mathbf{i}^\mathbf{t}\, \mathbf{v}_\boldsymbol{j} \neq 0 \quad (i \neq j) \tag{5.58}$$

We can normalize the eigen vectors so that:

$$\mathbf{w}_\mathbf{i}^\mathbf{t}\, \mathbf{v}_\mathbf{i} = 1, \mathbf{w}_\mathrm{i}^\mathbf{t}\, \mathbf{v}_\boldsymbol{j} \neq 0 \quad (i \neq j) \tag{5.59}$$

The left and right eigen vectors are used in computing the participation factor matrix. The deviation from an equilibrium point can be defined as

$$\Delta \dot{x} = \boldsymbol{A} \Delta x \tag{5.60}$$

If the initial deviation n corresponds to a right eigen vector, then the subsequent response is along this eigen vector since

$$\boldsymbol{A}\boldsymbol{v}_i = \lambda_i \boldsymbol{v}_i \tag{5.61}$$

From Equation (5.60), it is difficult to determine how parameters in A affect a particular x because of the variable coupling. To decouple the problem first define the matrices of the right and left eigen vectors i.e., the modal matrices:

$$\boldsymbol{V} = [v_1, v_2 \ldots v_n] \;\&\; \boldsymbol{W} = [w_1, w_2, \ldots w_n] \tag{5.62}$$

$$\boldsymbol{AV} = \boldsymbol{V\Lambda}$$

where $\Lambda = diag(\lambda_i)$

It follows that,

$$\boldsymbol{V^{-1}AV = \Lambda} \tag{5.63}$$

To decouple the variables, z is defined such that

$$\Delta x = \boldsymbol{V}z \tag{5.64}$$

Therefore

$$\Delta \dot{x} = \boldsymbol{V}\dot{z} = \mathbf{A}\Delta x = \boldsymbol{A}Vz \tag{5.65}$$

Then

$$\dot{z} = V^{-1}AVz = \boldsymbol{WAV}z = \boldsymbol{\Lambda}z \tag{5.66}$$

Since Λ is diagonal, the equations are now uncoupled with

$$\boldsymbol{\dot{z}_i} = \lambda_i \boldsymbol{z_i} \tag{5.67}$$

So

$$\Delta x(t) = \boldsymbol{V}\boldsymbol{z}(t) \tag{5.68}$$

Thus, the response can be written in terms of the individual eigen values and right eigen vectors as

$$\Delta x(t) = \sum_{i=1}^{n} \boldsymbol{v_i z_i}(0) e^{\lambda_i t} \tag{5.69}$$

Further with

$$\Delta x = \boldsymbol{VZ} \tag{5.70}$$

This implies

$$z = \boldsymbol{V^{-1}}x = \boldsymbol{W^T}x \tag{5.71}$$

So, $z(t)$ is written using the left eigen vectors as:

$$z(t) = \boldsymbol{W^t x}(t) = [w_1 \quad w_2 \quad w_3 \quad \dots \quad w_n]^t \begin{bmatrix} x_1(t) \\ \vdots \\ x_n(t) \end{bmatrix} \tag{5.72}$$

The eigen values must be distinct. We can then write the response $x(t)$ in terms of the modes of the system.

$$z_i(t) = \boldsymbol{w}_i^t \mathrm{x(t)} \tag{5.73}$$

$$z_i(0) = \boldsymbol{w}_i^t \mathrm{x(0)} \triangleq c_i$$

So,

$$x(t) = \sum_{i=1}^{n} \boldsymbol{v}_i c_i e^{\lambda_i t} \tag{5.74}$$

Expanding,

$$\Delta x_i(t) = v_{i1} c_1 e^{\lambda_1 t} + v_{i2} c_2 e^{\lambda_2 t} + \ \ldots \ v_{in} c_n e^{\lambda_n t} \tag{5.75}$$

So c_i is a scalar that represents the magnitude of excitation of the i^{th} mode from the initial conditions.

5.2.1 INEQUALITY CONSTRAINTS

Inequality constraints keep the damping ratio positive for the critical eigen value and maintain the real part of the critical eigen value as non–zero values [115]. It is given as:

$$min(\xi_{cri}) \geq 0 \tag{5.76}$$

where ξ is the damping ratio for critical eigen value. Also, real, and imaginary parts of eigen value should not be equal to zero.

$$|v^r| \neq 0 \tag{5.77}$$

$$\left|v^i\right| \neq 0 \tag{5.78}$$

where v^r and v^i are the real and imaginary parts of eigen value.

5.2.2 SMIB EIGEN ANALYSIS

To generate the results, a SMIB eigen analysis is carried out. After the analysis, positive eigen values are sorted by writing these in descending order and negative values with large magnitude are found by arranging these in ascending order. Potentially unstable system states are represented by the positive eigen values, whereas greater negative eigen values signify a rapid system state which may represent numerical instability.

The stability of a nonlinear system is given by the roots of the characteristic equation of the system of first approximations that is by the eigen values. The positive real

part of eigen values (at least one) indicates that the original system is unstable. When the eigen values have negative real parts, the original system is asymptotically stable. When the real part of the eigen values is zero, it is critically unstable.

The SMIB eigen value analysis has proven very useful during the checking of model data input. In this dynamic model, one generator is attached to an infinite bus. All the dynamic models of the generator namely machine model, exciter, governor, and stabilizer have been incorporated in this model. A linear matrix is developed for all the dynamic states at the steady-state solution and eigen value and eigen vector analysis is performed on this matrix.

After running the SMIB eigen analysis, the results are sorted in descending order by the maximum eigen value column to find out any positive eigen value or in ascending order by minimum eigen value to observe negative eigen values with a large magnitude. Positive eigen values correspond to possibly unstable system states, whereas large negative eigen values represent exceptionally fast states of the system which may result in numerical instability. The large negative eigen values are caused by exciter models which contain extremely fast feedback loops.

5.3 SEAMB METHOD FOR CALCULATING DATC

The SEAMB method for calculating DATC is a method wherein transient stability is limited by the highest permissible transfer. This process involves screening the contingencies. In the present work, a condition for critical sensitivity in terms of eigen values is observed. The transfer is increased from the base value till the HB point is reached. The final value of ATC obtained at this juncture is treated as Dynamic ATC. This method is more reliable than all the prevalent ones as it does not use any convergent algorithm.

5.3.1 RELATIONSHIP OF EIGEN VALUES WITH DATC

The system is asymptotically stable in the neighbourhood if the real part of all the eigen values is negative. If a complex pair of eigen values have zero real part, the system is marginally stable and may exhibit limit cycles. If, on the other hand, any of the eigen values have a positive real part, the system is unstable.

In the present study, SMIB Eigen Area-based Modal Bifurcation (SEAMB) sensitivity method has been used for the assessment of DATC. The eigen values have been

used as an index in determining the HB limit. The sudden change in the system behaviour is treated as a system parameter and is dealt with by the bifurcation theory. The change is brought out by a pair of complex conjugates eigen values crossing the imaginary axis leading to HB.

The information about eigen values, eigen vectors (left or right), participation factors, and mode shape is given by modal analysis. Modal analysis is the analysis of small-signal stability through eigen value analysis. The goal is to determine how the various parameters affect the response of the system.

5.3.2 SADDLE NODE BIFURCATION (SNB)

At saddle-node, an eigen value of the system Jacobian becomes zero. In the power system, saddle-node bifurcation has also been indicted by the non-convergence of the load-flow algorithm at the critical point where one of its eigen values becomes zero.

The SNB is characterized by a zero eigen value. The response of the system at a saddle-node is monotonic. In an autonomous system of ordinary differential equations:

$$\dot{y} = g(y, \dot{\beta}), \quad y \in R^n \tag{5.79}$$

depending on a parameter $\beta \in R$, where function g is smooth. Suppose that at

$$\beta = 0 \tag{5.80}$$

the system has an equilibrium,

$$y^0 = 0 \tag{5.81}$$

Further, assume that it's a Jacobian matrix

$$A_0 = g_y(0,0) \tag{5.82}$$

has a simple eigen value,

$$\lambda_1 = 0 \tag{5.83}$$

Then, generically, as β passes through $\beta = 0$, two equilibria collide, form a critical saddle-node equilibrium, and disappear. This bifurcation is characterized by a single bifurcation condition given by Equation (5.83).

5.3.3 HOPF BIFURCATION METHOD (HB)

HBs, referred to as oscillatory bifurcation, generate limit cycles resulting in oscillatory instabilities. SNB is, however, characterized by zero eigen values where the system response at the saddle is monotonous. It is a fact that forcing a pair of complex eigen values to cross the imaginary axis in the complex plane can make the system unstable. This oscillatory instability linked to nonlinear systems is called HB limit and further leads to dynamic voltage instability.

It is obtained by a pair of complex conjugate eigen values crossing the imaginary axis leading to HB. At this point, one pair of the complex eigen values become purely imaginary. If J_0 is the Jacobian of a continuous parametric dynamical system evaluated at a steady point Z_e and if all eigen values of J_0 have negative real part except for one conjugate nonzero purely imaginary pair $\pm j\beta$, a Hopf bifurcation arises when these two eigen values cross the imaginary axis because of a variation of the system parameters. The Hopf bifurcation limit is reached when one of the pairs of eigen values crosses the imaginary axis.

The change is brought about by the merging of two different points of equilibrium: stable and unstable (SNB), and by a pair of complex conjugate, eigen values crossing the imaginary axis (HB). HB limit is computed as per the procedure given below. A set of differential-algebraic equations are described as [115]:

$$\dot{x} = f(x, y, T) \tag{5.84}$$

$$0 = g(x, y, T) \tag{5.85}$$

where,

- x is described as a vector of state variables controlling the generators' dynamics, loads and controls,
- y is stated as the vector of variables (algebraic) of load flow equation and,
- T is the operating parameter for the HB limit.

The state matrix is computed by manipulating the complete Jacobian matrix J, which is defined by the linearization of the system equation at the initial operating point (x^*, y^*)

$$\begin{bmatrix} \dot{\Delta x} \\ 0 \end{bmatrix} = [\boldsymbol{J}] \begin{bmatrix} \Delta x \\ \Delta y \end{bmatrix} \tag{5.86}$$

where **J** is the unreduced Jacobian of the system,

$$\boldsymbol{J} = \begin{bmatrix} f_x & f_y \\ g_x & g_y \end{bmatrix} \tag{5.87}$$

To obtain a state matrix, eliminate the algebraic variables, and hence assume that g_y is non-singular from the above equation. Thus, the state matrix of the linearized system is obtained as:

$$\dot{\Delta x} = \begin{bmatrix} f_x & -f_y & {g_y}^{-1} & g_x \end{bmatrix} \Delta x = \boldsymbol{A}_{red} \Delta x \tag{5.88}$$

where

$$\boldsymbol{A}_{red} = \begin{bmatrix} f_x & -f_y & {g_y}^{-1} & g_x \end{bmatrix} \tag{5.89}$$

and **A** is known as the reduced Jacobian in contrast to the unreduced one. The eigen value of the **A** matrix describes the equilibrium point stability of this system for a given T. The eigen value of the reduced system matrix is given by:

$$\boldsymbol{A}_{red} v = \mu v \tag{5.90}$$

where μ is the eigen value and v is the associated right eigen vector. Figure 5.5 shows the complex eigen values of an arbitrary map (dots). In the case of the HB, two complex conjugate eigen values cross the imaginary axis where λ_i is the parameter of eigen value.

5.3.1 ALGORITHM AND FLOW CHART OF SEAMB METHOD

In the SEAMB method, firstly ATC is calculated considering all the constraints. Then ATC is calculated using a single linear step technique. This value is calculated considering line flow constraints. After that transient stability analysis is done and eigen values are observed using SMIB analysis. Further, the power is transferred between seller and buyer areas and is increased step by step after observing eigen values at every increased MW transfer. This is continued till the SNB limit. After that power is further increased to achieve the HB limit. The value thus obtained is noted as DATC.

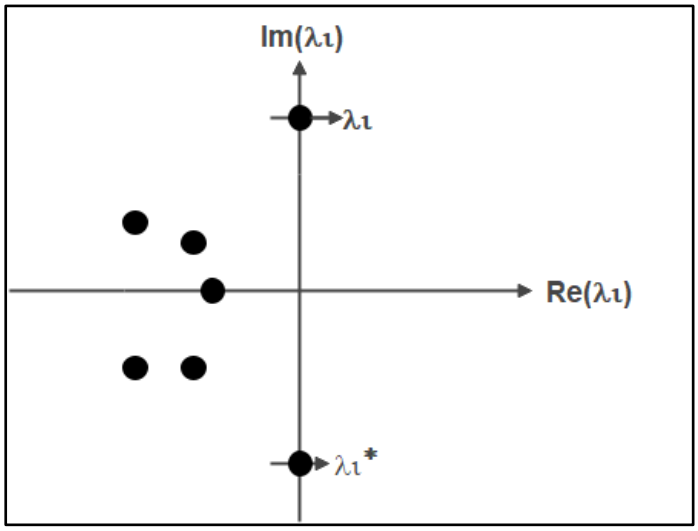

Figure 5.5 Complex eigen values of an arbitrary map (dots). In the case of the Hopf bifurcation, two complex conjugate eigen values cross the imaginary axis

The step-by-step procedure for calculating DATC by the SEAMB method is given below:

1. Load the bus data, line data, and the parameters of the power system model.
2. Identify areas and specify the transaction between areas.
3. Run power flow for base case loading condition and obtain base case ATC.
4. Perform transient stability analysis for specified contingency.
5. Compute eigen values through SMIB analysis.
6. Calculate the value of ATC.
7. Check if the HB limit has reached. If not, increase the power transaction in small steps and go to step 5.
8. Obtain the critical eigen value and treat ATC as DATC and stop.

5.4 RESULTS AND DISCUSSION

The DATC has been calculated by the SEAMB sensitivity method by dividing the system into areas. The dynamic ATC has been calculated for various fault conditions. These conditions include:

- 3 phase bus fault
- 3 phase line fault
- 3 phase bus fault and line opening

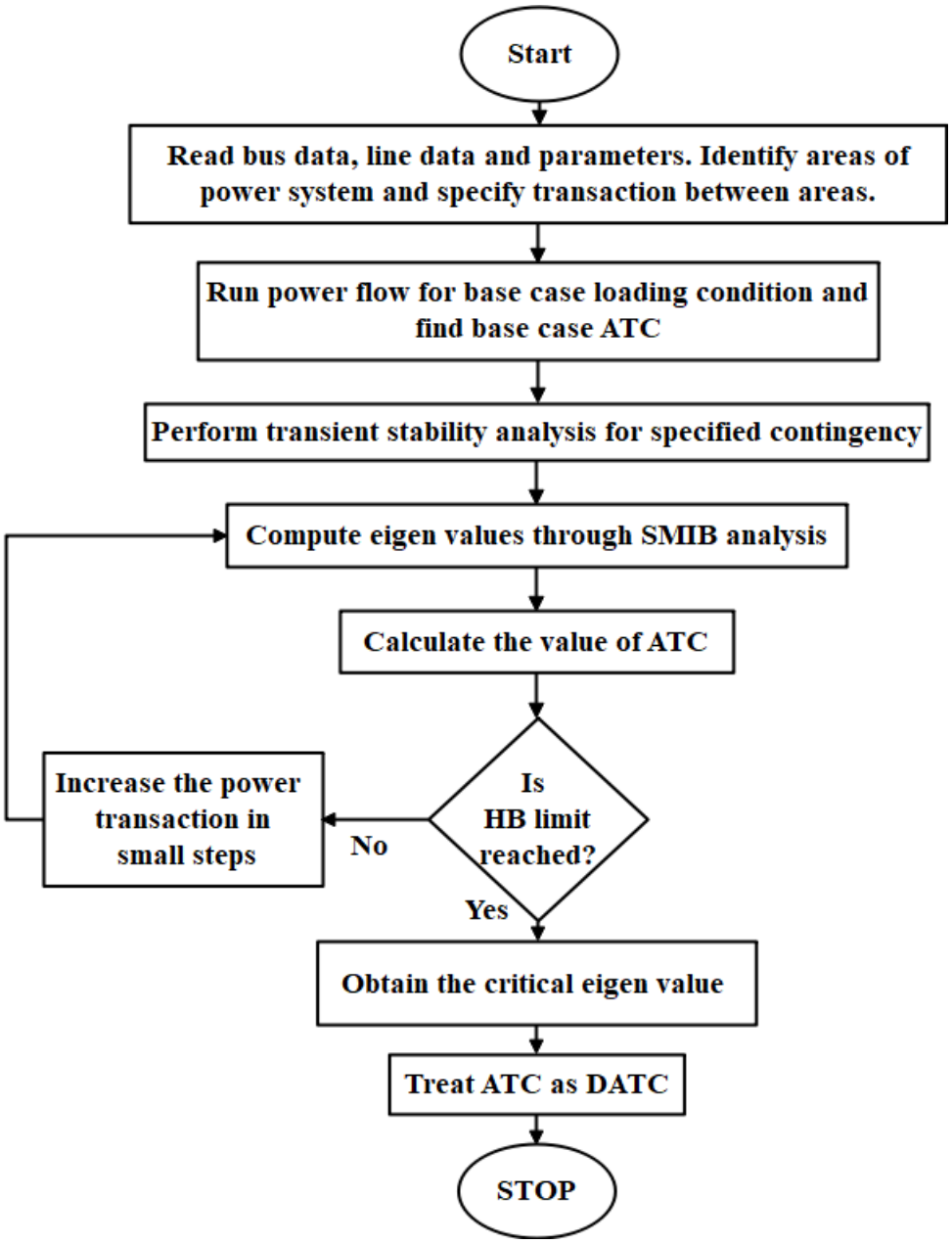

Figure 5.6 Flowchart of DATC using the SEAMB method

The performance has been carried out for two systems namely the 9-bus system and 39-bus system. The DATC has been calculated for the above-specified fault conditions with static load and dynamic composite load. The generator and excitation system parameters are presented in Table 5.1 and Table 5.2 respectively.

5.4.1 9 BUS SYSTEM ANALYSIS

A 9-bus three-machine system [20] shown in Figure 5.7 is used to validate the proposed algorithm. The system is represented as two areas equivalent for the analysis of DATC, where Area 1 consists of buses 1, 2, 4, 5, 7 and 8 while Area 2 consists of buses 3, 6 and 9.

Table 5.1 Generator Parameters

Parameters	Values
H	2.56
D	0
R_a	0
X_d	2.2395
X_q	2.161
X_{dp}	0.2995
X_{qp}	0.49225
X_{dpp}	0.225
X_l	0.15
T_{dop}	6
T_{qop}	0.53
T_{dopp}	0.03
T_{qopp}	0.05
S_1	0
S_{12}	0
R_{comp}	0
X_{comp}	0

The power transaction is assumed to take place between areas. The load as specified in Figure 5.7 is taken as the static load for ATC calculation. The load nature of bus 8 is changed to composite load for dynamic ATC calculation. The DATC for all the cases has been obtained using the proposed SEAMB algorithm.

- **DATC for three-phase fault at bus:**

The DATC has been calculated for three-phase short circuit fault at different buses corresponding to Area 1 and Area 2 for static and dynamic composite loads. These buses are number 9 (Area 2) and number 4 and 5 (Area 1) respectively. During each run, the system was assumed to be healthy and the three-phase balanced faults are initiated at 0.1s. The corresponding results are summarized in Table 5.3, where DATC values have been evaluated with the SEAMB method. The values found under dynamic load are found to be lesser as compared to that of static load.

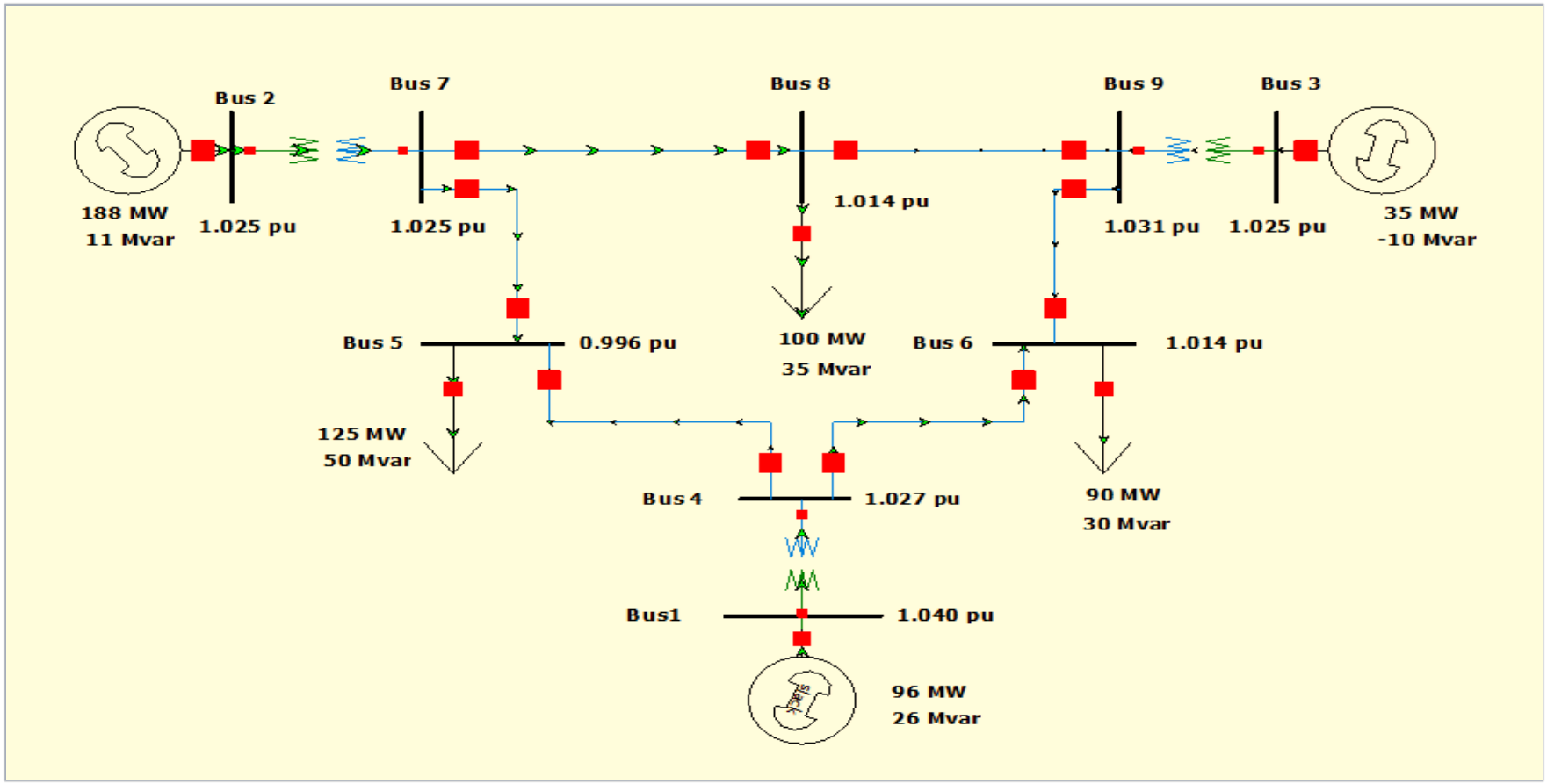

Figure 5.7 Line diagram of 9 bus system

Table 5.2 Exciter Parameters

Parameters	Values
T_r	0
K_a	20
T_a	0.2
V_{rmax}	3
V_{rmin}	-3
K_e	1
T_e	0.314
K_f	0.063
T_f	0.35
S_{witch}	0
E_1	2.8
SE_1	0.30338
E_2	3.73
SE_2	1.2884
S_{pdmit}	0

Table 5.3 Comparison of DATC values evaluated with SEAMB method under static and dynamic load for various faults at buses

Fault No.	Fault Bus	DATC (Static load) (MW)	DATC (Dynamic load) (MW)
1	9	3.53	2.53
2	4	29.63	28.14
3	5	3.08	3.36

The system ATC value was 29.63 MW when power transfer was not initiated and the system was in healthy condition. For a three-phase short circuit fault at bus 9, it is observed that the transfer can be increased by 26.1 MW from area 1 to area 2 till the HB limit is reached. The DATC value hence obtained under static load is 3.53 MW. Similarly, under dynamic load, the DATC value observed is 2.53 MW. The value observed under dynamic load is found to be 39.5% lesser than that of static load. For the three-phase short circuit fault at bus 4, the HB limit is reached after transferring 1.395 MW from area 1 to area 2 under dynamic load. Correspondingly, the DATC value thus obtained is 28.14 MW. Under static load, the HB limit is attained without any transfer and thus DATC value is 29.63 MW. The value observed under dynamic load is 5% less than that of static load. With a similar procedure, for a short circuit fault at bus 5, the power transfer can be increased by 26.451 MW and 26.17 MW from area 1 to area 2 till the HB limit is reached for static

and dynamic load respectively. The DATC value hence obtained are 3.08 MW and 3.36 MW for static and dynamic load respectively. The value observed under static load is found to be 9% lesser than that of dynamic load. The values obtained in Table 5.3 are shown in Figure 5.8. The values observed under dynamic load are lesser as compared to static load except at fault at bus 5. Table 5.4 summarizes minimum eigen values of the three generators of 9 bus system during three-phase bus fault at the respective fault numbers at HB limit.

Table 5.4 Minimum eigen values obtained after three phase bus fault at HB limit for DATC calculated by SEAMB method for 9 bus system

Generator No./Fault No.	1	2	3
1	-0.0506	0.0002	0.0005
2	-0.0080	-0.1413	-0.4732
3	0.0009	-0.2020	-0.0102

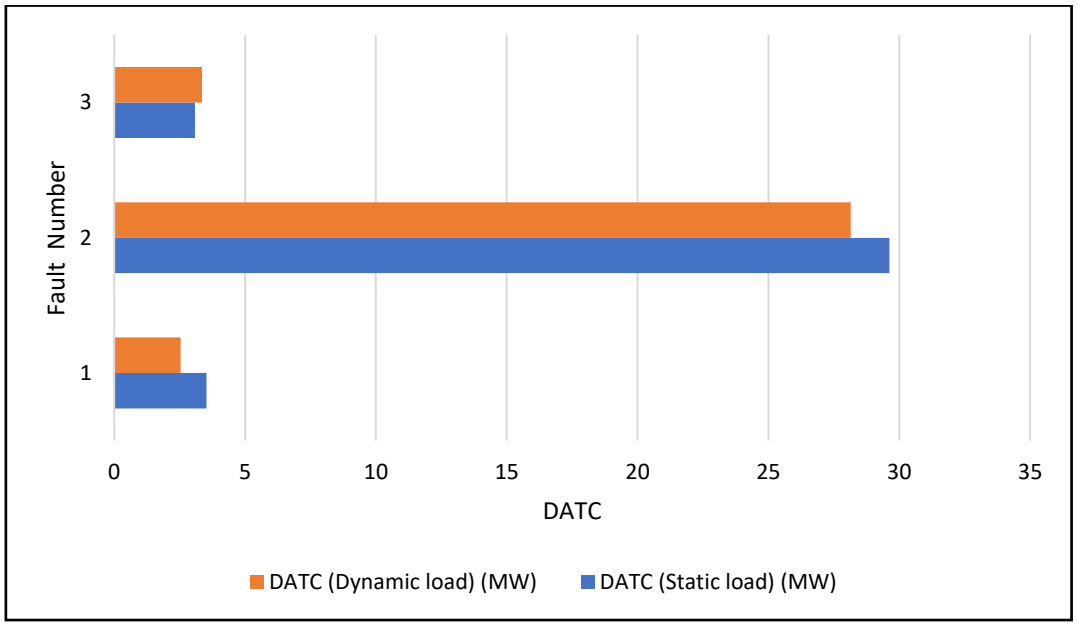

Figure 5.8 Assessment of DATC values calculated with the presented SEAMB method for various faults at buses under static and dynamic load

- **DATC for three-phase bus fault and line opening:**

In this case, the DATC has been calculated for three-phase short circuit fault at different buses followed by the opening of the respective line as shown in Table 5.5 corresponding to Area 1 and Area 2 for static and dynamic composite loads. These buses

are number 9 (Area 2) and number 4 and 5 (Area 1) respectively. During each run, the system was assumed to be healthy and the three-phase balanced faults are initiated at 0.1s. The respective line is tripped at 0.15s. The corresponding results are summarized in Table 5.5, where DATC values have been evaluated with the SEAMB method. The values found under dynamic load are found to be lesser as compared to that of static load.

Table 5.5 Evaluation of DATC values calculated with SEAMB method for 9 bus system for three-phase bus fault and consequent line opening under static and dynamic load

Fault No.	Fault Bus	From Bus	To Bus	SEAMB (Static load) (MW)	SEAMB (Dynamic load) (MW)
1	9	8	9	1.743	1.53
2	4	6	4	3.144	3.01
3	5	4	5	3.547	3.36

For the three-phase short circuit fault at bus 9 and subsequent opening of line 8-9, it is scrutinized that the transfer can be increased by 28 MW from area 1 to area 2 till the HB limit is reached. The DATC value hence obtained under dynamic load is 1.53 MW. Similarly, under static load, the DATC value observed is 1.743 MW. The value observed under dynamic load is found to be 14% lesser than that of static load. For the three-phase short circuit fault at bus 4 and corresponding opening of line 6-4, eigen values are observed. The HB limit is reached after transferring 26.5 MW from area 1 to area 2 under dynamic load. Correspondingly, the DATC value thus obtained is 3.01 MW.

Under static load, the HB limit is attained with the transfer of 26.4 MW and thus DATC value is 3.14 MW. The value observed under dynamic load is 4.3% less than that of static load. With a similar procedure, for a short circuit fault at bus 5, followed by the opening of line 4-5, the power transfer can be increased by 26.083 MW and 26.175 MW from area 1 to area 2 till the HB limit is reached for static and dynamic load respectively. The DATC value hence obtained are 3.547 MW and 3.36 MW for static and dynamic load respectively. The value observed under dynamic load is found to be 5.5% lesser than that of static load. The values obtained in Table 5.5 are shown in Figure 5.9. The values observed under dynamic load are lesser as compared to static load.

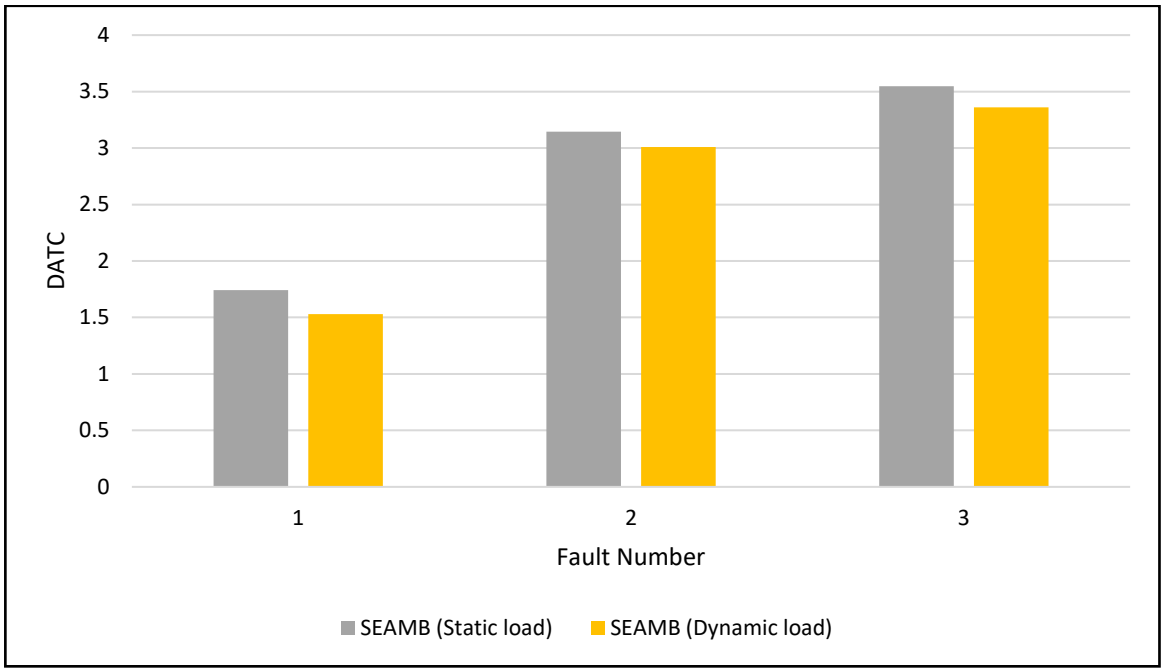

Figure 5.9 Comparison of Dynamic ATC values under static and dynamic load for three-phase bus fault and line opening for 9 bus system

5.4.2 39 BUS SYSTEM ANALYSIS

A 39-bus 10 machine system [24] shown in Figure 5.10 is used to validate the proposed algorithm. The system is represented as three area equivalent for the analysis of DATC, where Area 1 consists of buses 2, 3, 25, 26, 27, 28, 29, 30, 37 and 38 while Area 2 consists of buses 4, 5, 6, 7, 10, 11, 12, 13, 14, 15, 16, 17, 18, 19, 20, 21, 22, 23, 24, 31, 32, 33, 34, 35 and 36. Area 3 consists of buses 1, 8, 9 and 39. The power transaction is assumed to take place amongst areas. The load as specified in the Figure 5.10 is taken as a static load for ATC calculation. The load nature of bus 18 is changed to composite load for dynamic ATC calculation. The DATC for all the cases has been obtained using the proposed SEAMB algorithm.

- **DATC for three-phase fault at bus:**

The DATC has been calculated for a three-phase short circuit fault at bus number 39 corresponding to Area 3 as listed in Table 5.6 for dynamic composite load at various transactions as listed in Table 5.7. During each run, the system was assumed to be healthy and the three-phase balanced fault is initiated at 0.1s. The corresponding results are summarized in Table 5.8, where DATC values have been evaluated with the SEAMB

method. The observation of DATC done under transaction T2 through the dynamic load is found to be least as compared to the other two transactions.

Table 5.6 Configuration of buses into areas

Area	Buses
1	2, 3, 25, 26, 27, 28, 29, 30, 37, 38
2	4, 5, 6, 7, 10, 11, 12, 13, 14, 15, 16, 17, 18, 19, 20, 21, 22, 23, 24, 31, 32, 33, 34, 35, 36
3	1, 8, 9, 39

Table 5.7 Transactions involved based upon areas in 39 bus system

Transaction	Configuration
T1	Area 1 to Area 2
T2	Area 2 to Area 3
T3	Area 3 to Area 1

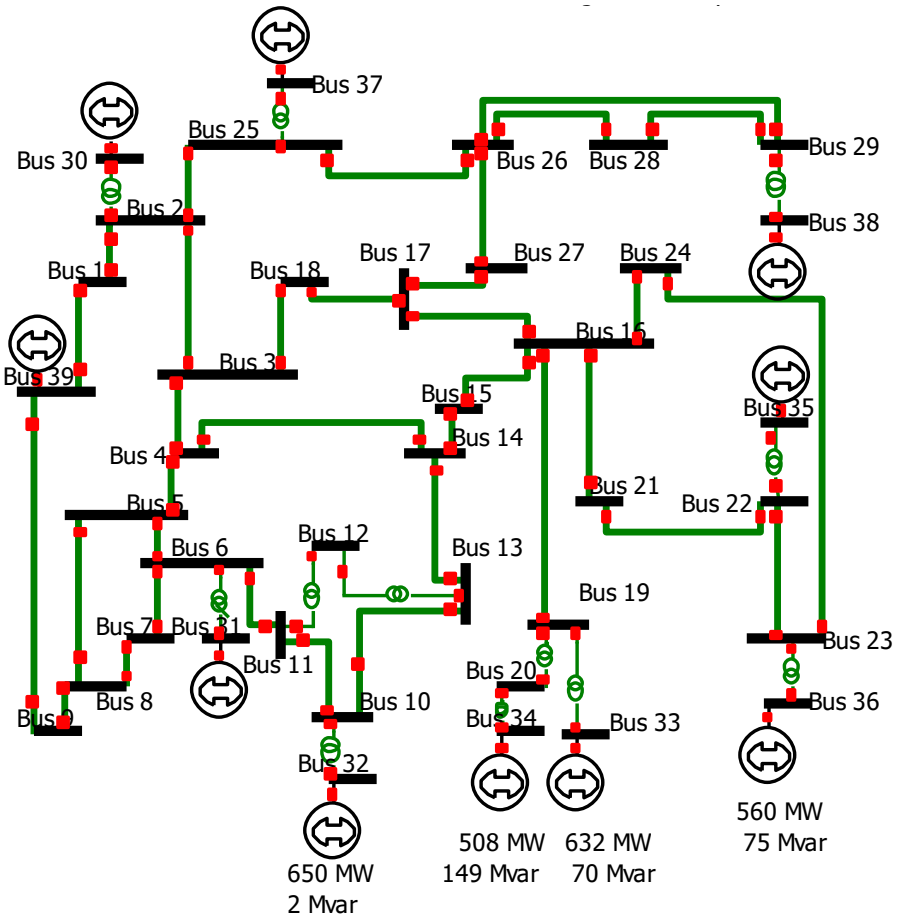

Figure 5.10 Line diagram of 39 – bus system

The system ATC value was 1954 MW during transaction T1, 1104 MW for transaction T2 and 2619 MW for transaction T3, when power transfer was not initiated and system was under healthy condition. For three phase short circuit fault at bus 39 at 0.1s, it is observed that the transfer can be increased by 300 MW from area 1 to area 2 till the HB limit is reached. The DATC value hence obtained under dynamic load is 1757 MW. For the transaction from area 2 to area 3, eigen values are observed. The HB limit is reached after transferring 30 MW between areas under dynamic load. Correspondingly, the DATC value thus obtained is 1074 MW. With the similar procedure, for transaction T3, the power transfer can be increased by 20 MW till the HB limit is reached for dynamic load. The DATC value hence obtained is 2597 MW. The values obtained in Table 5.8 are shown in Figure 5.11.

Table 5.8 DATC values calculated from SEAMB method at various transactions considering fault at bus 39 under dynamic load

S. No.	Transaction	DATC (Dynamic load) (MW)
1	T1	1757
2	T2	1074
3	T3	2597

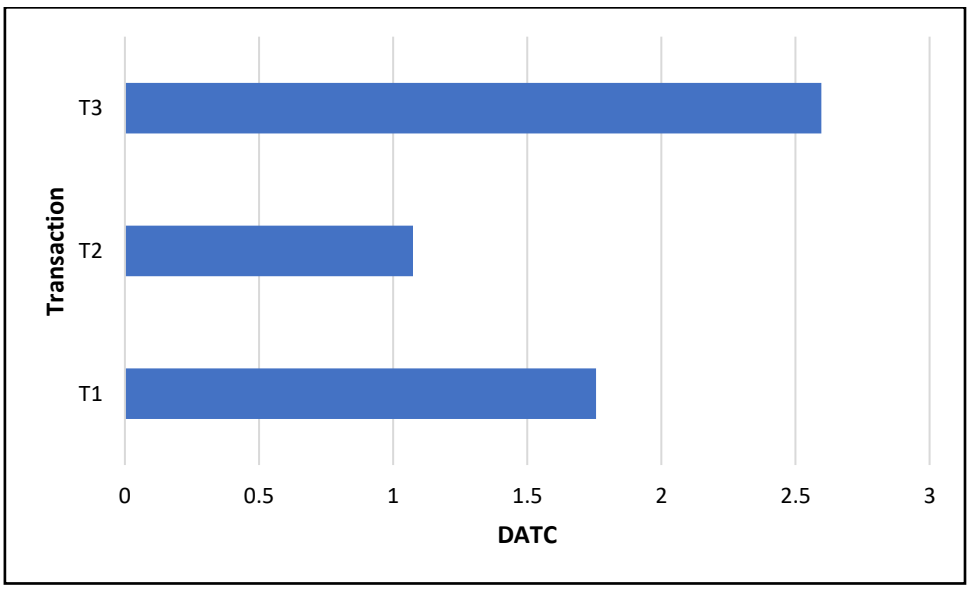

Figure 5.11 Comparison of DATC values evaluated by SEAMB method considering fault at bus 39 under various transactions between areas

- **DATC for three-phase fault at line:**

The DATC has been calculated for three-phase short circuit fault at different lines corresponding to transaction T1 for dynamic composite loads. These lines are 29-28, 10-13, 25-2 and 39-1 respectively. During each run, the system was assumed to be healthy and the three-phase balanced faults are initiated at 0.1s for all lines except at line 39-1, where the fault is initiated at 0.01s. All lines tripped at 0.15s one by one after experiencing the fault. The corresponding results are summarized in Table 5.9, where DATC values have been evaluated with the SEAMB method and are found under dynamic load.

The system ATC value was 1954 MW during transaction T1 when power transfer was not initiated and system was under healthy condition. For three phase short circuit fault at line 29-28 at 0.1s, it is observed that the transfer can be increased by 89 MW from area 1 to area 2 till the HB limit is reached. The DATC value hence obtained under dynamic load is 1866 MW For the transaction from area 1 to area 2 and three-phase short circuit fault at line 10-13, eigen values are observed. The HB limit is reached after transferring 192 MW between areas under dynamic load.

Table 5.9 DATC values evaluated after considering fault at lines under dynamic load for transaction T1

S. No.	From Bus	To Bus	DATC (Dynamic load) (MW)
1	29	28	1866
2	10	13	1765
3	25	2	1954
4	39	1	1811

Correspondingly, the DATC value thus obtained is 1765 MW With a similar procedure, for line 25-2, the HB limit is reached without any transfer. The DATC value obtained is 1954 MW. For fault at line 39-1, power transfer can be increased by 146 MW till the HB limit is reached for dynamic load. The DATC value hence obtained is 1811 MW. The values obtained in Table 5.9 are shown in Figure 5.12.

- **DATC for three-phase bus fault and line opening:**

In this case, the DATC has been calculated for a three-phase short circuit fault at different buses followed by the opening of the respective line as shown in Table 5.10 corresponding to transaction T1 for static and dynamic composite loads. These buses are

number 25 and 29 (Area 1), number 10 (Area 2) and number 39 (Area 3) respectively. During each run, the system was assumed to be healthy and the three-phase balanced faults are initiated at 0.1s. The respective line is tripped at 0.15s. The corresponding results are summarized in Table 5.10, where DATC values have been evaluated with the SEAMB method. The values found under dynamic load are found to be lesser as compared to that of static load.

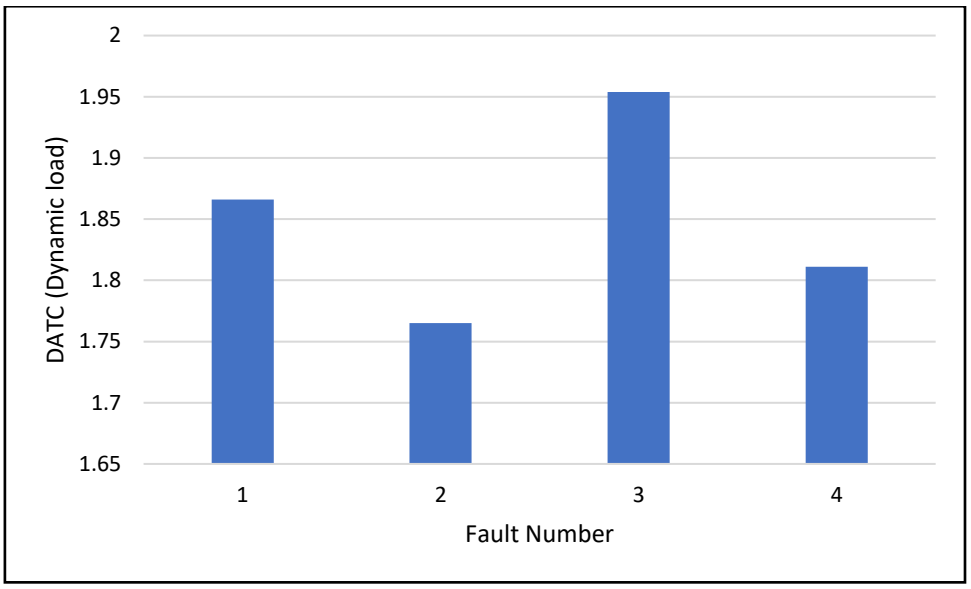

Figure 5.12 Comparison of DATC values calculated under dynamic load by SEAMB method for faults at different lines

Table 5.10 Transient contingencies and DATC results for transaction T1 by SEAMB technique under static load (39 bus system)

Fault No.	Fault Bus	From Bus	To Bus	Static Load (MW)	Dynamic Load (MW)
1	29	29	28	3547	1954
2	10	10	13	2958	2004
3	25	25	2	2960	1984
4	39	39	1	1957	1678

For the three-phase short circuit fault at bus 29 and subsequent opening of line 29-28, it is scrutinized that the HB limit is reached without any transfer. The DATC value hence obtained under dynamic load is 1954 MW. Similarly, under static load, the DATC value observed is 3547 MW. The value observed under dynamic load is found to be 81% lesser than that of static load. For the three-phase short circuit fault at bus 10 and corresponding opening of line 10-13, eigen values are observed as shown in Table 5.11.

The HB limit is reached after transferring 50MW from area 2 to area 1 under dynamic load. Correspondingly, the DATC value thus obtained is 2004 MW. Under static load, the DATC value is 2958 MW. The value observed under dynamic load is 48% less than that of static load. With a similar procedure, for a short circuit fault at bus 25, followed by the opening of line 25-2, the power transfer can be increased by 30 MW from area 2 to area 1 from area 1 to area 2 till the HB limit is reached for dynamic load. The DATC value hence obtained is 1984 MW for dynamic load respectively. The value observed under dynamic load is found to be 49.5% lesser than that of static load.

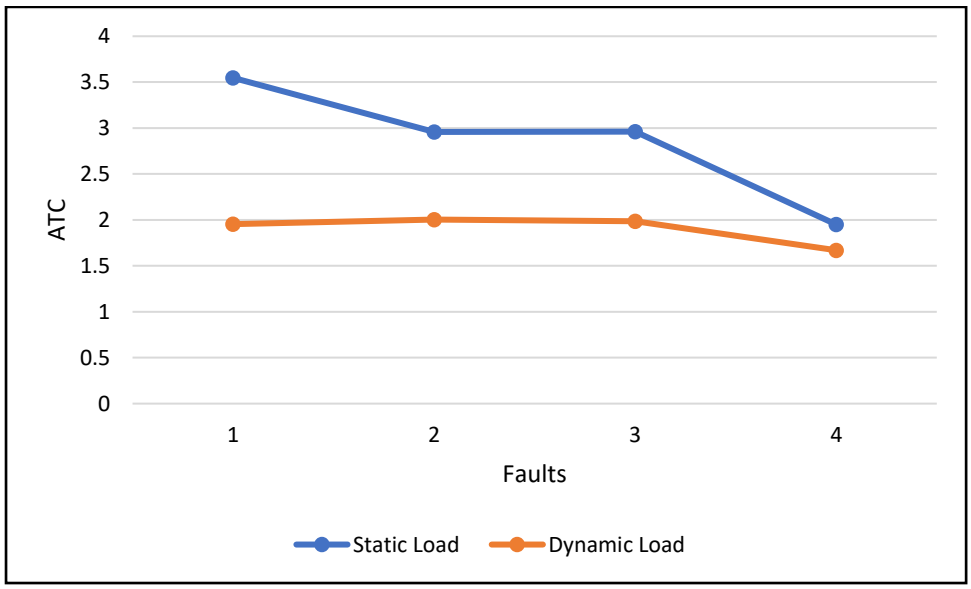

Figure 5.13 Comparison of DATC values under static and dynamic load for SEAMB technique

For the three-phase short circuit fault at bus 39 and corresponding opening of line 39-1, the HB limit is reached after transferring 280 MW from area 1 to area 2 under dynamic load. Correspondingly, the DATC value thus obtained is 1678 MW. Under static load, the DATC value is 1957 MW. The value observed under dynamic load is 17% less than that of static load. The values obtained in Table 5.10 are shown in Figure 5.13. The values observed under dynamic load are lesser as compared to static load. Table 5.11 summarizes the minimum eigenvalues obtained at HB point under dynamic load through the SEAMB method for calculating DATC for three-phase bus fault and line opening.

Table 5.11 Minimum eigen values obtained at HB point under dynamic load through SEAMB method for calculating DATC for three-phase bus fault and line opening

Generator No./Fault No.	1	2	3	4
30	-0.1	-0.1	-0.1	-0.1
31	-0.1	-0.1	-0.1	-0.1
32	-0.1	0.0004	-0.1	-0.1
33	-0.1001	-0.1001	-0.1001	-0.1001
34	-0.1001	-0.1001	-0.1001	-0.1001
35	-0.1002	-0.1002	-0.1002	-0.1002
36	-0.1006	-0.1003	-0.1006	-0.1003
37	-0.1001	-0.1001	0.0002	-0.1001
38	0.0002	-0.1001	-0.1001	0.0054
39	-0.1	-0.1	-0.1	0.0001

5.5 CHAPTER SUMMARY

The SEAMB technique is presented to analyze the DATC when the system is subjected to dynamic conditions. The analysis is carried out using PWS. The performance is evaluated by dividing the transmission lines into areas. It also summarizes the eigen value analysis using the bifurcation method. The DATC values are presented for WSCC 9 bus system and the New England 39-bus system when subjected to various faults and contingencies. The following conclusions are drawn from the investigation:

- The system is divided into areas and various transactions between them are considered under static and dynamic load.
- The values of DATC obtained from the proposed method are evaluated for three-phase bus faults, three-phase line faults and three-phase bus faults and line opening.
- The values of DATC are found to be depending on the areas where bilateral transactions are taking place.
- The values of ATC under dynamic conditions (DATC) are found to be lower than the respective pre-fault values.
- The values of DATC under dynamic load are found to be lower than that of static load.
- For 9 bus system, DATC obtained under dynamic load for three phase fault at bus number 9 followed by opening of line 8-9, is found to be 14% lesser than that of static load.

- Similarly, for 39 bus system, DATC obtained under dynamic load for three phase fault at bus number 29 followed by opening of line 29-28, is found to be 81% lesser than that of static load.

Chapter 6 Conclusions and Scope for Future Work

In deregulated structure, the system operator needs to calculate the Available Transfer Capability (ATC) of the network. Depending on operating static or dynamic operating conditions, the ATC can be classified as Static ATC (SATC) or Dynamic ATC (DATC). The most appropriate way to enhance the ATC is through the usage of a Thyristor Controlled Series Capacitor (TCSC). The TCSC acts as a series compensator to transmission line reactance and thus enhances the transfer capability. The optimal placement of TCSC complements the enrichment of ATC.

In the present work, the allocation of TCSC has been accomplished by the SPCR method. This method presents the technique of finding the optimal location of TCSC by computing the sensitivity of lines while utilizing the DC Power Flow Sensitivity Index and Reactive Power Loss Sensitivity Index. For optimizing the value of Static ATC, the novel MEEPSO method is suggested. The system performance is analyzed for the single area and multi-area arrangement. The PWS is used to deliberate on the performance of multi-area systems. The SEAMB technique is presented for calculating DATC at the HB limit. This chapter presents the summary of the main conclusions of the studies presented in previous chapters. It also enlists the direction for further research.

6.1 MAIN CONCLUSIONS

The main conclusions of each of the mentioned studies are summarized herewith.

In *Chapter - 3*, the SPCR method to optimally locate the TCSC has been devised to alleviate congestion. The optimization utilizes the DC power flow sensitivity index and reactive power loss sensitivity index. The TCSC placement has been decided based on a reduction in reactive and real power losses and a decrease in real power flow. The IEEE 6-bus and 30-bus test systems are used for validating the results. The following conclusions are drawn from the study:

- The potential list of lines where TCSC can be placed is obtained by both sensitivity factors.
- The TCSC location is one among the sensitive lines, which is resulting the most reduction in real and reactive power loss and decreased line flow.

- The allocation results in relieving congestion of these lines and, hence, allow them to be able to transfer power more than already committed usage and prevents overloading in the future.
- The results have been compared with published results based on PSAT and the performance is found comparable

In *Chapter – 4,* the power market operations have been analyzed based on a single area and multi-area arrangement. Both bilateral and multilateral transactions are analyzed in the study. A heuristic algorithm MEEPSO has been proposed to calculate SATC for single area arrangement while utilizing ACPTDF for bilateral transactions. The multi-area system has been analyzed for different transactions using PWS. The performance is validated through the analysis of 6-bus and 30-bus test systems. The efficacy of the presented algorithm is validated while comparing its performance with ACPTDF, DCPTDF and PWS. The comparison involves the performance with and without TCSC placement. The performance has been studied on 6-bus and 30-bus test systems for a different level of transactions. The following conclusions are drawn:

- The improved values of SATC are not resulted in all cases after placing TCSC at sensitive lines. However, the improvement in SATC results in most of the lines.
- The values of SATC obtained by the presented MEEPSO algorithm are compared with that of ACPTDF, DCPTDF, and PWS. The higher SATC value has resulted from the presented MEEPSO method.
- Among different transactions, the best arrangement is decided by the consideration of optimum cost, SATC and line loading.

In *Chapter – 5*, The SEAMB technique is presented to analyze the DATC when the system is subjected to dynamic conditions. The power system components are represented by dynamic equations. The generator is modelled as a *d-q* axis sub-transient round rotor GENROU model, while the exciter is represented as a dynamic IEEET1 model. The load is modelled as a composite load. The power system network is classified into areas to find DATC for the transactions between areas. The SEAMB eigen value analysis is carried out using the bifurcation method. The DATC values are presented for WSCC 9-bus system and the New England 39-bus system. The critical limits are obtained by Hopf Bifurcation (HB) limit. The result has been analyzed using Power World Simulator for transient

conditions due to bus fault and line outage. The analysis is carried out for both static and dynamic loads. The following conclusions are drawn from the investigation:

- The values of DATC are found to be depending on the areas where bilateral transactions are taking place.
- Different values of DATC are resulted when the same shunt fault is initiated at different buses. Thus, the DATC is found to be sensitive to the fault location. Similar observations are observed for line outage contingency.
- The values of ATC under dynamic fault and line outage contingency conditions are found to be lower than the respective pre-fault values.
- The values of DATC under dynamic load are found to be lower than that of static load.

6.2 SCOPE FOR FUTURE WORK

The research work, an exploration exercise, is a continuous endeavour. The culmination of a research project opens many more avenues for further research. After successful completion of the doctoral research work, the scope of further research is identified in the following related areas:

- Future work can be extended to include the demand response in the congestion management problem as it provides an opportunity to alleviate transmission congestion.
- The scope is identified to investigate the congestion management problem with renewable energy sources integration.
- Multi-lateral transactions can be considered in the work along with the bilateral transactions in a deregulated system.
- The investigation can be extended to analyze DATC with the solar and wind integrated systems.
- The work can be extended for placement of FACTS devices in a multi objective optimization arrangement with ATC and the voltage stability measures as the objective.
- There is a scope to analyze the effect of series compensated systems for computing DATC.

List of Publications

JOURNAL PUBLICATIONS (SCI)

- Divya Gupta and Sanjay K. Jain, "Analysis of operations in the energy market in a deregulated environment," ***Energy Sources Part B Economics Planning and Policy,*** vol. 11, pp. 1173-1179, 2016. (Impact Factor: 3.24)
  doi: 10.1080/15567249.2016.1176089

- Divya Gupta and Sanjay K. Jain, "Available Transfer Capability Enhancement by FACTS Devices Using Metaheuristic Evolutionary Particle Swarm Optimization (MEEPSO) Technique," ***Energies,*** vol. 14, pp. 869-896, 2021. (Impact Factor: 3.34)
  doi: https://doi.org/10.3390/en14040869

CONFERENCE PUBLICATIONS

- Divya Gupta and Sanjay K. Jain, "Scrutinizing market behaviors for increasing reliability in power systems," *2016 7th India International Conference on Power Electronics (IICPE),* IEEE, pp. 1-6, 17 - 19 November 2016, Patiala, India.

- Divya Gupta and Sanjay K. Jain, "Analyzing power transferred physically over committed usage by adding series compensation using birds' intelligence." *2016 7th India International Conference on Power Electronics (IICPE),* IEEE, pp. 1-7, 17 - 19 November 2016, Patiala, India.

References

[1] P. Venkatesh, B. Manikandan, S. C. Raja, and A. Srinivasan, *Electrical power systems: analysis, security and deregulation*. PHI Learning Pvt. Ltd., 2012.

[2] F. E. R. Commission, "Open access same-time information system and standards of conduct. Docket No," RM 95-9-000, Order 889, Washington, 1996.

[3] M. H. Gravener, C. Nwankpa, and T.-S. Yeoh, "ATC computational issues [electricity supply]," in *IEEE Proceedings of the 32nd Annual Hawaii International Conference on Systems Sciences, 1999. HICSS-32.*, vol. Track 3, pp. 6, 05-08 January 1999, Maui, USA.

[4] M. H. Gravener and C. Nwankpa, "Available transfer capability and first order sensitivity," *IEEE Transactions on Power Systems,* vol. 14, no. 2, pp. 512-518, May 1999.

[5] A. S. Siddiqui and T. Deb, "Congestion management using FACTS devices," *International Journal of System Assurance Engineering and Management,* vol. 5, no. 4, pp. 618-627, 2014.

[6] T. T. Nguyen and F. Mohammadi, "Optimal Placement of TCSC for Congestion Management and Power Loss Reduction Using Multi-Objective Genetic Algorithm," *Sustainability,* vol. 12, no. 7, p. 2813, 2020, doi: 10.3390/su12072813.

[7] M. Mandala and C. Gupta, "Congestion management by optimal placement of FACTS device," in *2010 Joint International Conference on Power Electronics, Drives and Energy Systems & 2010 Power India*, December 2010: IEEE, pp. 1-7, 20-23 December 2010, New Delhi, India.

[8] F. Galiana, "Assessment and control of the impact of FACTS devices on power system performance," *IEEE Transactions on power systems,* vol. 11, no. 4, pp. 1931-1936, November 1996.

[9] S. Singh and A. David, "Optimal location of FACTS devices for congestion management," *Electric Power Systems Research,* vol. 58, no. 2, pp. 71-79, June 2001.

[10] S. Kumar, A. Kumar, and N. K. Sharma, "Sensitivity analysis-based performance and economic operation of wind-integrated system with FACTS devices for optimum load dispatch," *Renewables: Wind, Water, and Solar,* vol. 4, no. 2, 2017.

[11] F. Ahmad, "Enhancement of the Voltage Profile for an IEEE-14 Bus System by Using FACTS Devices," in *Applications of Computing, Automation and Wireless Systems in Electrical Engineering*: Springer, pp. 1243-1257, 01 June 2019, Singapore.

[12] M. Mbae and N. Nwulu, "Impact of hybrid FACTS devices on the stability of the Kenyan power system," *International Journal of Electrical & Computer Engineering,* vol. 12, no. 1, pp. 12-21, 2022.

[13] O. O. Mohammed, M. W. Mustafa, D. S. S. Mohammed, and A. O. Otuoze, "Available transfer capability calculation methods: A comprehensive review," *International Transactions on Electrical Energy Systems,* vol. 29, no. 6, p. e2846, 2019.

[14] A. Narain, S. Srivastava, and S. Singh, "Impact of wind power generation on ATC calculation with uncertain equal load," *Electrical Engineering,* vol. 104. pp. 1-9, 2021.

[15] P. Kerur, M. Hudedmani, and R. Chakrasali, "Determination of ATC and Shortest Path Power Flow in Deregulated Power System," *International Journal of Science and Engineering,* vol. 6, no. 4, 2020.

[16] A. Kumar and J. Kumar, "ATC with ZIP load model – A comprehensive evaluation with third generation FACTS in restructured electricity markets," *International Journal of Electrical Power & Energy Systems,* vol. 54, no. 1, pp. 546-558, 2014.

[17] K. Y. Lee and Z. A. Vale, *Applications of Modern Heuristic Optimization Methods in Power and Energy Systems*. John Wiley & Sons, 2020.

[18] A. Al Ahmad and R. Sirjani, "Optimal placement and sizing of multi-type FACTS devices in power systems using metaheuristic optimisation techniques: An updated review," *Ain Shams Engineering Journal,* vol. 11, no. 3, pp. 611-628, 2020.

[19] M. Eidiani, "An efficient differential equation load flow method to assess dynamic available transfer capability with wind farms," *IET Renewable Power Generation,* vol. 15, no. 16, pp. 3843-3855, 2021.

[20] X. Zhang, Y. Song, Q. Lu, and S. Mei, "Dynamic available transfer capability (ATC) evaluation by dynamic constrained optimization," *IEEE Transactions on Power Systems,* vol. 19, no. 2, pp. 1240-1242, 2004.

[21] F. Shahnia, S. Rajakaruna, and A. Ghosh, *Static compensators (STATCOMs) in power systems*. Springer, 2015.

[22] W. Liu, L. Wang, and Q. Wan, "Calculation of available transfer capability considering economic and emission dispatch," in *2008 Third International Conference on Electric Utility Deregulation and Restructuring and Power Technologies*, IEEE, pp. 551-556, 06-09 April 2008, Nanjing.

[23] B. Mozafari, A. Ranjbar, A. Shirani, and A. Barkeseh, "A comprehensive method for available transfer capability calculation in a deregulated power," in *2004 IEEE International Conference on Electric Utility Deregulation, Restructuring and Power Technologies. Proceedings*, 2004, vol. 2, IEEE, pp. 680-685, 05-08 April, 2004, Hong Kong, China.

[24] T. Jain, S. Singh, and S. Srivastava, "Dynamic available transfer capability computation using a hybrid approach," *IET generation, transmission & distribution,* vol. 2, no. 6, pp. 775-788, 2008.

[25] A. I. S. Velusamy, N. B. Ramu, D. Durairaj, and K. Murugesan, "Differential evolutionary algorithm-based optimal support vector machine for online dynamic available transfer capability estimation incorporating transmission capacity margins," *International Transactions on Electrical Energy Systems*, vol. 27, no. 7, p. e2331, 2017.

[26] W. Li, M. Shaaban, Z. Yan, Y. Ni, and F. F. Wu, "Available transfer capability calculation with static security constraints," in *2003 IEEE Power Engineering Society General Meeting*, 2003, vol. 1: IEEE, pp. 306-310, 13-17 July 2003, Toronto, Canada.

[27] V. Bhavithira and A. Amudha, "Enhancement of Available Transfer Capability using FACTS controller," in *Applied Mechanics and Materials*, 2014, vol. 573: Trans Tech Publ, pp. 340-345.

[28] M. Eidiani and M. H. M. Shanechi, "FAD-ATC: A new method for computing dynamic ATC," *International Journal of Electrical Power & Energy Systems,* vol. 28, no. 2, pp. 109-118, 2006.

[29] M. Eidiani, M. H. Modir Shanechi and E. Vaahedi, , "Assessment of ATC using Voltage and Transient Stability simultaneously," *Journal of Computational Methods in Engineering,* vol. 23, no. 2, pp. 11-24, 2005.

[30] L. L. Lai, *Power system restructuring and deregulation: trading, performance and information technology*. John Wiley & Sons, 2001.

[31] G. Srinivsulu, B. Pamulaparthy, and A. Sharma, "Review of congestion management methods from conventional to smart grid scenario," *International Journal of Emerging Electric Power Systems,* vol. 20, no. 3, 2019.

[32] M. M. Gajjala and A. Ahmad, "A survey on recent advances in transmission congestion management," *International Review of Applied Sciences and Engineering,* vol. 13, no. 1, pp. 29-41, 2021.

[33] T. T. Lie and W. Deng, "Optimal flexible AC transmission systems (FACTS) devices allocation," *International Journal of Electrical Power & Energy Systems,* vol. 19, no. 2, pp. 125-134, Feb. 1997.

[34] E. V. Larsen, N. W. Miller, S. L. Nilsson, and S. R. Lindgren, "Benefits of GTO-based compensation systems for electric utility applications," *IEEE Transactions on Power Delivery,* vol. 7, no. 4, pp. 2056-2064, Oct. 1992.

[35] B. Monisha, D. Karthikaikannan, and K. Balamurugan, "Study of Optimal Power Flow on IEEE Test Systems with TCSC Using Power World Simulator," Proceedings of ICICA 2018," in *Advances in Intelligent Systems and Computing*, Springer, pp. 321-336, 2019.

[36] B. Manikandan, S. C. Raja, and P. Venkatesh, "Multi-area available transfer capability determination in the restructured electricity market," in *2008 Joint International Conference on Power System Technology and IEEE Power India Conference*, 2008, pp. 1-7, 12-15 October 2008, New Delhi, India.

[37] M. S. Sureban and S. G. Ankaliki, "Evaluation of Available Transfer Capability using Power World Simulator," *I-Manager's Journal on Power Systems Engineering,* vol. 5, no. 4, p. 34, 2017.

[38] A. Kumar and M. Kumar, "Available transfer capability determination using power transfer distribution factors," *International Journal of Emerging Electrical Power Systems,* vol. 3, pp. 1171-1176, 2013.

[39] M. Venkateswara Rao, S. Sivanagaraju, and C. V. Suresh, "Available transfer capability evaluation and enhancement using various FACTS controllers: Special focus on system security," *Ain Shams Engineering Journal,* vol. 7, no. 1, pp. 191-207, 2016.

[40] K. Sörensen and F. Glover, "Metaheuristics," in *Encyclopedia of operations research and management science,* Gass S.I., Fu M.C. (eds), Springer, Boston vol. 62, pp. 960-970, 2013.

[41] T. T. Capability, "A Reference Document for calculating and reporting the Electric Power Transmission Capacity of interconnected electric systems," *North American Electric Reliability Council,* 1995.

[42] T. T. C. T. Force, "Transmission transfer capability," *North American Reliability Council, Princeton, New Jersey,* 1995.

[43] N. Rep, "Available transfer capability Definitions and determinations," *North American Electric Reliability Council (NERC),* 1996.

[44] M. Patel and A. A. Girgis, "Review of available transmission capability (ATC) calculation methods," in *2009 Power Systems Conference*, 2009: IEEE, pp. 1-9, 10-13 March 2009, Clemson, USA.

[45] H. Farahmand, Rashidinejad, M., & Gharaveici, A. A. , "A combinatorial approach of real GA & fuzzy to ATC enhancement, " *Turkish Journal of Electrical Engineering & Computer Sciences,* vol. 15, no. 1, pp. 77-88, 2007.

[46] J. A. Momoh, Ma, X. W., Tomsovic, K. , "Overview and literature survey of fuzzy set theory in power systems," *IEEE Transactions on power systems,* vol. 10, no. 3, pp. 1676-1690, Aug. -1995.

[47] J. S. R. Jang, C. T. Sun, and E. Mizutani, "Neuro-fuzzy and soft computing-a computational approach to learning and machine intelligence," *IEEE Transactions on automatic control,* vol. 42, no. 10, pp. 1482-1484, 1997.

[48] Zimmermann, "Fuzzy programming and linear programming with several objective functions," *Fuzzy Sets and Systems,* vol. 1, no. 1, pp. 45-55, 1978.

[49] V. Miranda, & J. P. Saraiva, "Fuzzy modelling of power system optimal load flow," *IEEE Transactions on Power Systems,* vol. 7, no. 2, pp. 843-849, 1992.

[50] E. De Oliveira, J. M. Lima, and J. Pereira, "Flexible AC transmission system devices: allocation and transmission pricing," *International Journal of Electrical Power & Energy Systems,* vol. 21, no. 2, pp. 111-118, 1999.

[51] K. Verma, S. Singh, and H. Gupta, "FACTS devices location for enhancement of total transfer capability," in *2001 IEEE Power Engineering Society Winter Meeting. Conference Proceedings*, 2001, vol. 2: IEEE, pp. 522-527, 28 January 2001 – 01 February 2001, Columbus, USA.

[52] P. Bhatt, N. Zaveri, and H. Patel, "Role of FACTS Devices in Competitive Electricity Market: A Review." *in International Conference on Recent Advances in Computer and Electrical Engineering*, March 2007, Bikaner, Rajsthan, India.

[53] T. Jain, S. Singh, and S. Srivastava, "Dynamic ATC enhancement through optimal placement of FACTS controllers," *Electric Power Systems Research,* vol. 79, no. 11, pp. 1473-1482, 2009.

[54] R. Rajathy, "Investigations on power system operation and management in restructured market," Dept. of Electrical & Electronics Engg., Pondicherry University, 2011.

[55] G. C. Ejebe, J. Tong, J. Waight, J. Frame, X. Wang, and W. Tinney, "Available transfer capability calculations," *IEEE Transactions on Power systems,* vol. 13, no. 4, pp. 1521-1527, 1998.

[56] Y. Ou and C. Singh, "Assessment of available transfer capability and margins," *IEEE Transactions on Power Systems,* vol. 17, no. 2, pp. 463-468, 2002.

[57] M. Shaaban, Y. Ni, and F. F. Wu, "Transfer capability computations in deregulated power systems," in *IEEE Proceedings of the 33rd Annual Hawaii International Conference on System Sciences*, pp. 5, 07 January 2000, Maui, USA.

[58] G. Hamoud, "Assessment of available transfer capability of transmission systems," *IEEE Transactions on Power systems,* vol. 15, no. 1, pp. 27-32, Feb. 2000.

[59] M. D. Ilic, Y. T. Yoon, and A. Zobian, "Available transmission capacity (ATC) and its value under open access," *IEEE transactions on power systems,* vol. 12, no. 2, pp. 636-645, 1997.

[60] A. J. Wood, B. F. Wollenberg, and G. B. Sheblé, *Power generation, operation, and control*. John Wiley & Sons, 2013.

[61] S. Grijalva, P. W. Sauer, and J. D. Weber, "Enhancement of linear ATC calculations by the incorporation of reactive power flows," *IEEE Transactions on Power Systems,* vol. 18, no. 2, pp. 619-624, 2003.

[62] A. Kumar and S. Srivastava, "AC power transfer distribution factors for allocating power transactions in a deregulated market," *IEEE Power Engineering Review,* vol. 22, no. 7, pp. 42-43, 2002.

[63] P. Venkatesh, R. Gnanadass, and N. P. Padhy, "Available transfer capability determination using power transfer distribution factors," *International journal of emerging electric power systems,* vol. 1, no. 2, Jan. 2004.

[64] A. Kumar, S. Srivastava, and S. Singh, "Available transfer capability assessment in a competitive electricity market using a bifurcation approach," *IEE Proceedings-Generation, Transmission and Distribution,* vol. 151, no. 2, pp. 133-140, March 2004.

[65] M. Hojabri, Hizam, H., Mariun, N., & Abdullah, S. M., "Comparative analysis of ATC probabilistic methods," *Journal of American Science,* vol. 6, no. 9, 2010.

[66] L. L. Lai, J. T. Ma, R. Yokoyama, M. Zhao., "Improved genetic algorithms for optimal power flow under both normal and contingent operation states," *International Journal of Electrical Power & Energy Systems,* vol. 19, no. 5, pp. 287-292, June 1997.

[67] S. R. Paranjothi and K. Anburaja, "Optimal Power Flow Using Refined Genetic Algorithm," *Electric Power Components and Systems,* vol. 30, no. 10, pp. 1055-1063, Oct. 2002.

[68] D. Devaraj and B. Yegnanarayana, "Genetic-algorithm-based optimal power flow for security enhancement," *IEE Proceedings - Generation, Transmission and Distribution,* vol. 152, no. 6, December 2005.

[69] C. W. Richter and G. B. Sheblé, "Genetic algorithm evolution of utility bidding strategies for the competitive marketplace," *IEEE transactions on power systems,* vol. 13, no. 1, pp. 256-261, Feb. 1998.

[70] C. W. Richter, G. B. Sheblé and D. Ashlock, "Comprehensive bidding strategies with genetic programming/finite state automata," *IEEE Transactions on Power systems,* vol. 14, no. 4, pp. 1207-1212, Nov. 1999.

[71] V. P. Gountis and A. G. Bakirtzis, "Bidding Strategies for Electricity Producers in a Competitive Electricity Marketplace," *IEEE Transactions on Power Systems,* vol. 19, no. 1, pp. 356-365, Feb. 2004..

[72] M. M. Othman, A. Mohamed, and A. Hussain, "Available transfer capability assessment using evolutionary programming based capacity benefit margin," *International Journal of Electrical Power & Energy Systems,* vol. 28, no. 3, pp. 166-176, Mar. 2006.

[73] M. E. H. Pedersen, "Tuning & simplifying heuristical optimization " Doctoral thesis, University of Southampton, 2010.

[74] M. A. Abido, "Optimal power flow using particle swarm optimization," *International Journal of Electrical Power & Energy Systems,* vol. 24, no. 7, pp. 563-571, Oct. 2002.

[75] N. Mo, Z. Y. Zou, K. W. Chan, and T. Y. G. Pong, "Transient stability constrained optimal power flow using particle swarm optimisation," *IET Generation, Transmission & Distribution,* vol. 1, no. 3, May 2007.

[76] P. E. Onate Yumbla, J. M. Ramirez, and C. A. Coello Coello, "Optimal Power Flow Subject to Security Constraints Solved With a Particle Swarm Optimizer," *IEEE Transactions on Power Systems,* vol. 23, no. 1, pp. 33-40, Feb. 2008..

[77] B. Zhao, C. X. Guo, and Y. J. Cao, "A Multiagent-Based Particle Swarm Optimization Approach for Optimal Reactive Power Dispatch," *IEEE Transactions on Power Systems,* vol. 20, no. 2, pp. 1070-1078, May 2005.

[78] J. Kennedy and R. Eberhart, "Particle swarm optimization," in *IEEE Proceedings of ICNN'95-International Conference on Neural Networks*, vol. 4, pp. 1942-194, 27 November 1995 - 01 December 1995, Perth, Australia.

[79] H. Farahmand, M. Rashidinejad, A. A. Gharaveici and M. Shojaee, "An Application of Hybrid Heuristic Approach for ATC Enhancement," in *IEEE Large Engineering Systems Conference on Power Engineering*, pp. 125-130, 26-28 July 2006, Halifax, Canada.

[80] V. C. Ramesh and X. Li, "A fuzzy multiobjective approach to contingency constrained OPF," *IEEE Transactions on Power Systems,* vol. 12, no. 3, pp. 1348-1354, Aug. 1997.

[81] A. B. Khairuddin, S. S. Ahmed, M. W. Mustafa, A. A. M. Zin, and H. Ahmad, "A Novel Method for ATC Computations in a Large-Scale Power System," *IEEE Transactions on Power Systems,* vol. 19, no. 2, pp. 1150-1158, May 2004.

[82] S. S. Kim, M. K. Kim, and J. K. Park, "Consideration of multiple uncertainties for evaluation of available transfer capability using fuzzy continuation power flow," *International Journal of Electrical Power & Energy Systems,* vol. 30, no. 10, pp. 581-593, Dec. 2008.

[83] T. K. Hahn, M. K. Kim, D. Hur, J.-K. Park, and Y. T. Yoon, "Evaluation of available transfer capability using fuzzy multi-objective contingency-constrained optimal power flow," *Electric Power Systems Research,* vol. 78, no. 5, pp. 873-882, May 2008.

[84] S. Greene, I. Dobson, and F. L. Alvarado, "Sensitivity of transfer capability margins with a fast formula," *IEEE Transactions on Power Systems,* vol. 17, no. 1, pp. 34-40, 2002.

[85] A. Kumar, S. Srivastava, and S. Singh, "Available transfer capability (ATC) determination in a competitive electricity market using AC distribution factors," *Electric Power Components and Systems,* vol. 32, no. 9, pp. 927-939, 2004.

[86] R. D. Christie, B. F. Wollenberg, and I. Wangensteen, "Transmission management in the deregulated environment," *Proceedings of the IEEE,* vol. 88, no. 2, pp. 170-195, 2000.

[87] Y. Ou and C. Singh, "Calculation of risk and statistical indices associated with available transfer capability," *IET Proceedings-Generation, Transmission and Distribution,* vol. 150, no. 2, pp. 239-244, Mar. 2003.

[88] M. Shaaban, W. Li, Z. Yan, Y. Ni, and F. F. Wu, "Calculation of total transfer capability incorporating the effect of reactive power," *Electric Power Systems Research,* vol. 64, no. 3, pp. 181-188, 2003.

[89] W. Ongsakul and P. Jirapong, "Calculation of total transfer capability by evolutionary programming," in *2004 IEEE Region 10 Conference TENCON 2004.*, vol. 3, pp. 492-495, 24 November 2004, Chiang Mai, Thailand.

[90] H.-h. Chen, G.-q. Li, and H.-l. Liao, "A self-adaptive improved particle swarm optimization algorithm and its application in available transfer capability calculation," in *2009 IEEE Fifth International Conference on Natural Computation*, vol. 3, IEEE, pp. 200-205, 14 – 16 August 2009, Tianjian, China.

[91] I. Hiskens, M. Pai, and P. Sauer, "An iterative approach to calculating dynamic ATC," *Proceedings of Bulk Power System Dynamics and Control IV-Restructuring,* pp. 585-590, Aug. 1998.

[92] E. De Tuglie, M. Dicorato, M. La Scala, and P. Scarpellini, "A static optimization approach to assess dynamic available transfer capability," in *IEEE Proceedings of the 21st International Conference on Power Industry Computer Applications. Connecting Utilities, PICA 99,* pp. 269-277, 21 May 1999, Santa Clara, CA, USA.

[93] R. Gnanadass and V. Ajjarapu, "Assessment of dynamic available transfer capability using FDR PSO algorithm," *Elektrika Journal of Electrical Engineering,* vol. 10, no. 1, pp. 20-25, Jan. 2008.

[94] C. A. Canizares, "On bifurcations, voltage collapse and load modeling," *IEEE transactions on power systems,* vol. 10, no. 1, pp. 512-522, Feb. 1995.

[95] I. Dobson and L. Lu, "New methods for computing a closest saddle node bifurcation and worst case load power margin for voltage collapse," *IEEE Transactions on Power Systems,* vol. 8, no. 3, pp. 905-913, 1993.

[96] K. Srivastava and S. Srivastava, "Elimination of dynamic bifurcation and chaos in power systems using facts devices," *IEEE Transactions on Circuits and Systems I: Fundamental Theory and Applications,* vol. 45, no. 1, pp. 72-78, Jan. 1998.

[97] M. Rashidinejad, H. Farahmand, M. Fotuhi-Firuzabad, and A. Gharaveisi, "ATC enhancement using TCSC via artificial intelligent techniques," *Electric Power Systems Research,* vol. 78, no. 1, pp. 11-20, Jan. 2008.

[98] Y. Esmaili and A. Hemmatyar, "ATC enhancement using SSSC, a case study of harmony search vs PSO," *Journal of Basic and Applied Scientific Research,* vol. 2, no. 4, p. 10, pp. 3416-3425, 2012.

[99] T. S. Sudheer, J. S. Rao, and J. Amarnnath, "Optimal location of the facts devices using the sensitivity approach for the enhancement of ATC and voltage profile in deregulated power system," *International Journal of Compute-r Applications,* vol. 76, no. 10, 2013.

[100] R. H. Bhesdadiya, & Patel, R. M, "Available transfer capability calculation methods: A Review.," *International journal of Advanced Research in Electrical, Electronics and Instrumentation engineering,* vol. 3, no. 1, pp. 1-6, 2014.

[101] M. Hassan, S. Cheng, and Z. Zakaria, "Steady-state modeling of static synchronous compensator and thyristor controlled series compensator for power flow analysis," *Information Technology Journal,* vol. 8, no. 3, pp. 347-353, 2009.

[102] M. S. Nobile, Pasi, G., Cazzaniga, P., Besozzi, D., Colombo, R., & Mauri, G., "Proactive particles in swarm optimization: a self-tuning algorithm based on fuzzy logic," in *2015 IEEE International Conference on Fuzzy Systems (FUZZ-IEEE)*, pp. 1–8, 02 05 August 2015, Istanbul, Turkey.

[103] S. Chansareewittaya and P. Jirapong, "Power transfer capability enhancement with optimal maximum number of facts controllers using evolutionary programming," in *IECON 2011-37th Annual Conference of the IEEE Industrial Electronics Society*, pp. 4733-4738, 07 - 10 November 2011, Melbourne, VIC, Australia.

[104] Y. Shi and R. C. Eberhart, "Parameter selection in particle swarm optimization," in *Evolutionary Programming VII*, Lecture Notes in Computer Science, Berlin, Heidelberg, 1998, vol. 1447, pp. 591–600.

[105] J. Yuryevich and K. P. Wong, "Evolutionary Programming Based Optimal Power Flow Algorithm," *IEEE transactions on Power Systems,* vol. 14, no. 4, pp. 1245-1250, 1999.

[106] N. Ghawghawe and K. L. Thakre, "Application of power flow sensitivity analysis and PTDF for determination of ATC," in *2006 IEEE International Conference on Power Electronic, Drives and Energy Systems*, pp. 1-7, 12 – 15 December 2006, New Delhi, India.

[107] N. Mat, M. Othman, I. Musirin, A. Mohamed, and A. Hussain, "Determination of Available Transfer Capability (ATC) considering Integral Square Generator Angle (ISGA)," in *Proceedings of the 2nd WSEAS International Conference on Circuits, Systems, Signal and Telecommunications (CISSTs' 08),* pp. 126-131, 25 -27 January 2008, Acapulco, Mexico.

[108] K. R. Susmitha and D. G. S. Rao, " Determination of ATC by using DCPTDF and ACPTDF methods," *International Journal of Applied Engineering Research,* vol. 12, no. 1, pp. 339-345, 2017.

[109] T. Jain, S. N. Singh and S. C. Srivastava, "Dynamic Available Transfer Capability Evaluation Considering Hopf Bifurcation Limit," in *Fifteenth National Power Systems Conference (NPSC),* pp. 55-60, December 2008, IIT Bombay.

[110] T. Jain, S. N. Singh and S. C. Srivastava, "Dynamic ATC enhancement through optimal placement of FACTS controllers " *Electric Power Systems Research,* vol. 79, no. 11, pp. 1473–1482, Nov. 2009.

[111] T. Jain, S. Singh, and S. Srivastava, "Adaptive wavelet neural network-based fast dynamic available transfer capability determination," *IET generation, transmission & distribution,* vol. 4, no. 4, pp. 519-529, April 2010.

[112] D. V. Kumar and C. Venkaiah, "Dynamic Available Transfer Capability (DATC) computation using intelligent techniques," in *2008 Joint International Conference on Power System Technology and IEEE Power India Conference*, pp. 1-6, 2008.

[113] B. H. Lee and K. Y. Lee, "Dynamic and static voltage stability enhancement of power systems," *IEEE Transactions on Power systems,* vol. 8, no. 1, pp. 231-238, February 1993.

[114] M. Mahmoudian and G. R. Yousefi, "ATC improvement and losses estimation considering dynamic transmission line ratings," in *20th IEEE Iranian Conference on Electrical Engineering (ICEE2012)*, pp. 404-409, 15 – 17 May 2012, Tehran, Iran.

[115] V. A. I. Selvi, R. N. Banu, D. Devaraj, and M. Karuppasamypandiyan, "Estimation of dynamic available transfer capability including Hopf bifurcation limit using step

by step algorithm," *International Journal of Power and Energy Conversion,* vol. 8, no. 2, pp. 113-131, Feb. 2017.

[116] N. Magaji, & Mustafa, M. W., "Determination of best location of FACTS devices for damping oscillations," *International Review of Electrical Engineering,* vol. 5, no. 3, pp. 1119-1126, May 2010.

[117] S. N. Malival, K. C. Chande and R.S. Parikh, "Optimal Placement of TCSC by Sensitivity Methods Using PSAT," *International Journal for Scientific Research & Development,* vol. 1, Issue 11, pp. 2554-2558, 2014.

[118] N. D. Ghawghawe and K. L. Thakre, "Computation of TCSC reactance and suggesting criterion of its location for ATC improvement," *International Journal of Electrical Power & Energy Systems,* vol. 31, no. 2, pp. 86-93, 2009.

[119] G. M. Huang, & P. Yan, "TCSC and SVC as re-dispatch tools for congestion management and TTC improvement," in *2002 IEEE Power Engineering Society Winter Meeting. Conference Proceedings*, vol. 1, pp. 660–665, Jan. 2002.

[120] D. Gan, R. J. Thomas, and R. D. Zimmerman, "Stability-constrained optimal power flow " *IEEE Transactions on Power Systems,* vol. 15, no. 2, pp. 535-540, 2000.

[121] F. M. Albatsh, S. Mekhilef, S. Ahmad, H. Mokhlis, and M. A. Hassan, "Enhancing power transfer capability through flexible AC transmission system devices: a review," *Frontiers of Information Technology & Electronic Engineering,* vol. 16, no. 8, pp. 658-678, 2015..

[122] N. Schnurr, & W. H. Wellssow, "Determination and enhancement of the available transfer capability in FACTS," in *2001 IEEE Porto Power Tech Proceedings*, vol. 4, pp. 6, 10 – 13 September 2001, Porto, Portugal.

[123] P. P. Kulkarni and N. Ghawghawe, "Optimal placement and parameter setting of TCSC in power transmission system to increase the power transfer capability," in *2015 IEEE International Conference on Energy Systems and Applications*, pp. 735-739, 30 October 2015 - 01 November 2015, Pune, India.

[124] M. A. Kamarposhti and H. Lesani, "Effects of STATCOM, TCSC, SSSC and UPFC on static voltage stability," *Electrical Engineering,* vol. 93, no. 1, pp. 33-42, March 2011.

[125] L. Vanfretti and F. Milano, "Facilitating constructive alignment in power systems engineering education using free and open-source software," *IEEE Transactions on Education,* vol. 55, no. 3, pp. 309-318, Aug. 2012.

[126] F. Milano, "An open source power system analysis toolbox," *IEEE Transactions on Power systems,* vol. 20, no. 3, pp. 1199-1206, 2005.

[127] N. S. Rao, J. Amarnath, and V. P. Rao, "Comparison for performance of multitype FACTS devises on available transfer capability in a deregulated power system," in *2014 IEEE International Conference on Smart Electric Grid (ISEG)*, pp. 1-6, 19-20 September 2014, Guntur, India.

[128] Y. Xiao, Y. Song, C.-C. Liu, and Y. Sun, "Available transfer capability enhancement using FACTS devices," *IEEE transactions on power systems,* vol. 18, no. 1, pp. 305-312, Feb. 2003.

[129] I. Dobson, Greene, S., Rajaraman, R., DeMarco, C. L., Alvarado, F. L., Glavic, M., Zimmerman, R., *Electric power transfer capability: concepts, applications, sensitivity and uncertainty*. PSERC Publication, 2001.

[130] G. C. Ejebe, J. G. Waight, M. Sanots-Nieto, and W. F. Tinney, "Fast calculation of linear available transfer capability," *IEEE Transactions on Power Systems,* vol. 15, no. 3, pp. 1112-1116, 2000.

[131] I. Dobson *et al.*, "Electric power transfer capability: concepts, applications, sensitivity and uncertainty," *PSERC Publication,* no. 01-34, 2001.

[132] O. O. Mohammed, M. W. Mustafa, D. S. S. Mohammed, and A. O. Otuoze, "Available transfer capability calculation methods: A comprehensive review," *International Transactions on Electrical Energy Systems,* vol. 29, no. 6, 2019.

[133] G. C. Ejebe, Tong, J., Waight, G.G., Frame, J.G., Wang, X., and Tinney, W.F, "Available transfer capability calculations," *IEEE Trans. Power Syst,* vol. 13, no. 4, pp. 1521–1527, 1998.

[134] B. Corniere, L. Martin, S. Vitet, N. Hadjsaid, and A. G. Phadke, "Assessment of the congestion cost and the risk of curtailment associated with available transfer capability (ATC)," in *2000 IEEE Power Engineering Society Winter Meeting. Conference Proceedings*, vol. 2, pp. 891-896, 23 – 27 January 2000, Singapore.

[135] J. Weber, "Efficient available transfer capability analysis using linear methods," in *PSERC Internet Seminar*, *Urbana,* 2000, vol. 7.

[136] S. Nagalakshmi, S. Kalyani, V. A. Shobana, R. N. Ranjeni, and P. Deepamangai, "Estimation of Available Transfer Capability under normal and contingency conditions in Deregulated Electricity Market," in *IEEE-International Conference On*

Advances In Engineering, Science And Management (ICAESM-2012), 2012: IEEE, pp. 453-459, 30-31 March 2012, Nagapattinam, India.

[137] K. R. Susmitha and G. S. Rao, "Determination of ATC by using DCPTDF and ACPTDF methods," *International Journal of Applied Engineering Research,* vol. 12, no. 1, pp. 339-345, 2017.

[138] A. Kumar, "Available transfer capability determination and congestion management in competitive electricity markets ", Electrical Engineering, IIT Kanpur, Kanpur, 2003.

[139] X. Luo, Patton, A. D., Singh, C., "Real power transfer capability calculations using multi-layer feed forward neural networks," *IEEE Transactions on Power Systems,* vol. 15, no. 2, pp. 903-908, 2000.

[140] S. N. Pandey, N. K. Pandey, S. Tapaswi, and L. Srivastava, "Neural Network-Based Approach for ATC Estimation Using Distributed Computing," *IEEE Transactions on Power Systems,* vol. 25, no. 3, pp. 1291-1300, 2010.

[141] T. Jain, S. N. Singh, and S. C. Srivastava, "Fast static available transfer capability determination using radial basis function neural network," *Applied Soft Computing,* vol. 11, no. 2, pp. 2756-2764, Mar. 2011.

[142] N. K. T. El-Omari, "Sea Lion Optimization Algorithm for Solving the Maximum Flow Problem," *IJCSNS,* vol. 20, no. 8, p. 30, Aug. 2020.

[143] K. Hussain, M. N. Mohd Salleh, S. Cheng, and Y. Shi, "Metaheuristic research: a comprehensive survey," *Artificial Intelligence Review,* vol. 52, no. 4, pp. 2191-2233, Dec. 2019.

[144] Z. H. Ahmed, "A comparative study of eight crossover operators for the maximum scatter travelling salesman problem," *operations research,* vol. 11, no. 6, pp. 317-329, 2020.

[145] H. Yoshida, K. Kawata, Y. Fukuyama, S. Takayama, and Y. Nakanishi, "A particle swarm optimization for reactive power and voltage control considering voltage security assessment," *IEEE Transactions on power systems,* vol. 15, no. 4, pp. 1232-1239, 2000.

[146] M. A. Abido, "Optimal power flow using particle swarm optimization," *International Journal of Electrical Power & Energy Systems,* vol. 24, no. 7, pp. 563-571, 2002.

[147] P. Acharjee, "Optimal power flow with UPFC using security constrained self-adaptive differential evolutionary algorithm for restructured power system,"

International Journal of Electrical Power & Energy Systems, vol. 76, pp. 69-81, 2016.

[148] S. Madadi, B. Mohammadi-Ivatloo, and S. Tohidi, "Probabilistic Available Transfer Capability Evaluation Considering Dynamic Line Rating Based on a Sequential Game-Theoretic Approach," *IEEE Systems Journal,* vol. 16, no. 1, pp. 891-901, 2022.

[149] W. Li, P. Wang, and Z. Guo, "Determination of Optimal Total Transfer Capability Using a Probabilistic Approach," *IEEE Transactions on Power Systems,* vol. 21, no. 2, pp. 862-868, 2006..

[150] M. Rashidinejad, H. Farahmand, M. Fotuhi-Firuzabad, and A. A. Gharaveisi, "ATC enhancement using TCSC via artificial intelligent techniques," *Electric Power Systems Research,* vol. 78, no. 1, pp. 11-20, 2008.

[151] J.-B. Park, K.-S. Lee, J.-R. Shin, and K. Y. Lee, "A particle swarm optimization for economic dispatch with nonsmooth cost functions," *IEEE Transactions on Power systems,* vol. 20, no. 1, pp. 34-42, 2005.

[152] M. Karthik and A. Reddy, "Particle swarm optimization to solve economic dispatch considering generator constraints," *The International Journal of Engineering and Science,* vol. 3, no. 10, pp. 94-100, 2014.

[153] L. Wang and C. Singh, "Stochastic economic emission load dispatch through a modified particle swarm optimization algorithm," *Electric Power Systems Research,* vol. 78, no. 8, pp. 1466-1476, 2008.

[154] T. Ting, M. Rao, and C. Loo, "A novel approach for unit commitment problem via an effective hybrid particle swarm optimization," *IEEE transactions on power systems,* vol. 21, no. 1, pp. 411-418, 2006.

[155] A. A. Sadiq, M. Buhari, S. S. Adamu, and H. Musa, "Coordination of multi-type FACTS for available transfer capability enhancement using PI–PSO," *IET Generation, Transmission & Distribution,* vol. 14, no. 21, pp. 4866-4877, 2020.

[156] S. M. Prajapati and P. Gandhi, "Impact of FACTS device for ATC enhancement in deregulated market," in *2018 IEEE International Conference on Power Energy, Environment and Intelligent Control (PEEIC)*, pp. 482-487, 13-14 April 2018, Greater Noida, India.

[157] D. Gaur and L. Mathew, "Optimal placement of FACTS devices using optimization techniques: A review," in *IOP conference series: materials science and engineering*, 2018, vol. 331, no. 1: IOP Publishing, p. 012023.

[158] M. S. Sureban and S. Ankaliki, "Enhancement of Available Transfer Capability of Transmission Lines Using Thyristor Controlled Reactor," in *2018 IEEE International Conference on Computation of Power, Energy, Information and Communication (ICCPEIC)*, pp. 375-380, 28-29 March 2018, Chennai, India.

[159] N. Ghawghawe and K. Thakre, "Computation of TCSC reactance and suggesting criterion of its location for ATC improvement," *International Journal of Electrical Power & Energy Systems,* vol. 31, no. 2-3, pp. 86-93, Feb. - Mar. 2009.

[160] S. V. Padmavathi, S. Sahu, and A. Jayalakshmi, "Available transfer capability enhancement by using Particle Swarm Optimization algorithm based FACTS allocation," in *2012 IEEE Asia Pacific Conference on Postgraduate Research in Microelectronics and Electronics*, pp. 184-187.

[161] D. Shukla, E. S. Lakshmi, and S. Singh, "Estimation of atc using ps-nr," in *2017 6th IEEE International Conference on Computer Applications In Electrical Engineering Recent Advances (CERA)*, pp. 111-116, 05-07 October 2017, Roorkee, India.

[162] E. Shayesteh, A. Yousefi, M. P. Moghaddam, and G. R. Yousefi, "An economic comparison between incorporation of FACTS devices and demand response programs for ATC enhancement," in *2008 IEEE Canada Electric Power Conference*, pp. 1-6, 06-07 October 2008, Vancouver, Canada.

[163] R. K. Poluru and R. L. Kumar, "Enhancement of ATC by optimizing TCSC configuration using adaptive Moth flame optimization algorithm," *J Comput Mech Power Syst Contr,* vol. 2, no. 3, pp. 1-9, Jul. 2019.

[164] S. Kesherwani, A. Mohapatra, and S. C. Srivastava, "An efficient holomorphic embedded based approach for available transfer capability evaluation," *International Journal of Electrical Power & Energy Systems,* vol. 122, p. 106164, Nov. 2020.

[165] K. N. Rao, J. Amarnath, and K. A. Kumar, "Voltage constrained available transfer capability enhancement with FACTS devices," *ARPN Journal of Engineering and Applied Sciences,* vol. 2, no. 6, pp. 1-9, Dec. 2007.

[166] N. Sinha, S. Karan, and S. K. Singh, "Modified de based atc enhancement using facts devices," in *2015 IEEE International Conference on Computational Intelligence and Networks*, Jan. 2015, pp. 3-8, 12-13 January 2015, Odisha, India.

[167] R. M. Idris, A. Khairuddin, and M. Mustafa, "Optimal allocation of FACTS devices for ATC enhancement using Bees algorithm," *World Academy of Science, Engineering and Technology,* vol. 54, no. 1, pp. 318-325, 2009.

[168] I. A. Hiskens, Pai, M.A., and Sauer, P.W, "An iterative approach to calculating dynamic ATC," in *Proceedings of Bulk Power System Dynamics and Control IV-restructuring,* Santorini, Greece, 1998.

[169] E. De Tuglie, M. Dicorato, M. La Scala, and P. Scarpellini, " A static optimization approach to assess dynamic available transfer capability," *IEEE Transactions on Power Systems,* vol. 15, no. 3, pp. 1069–1076, Aug. 2000.

[170] M. N. I. Maruf, A. Mohsin, M. Shoeb, M. Islam, and M. Hossain, "Study of thyristor controlled series capacitor (TCSC) as a useful FACTS device," *International Journal of Engineering, Science and Technology,* vol. 2, no. 9, pp. 4357-4360, 2010.

[171] E. W. Kimbark, "Improvement of system stability by switched series capacitors," *IEEE Transactions on power apparatus and systems,* vol. PAS - 85, no. 2, pp. 180-188, Feb. 1966..

[172] E. W. Kimbark, "Improvement of power system stability by changes in the network," *IEEE Transactions on Power Apparatus and Systems, v*ol. PAS – 88, no. 5, pp. 773-781, May 1969.

[173] N. Ratmarao and D. K. Reitan, "Improvement of power system transient stability using optimal control: bang-bang control of reactance," *IEEE Transactions on Power Apparatus and Systems, v*ol. PAS – 89, no. 5, pp. 975-984, May 1970.

[174] S. Meikandasivam, R. K. Nema and S. K. Jain, "Behavioral Study of TCSC Device–A MATLAB/Simulink Implementation 1," *International Journal of Electrical and Computer Engineering*, vol. 2, no. 9, pp. 1958–1963, Sep. 2008.

[175] L. Rajalakshmi, M. Suganyadevi, and S. Parameswari, "Congestion management in deregulated power system by locating series FACTS devices," *International journal of Computer applications,* vol. 13, no. 8, pp. 19-22, Jan. 2011.

[176] M. Gad, P. Shinde, and S. Kulkarni, "Optimal location of TCSC by sensitivity methods," *International Journal of Computational Engineering Research,* vol. 2, no. 6, pp. 162-168, Oct. 2012.

[177] A. K. Jain and S. Srivastava, "Price responsive demand management of an industrial buyer in day-ahead electricity market," *International Journal of Emerging Electric Power Systems,* vol. 18, no. 1, Feb. 2017.

[178] N. Sambasivarao, J. Amarnath, and V. Purnachandrarao, "Enhancement of available transfer capability in deregulated powersystem using series facts device (TCSC)," *Int. J. Eng. Res. Technol.,* vol. 2, no. 11, pp. 192-199, Nov. 2013.

[179] C. A. Canizares and F. L. Alvarado, "Point of collapse and continuation methods for large AC/DC systems," *IEEE transactions on Power Systems,* vol. 8, no. 1, pp. 1-8, Feb. 1993.

[180] R. E. Bohn, M. C. Caramanis, and F. C. Schweppe, "Optimal pricing in electrical networks over space and time," *The Rand Journal of Economics,* vol. 15, no. 3, pp. 360-376, 1984.

[181] S. K. Nallagalva, M. K. Kirar, and G. Agnihotri, "Transient stability analysis of the IEEE 9-bus electric power system," *International Journal of Scientific Engineering and Technology,* vol. 1, no. 3, pp. 161-166, 2012.

[182] Y. Shi and R. Eberhart, "A modified particle swarm optimizer," in *1998 IEEE international conference on evolutionary computation proceedings. IEEE world congress on computational intelligence*, pp. 69-73, 04 - 09 May 1998, Anchorage, AK, USA.

[183] R. C. Eberhart, Y. Shi, and J. Kennedy, *Swarm intelligence*. Elsevier, 2001.

[184] R. Poli, "An analysis of publications on particle swarm optimization applications " in "Technical Report CSM-469," Department of Computer Science, University of Essex, 2007.

[185] R. Poli, "Analysis of the Publications on the Applications of Particle Swarm Optimisation," *Journal of Artificial Evolution and Applications,* vol. 2008, pp. 1-10, Jan. 2008.

[186] M. R. Bonyadi and Z. Michalewicz, "Particle Swarm Optimization for Single Objective Continuous Space Problems: A Review," *Evol Comput,* vol. 25, no. 1, pp. 1-54, Mar. 2017.

[187] M. Clerc and J. Kennedy, "The particle swarm-explosion, stability, and convergence in a multidimensional complex space," *IEEE transactions on Evolutionary Computation,* vol. 6, no. 1, pp. 58-73, February 2002.

[188] P. Kundur, *Power system stability and control,* McGraw Hill Education, 2006.

[189] Z. Ma, Z. Wang, Y. Wang, R. Diao, and D. Shi, "Mathematical representation of WECC composite load model," *Journal of Modern Power Systems and Clean Energy,* vol. 8, no. 5, pp. 1015-1023, September 2020.